Terms and Conditions of Use of Digitised Theses from Trinity College Library Dublin

Copyright statement

All material supplied by Trinity College Library is protected by copyright (under the Copyright and Related Rights Act, 2000 as amended) and other relevant Intellectual Property Rights. By accessing and using a Digitised Thesis from Trinity College Library you acknowledge that all Intellectual Property Rights in any Works supplied are the sole and exclusive property of the copyright and/or other IPR holder. Specific copyright holders may not be explicitly identified. Use of materials from other sources within a thesis should not be construed as a claim over them.

A non-exclusive, non-transferable licence is hereby granted to those using or reproducing, in whole or in part, the material for valid purposes, providing the copyright owners are acknowledged using the normal conventions. Where specific permission to use material is required, this is identified and such permission must be sought from the copyright holder or agency cited.

Liability statement

By using a Digitised Thesis, I accept that Trinity College Dublin bears no legal responsibility for the accuracy, legality or comprehensiveness of materials contained within the thesis, and that Trinity College Dublin accepts no liability for indirect, consequential, or incidental, damages or losses arising from use of the thesis for whatever reason. Information located in a thesis may be subject to specific use constraints, details of which may not be explicitly described. It is the responsibility of potential and actual users to be aware of such constraints and to abide by them. By making use of material from a digitised thesis, you accept these copyright and disclaimer provisions. Where it is brought to the attention of Trinity College Library that there may be a breach of copyright or other restraint, it is the policy to withdraw or take down access to a thesis while the issue is being resolved.

Access Agreement

By using a Digitised Thesis from Trinity College Library you are bound by the following Terms & Conditions. Please read them carefully.

I have read and I understand the following statement: All material supplied via a Digitised Thesis from Trinity College Library is protected by copyright and other intellectual property rights, and duplication or sale of all or part of any of a thesis is not permitted, except that material may be duplicated by you for your research use or for educational purposes in electronic or print form providing the copyright owners are acknowledged using the normal conventions. You must obtain permission for any other use. Electronic or print copies may not be offered, whether for sale or otherwise to anyone. This copy has been supplied on the understanding that it is copyright material and that no quotation from the thesis may be published without proper acknowledgement.

An X-ray Search for Active Cores in Local Group Galaxies

by

Zhiyun Zang
M.Sc.

A Thesis submitted to
The University of Dublin
for the degree of

Doctor in Philosophy

Department of Physics
University of Dublin
Trinity College

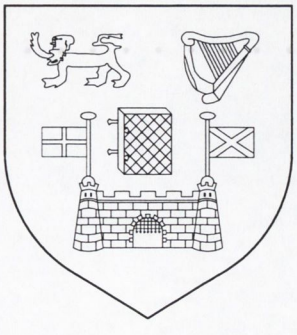

October, 1999

Declaration

This thesis has not been submitted as an exercise for a degree at any other University. Except the following listed articles and where otherwise stated, the work described herein has been carried out by the author alone. This thesis may be borrowed or copied upon request with the permission of the Librarian, University of Dublin, Trinity College. The copyright belongs jointly to the University of Dublin, Dunsink Observatory and Zhiyun Zang.

ROSAT PSPC observations of three Sculptor Group galaxies: NGC 55, NGC 247 and NGC 300
Z. Zang, R. S. Warwick and E. J. A. Meurs, 1997, *Irish A. J.*, 24, 45.

ROSAT HRI and PSPC observations of M32
Z. Zang and E. J. A. Meurs, 1998, in *The Stellar Content of Local Group Galaxies*, IAU Symp. 192, Cape Town, South Africa, eds. P. Whitelock and R. Cannon, p334.

The case for a low-level active nucleus in M32
Z. Zang and E. J. A. Meurs, 1999, *New A.*, in press.

X-ray candidates for a population of nuclear cores in Local Group galaxies
E. J. A. Meurs and Z. Zang, 1999, in *Black holes in Binaries and Galactic Nuclei*, ESO Workshop, Garching, Germany, in press.

Signature of Author 

Zhiyun Zang

臧志云

October, 1999

Summary

The nuclei of galaxies are sometimes sites of very energetic process, resulting in high levels of electromagnetic radiation being emitted. Such active galactic nuclei (AGNs) are thought to be powered by accretion of mass onto a centrally collapsed object, a supermassive black hole of typically $10^6 - 10^8$ solar masses. When gravitational energy of the accreting material is liberated it is radiated away, causing the nucleus to appear very bright. The extreme manifestation of this phenomenon is probably seen in the famous Quasi Stellar Objects.

In this thesis, a dedicated search for X-ray emission from the cores in the Local Group galaxies is performed to establish whether low levels of nuclear activity in these nearest galaxies may be found. The data are from ROSAT HRI or PSPC pointing observations which are available for 21 Local Group galaxies in the centre of the observing fields, and for another 3 in the outer area, covering 70% of all Local Group members. The HRI data are particular useful, since the nuclear source may be better resolved from the HRI images.

M31 is the brightest galaxy of the group, in which a source has been detected coincident with its nucleus. M32, a satellite galaxy of M31, is a small Elliptical with a clear central concentration. The HRI observation in 1994 shows a little extension ($\sim 2.7''$) of the X-ray source in M32, PSPC spectral models give higher absorption columns than the Galactic one; no choice can be made between Power Law or Thermal Bremsstrahlung models. In the view of the small source extension and still uncertain central or non-central position of the source, conceivable interpretations are either a Supernova Remnant or a mini-AGN. An ASCA spectrum and a radio upper limit suggest that a low-level AGN is a more attractive explanation.

Only in two other cases sources are found close to the centre of the galaxy. The HRI observation of NGC 6822 reveals a week source coincident with the nominal optical centre, which may exhibit a hard spectrum. The WLM galaxy has also an HRI source detected in 1996 near the central position. In both cases the galaxy is in a Irregular system and the optical position will refer to the centroid of the overall light distribution rather than a well-defined centre. These two central sources can therefore only be considered suspicious cases until there nature is firmly established

with help of data from other wavebands and from new high-energy measurements. Among the rest of the Local Group galaxies, no sources are detected in their central area. The upper limits of the X-ray luminosities derived for the central regions show that most dwarf Ellipticals has little X-ray emission ($L_X \lesssim 10^{35}$ ergs s^{-1}). The results on the Local Group members suggest that galaxies with total blue magnitude $L_B \simeq 10^8\ L_{\odot,B}$ or more may have some central X-ray emission at the level of the central object in the Milky Way.

For the sake of comparison, ROSAT observation of the next nearest group of galaxies, the Sculptor Group, were also examined. Among 5 large members of Sculptor Group galaxies, NGC 253 is a well-known starburst galaxy; NGC 7793 has some diffuse emission detected all over the galaxy but without significant enhancement near the centre position. For NGC 55, 247 and 300 no sources are detected in the central regions, down to X-ray luminosity $L_X \simeq 10^{36}$ ergs s^{-1}.

As seen from the example of M32, the X-ray luminosities of the central X-ray sources are several orders of magnitude less than typical Seyfert galaxies, which could be due to a lower black hole mass (*e.g.* $\sim 10^4\ M_\odot$) or a lower accretion rate. For such a low mass accretion rate, the standard thin disk model for accretion is probably not applicable and the model for Advection-Dominated Accretion Flows provides possible solutions, in which very little energy is radiated away during the accretion process. Masses for the central condensed objects have been determined for the Milky Way and M32. In both cases the accretion rate is extremely low and well into the expected Advection Dominated Accretion Flow regime.

In brief, central X-ray sources are only found among the most luminous members of the Local Group. These are candidate massive Black Holes, for which confirmation can be found from data at other wavelengths in the cases of the Milky Way and M31. If also M32 and M33 have massive Black Holes in their nuclei, there could be at least four massive Black Holes immediately around us. For the moment one could conclude that the 20 or so smaller and/or Irregular and dwarf-Spheroidal systems do not seem to possess massive Black Holes, but the sample of M32 shows that the activity level can be so low that a non-detection at high energy may not necessarily imply no Black Hole.

Acknowledgements

Firstly, I would like to thank my supervisor, Professor Evert Meurs, for all his help and advise during these years. I am very grateful to him for proof-reading this thesis as it was being written and providing me with invaluable comments on it. Thanks are also due to Dr. Sara McMurry, my internal supervisor in Physics Department of TCD, for all her help. I would like to thank Dr. Laura Norci for her advise on many aspects of my research work during these years. I am very grateful to Michael Carr for his comments on part of my transfer report which was the starting point of this thesis. I am also very grateful to Dr. Stefan Döbereiner (MPE, Garching) for correcting one of the ROSAT data sets for this study. I would like to acknowledge the financial support given to me by the Dublin Institute for Advanced Studies and by Forbairt under the Basic Research Grant Scheme. This research is based mainly on the data from ROSAT Public Data Archive and the MIDAS/EXSAS software. The Starlink and the XANADU are also used for data reduction. The databases from NED, SIMBAD, ADS and Skyview are used as well to obtain the various astronomical informations. Thanks to all the people who make those services available. This research is carried out at Dunsink Observatory, Dublin, and I am very grateful to everyone at the Observatory who helped me during these years, especially Wai Ming Tai, Mike Smyth and John Cunniffe who created the computer system 'giacobini' and kept it running for me. I am very grateful to the Head of the Observatory, Professor Evert Meurs, for the possibility to stay in the Observatory, otherwise it would not have been possible to start this study. I would like to thank all my friends for their encouragement they gave me during these years. Finally, I would like to thank my family, and especially my wife, Xiaoqin Wu and my daughter, Yi Zang, for all the support they have given me throughout my studies.

Abbreviations

AGN	Active Galactic Nuclei
ASCA	Advanced Satellite for Cosmology and Astrophysics
AXAF	Advanced X-ray Astronomy Facility
BH	Black Hole
CDS	Strasbourg astronomical Data Centre
EXSAS	Extended Scientific Analysis System
FOV	Field of View
HR	Hardness Ratio
HRI	High Resolution Imager
HST	Hubble Space Telescope
IPC	Imaging Proportional Counter
LINER	Low-Ionization Nuclear Emission-line Region
MC	Magellanic Cloud
MDO	Massive Dark Object
ML	Maximum Likelihood
MPC	Monitor Proportional Counter
MPE	Max Planck Institute for Extraterrestrial Physics
NED	NASA/IPAC Extragalactic Database
PET	Photon Event Table
PSF	Point Spread Function
PSPC	Position Sensitive Proportional Counter
ROSAT	Röntgen Satellite
SASS	Standard Analysis Software System
SIMBAD	Set of Identifications, Measurements and Bibliography for Astronomical Data
SNR	Supernova Remnant
XMM	X-ray Multi-Mirror
XRT	X-ray Telescope

Contents

List of Figures

List of Tables

Chapter 1

Introduction

Active galactic nuclei

The active galaxies, as a distinct from normal galaxies, were discovered by Carl Seyfert. He found that some spiral galaxies possessed extraordinary bright and point-like nuclei. On short exposure photographs, these nuclei looked like stars but spectroscopic studies revealed they possessed strong and broad emission lines (Seyfert 1943). We use the term of AGN (Active Galactic Nuclei) to define these objects because it is the very central region of a galaxy that is active, not the entire galaxy.

Now, nuclear activity in galaxies has been recognized as a wide-spread phenomenon. Yet, for how many active galaxies are known as of today, such highly energetic activity affects only about 10 percent of all galaxies. Nevertheless, it has become increasingly evident that weaker forms of nuclear activity can occur but may easily be overlooked. An important category with activity level between the above mentioned Seyferts and normal galaxies is represented by the LINER galaxies (Low Ionization Nuclear Emission line Regions), including several well-known brighter galaxies (Heckman 1980). Cases with LINER or near-LINER nuclear activity among bright galaxies that had been overlooked previously were presented by Filippenko and Sargent (1985). At the bottom end of the scale, the lowest level of nuclear activity is probably found in the Galactic Center.

The weak activity in the Galactic nucleus suggests that all galaxies may have some form of nuclear activity. It is therefore of great interest to establish the prevalence of nuclear activity of any level among the galaxies. This is not only important for the dynamics and evolution of galaxies in general, it is also relevant to astrophysical and cosmological questions such as the faint tail of the AGN luminosity function and, given the ubiquity of the smaller galaxies, the ionization flux in the universe and the expected contributions to the X-ray background (*e.g.* Griffiths and Padovani 1990).

The link between nuclear activity and X-ray emission is very well established. Probably, X-ray emission is one of the better ways to assess nuclear activity in galaxies, also when in other wavebands like optical there is no obvious central core. The Local Group galaxies are the nearest specimen to be examined and therefore allow low levels of nuclear activity to be detected. The ROSAT HRI data (see 3.1) are particularly appropriate for an investigation of the nuclear regions of the Local Group galaxies. The combination of high spatial resolution of the detector and small distance of the targets is very advantageous. When no HRI data are available, ROSAT PSPC data are an alternative.

Organization of this thesis

Following this introduction, *Chapter 2* gives an overview of the Local Group galaxies, including their optical contents and commonly used parameters.

The *Chapter 3* summarizes the known X-ray properties of the Local Group galaxies. After a brief history of X-ray astronomy, the two major X-ray imaging observatories that have flown until now, Einstein and ROSAT, are described with characteristics of their detectors, and the observations of two large systems of the Local Group, M31 and M33, are summarized in the end.

The next three chapters form the major part of this thesis. In *Chapter 4* analyses of ROSAT data for most of the Local Group galaxies are presented in detail. Beginning with a brief description of the data handling procedures, individual galaxies

follow and their X-ray emission properties based on the ROSAT data are presented.

Chapter 5 is all about the galaxy M32. This chapter is based on an article which has been accepted by "*New Astronomy*" and therefore is mostly self-contained. It includes a review of the known X-ray properties of the galaxy, then the improved results of the ROSAT PSPC and HRI data, and a discussion of the possible nature of the X-ray source in this galaxy.

Chapter 6 summarizes the X-ray results obtained for the central regions of the Local Group galaxies for which X-ray data are available. The overall X-ray characteristics of the central source and the possibility of low level activity are discussed.

The Sculptor Group is another nearby group, which is immediately beyond the Local Group. In the *Chapter 7*, the ROSAT results of the Sculptor Group galaxies are presented briefly. The possible occurrence of nuclear X-ray emission is discussed.

Chapter 2

An overview of the Local Group of galaxies

The Local Group was first recognized by Hubble in the early days of extragalactic research when distances to galaxies were first being measured. There was a distinct difference between those galaxies that resolved easily into stars and those that did not, implying that the Milky Way is part of a small local cluster of galaxies, that condensed out of the general expansion of the Universe. Now more then 30 members have been recognized for this condensation (Table 2.1, Whiting et al. 1997a), which is called The Local Group (LG).

The M31 and Milky Way galaxies are the most luminous and massive of the group. M31 is a Hubble Sb type, with a luminous large bulge of old stars, surrounded by a less luminous disk with gas, dust and young stars, arranged in spiral arms. Its diameter is $\sim$ 60 kpc and its mass $\sim 7 \times 10^{11}\ M_{\odot}$. Within it there are about 300 globular clusters, 400 open clusters, supernova remnants (SNRs), and other components. The Milky Way galaxy is a Sb/Sc type, with somewhat less-conspicuous central bulge and a brighter disc and looser arms than M31. It has a diameter of $\sim$ 40 kpc and a mass of $5 \times 10^{9}\ M_{\odot}$. M33 is another spiral galaxy (Sc) of the group, but smaller ($d \sim 14$ kpc) and fainter than the above two. It contains many blue stars in its complex, thick spiral arms, and has several giant H II regions.

Two of the best studied irregular galaxies in the Local Group are the two Mag-

Table 2.1: Local Group galaxies

Name		α_{1950} h m	δ_{1950} $^\circ$ $'$	Type	$D(kpc)$	M_V
Pegasus	DDO 216	23 26.1	+14 28	Irr	1800	−14.6
Sextans B	DDO 70	09 57.4	+05 34	Irr	1300	−14.3
Sextans A	DDO 75	10 08.6	−04 28	Irr	1300	−14.2
NGC 3109	DDO 236	10 00.8	−25 55	Irr	1260	−15.8
IC 10		00 17.7	+59 01	Irr	1250	−17.6
SagDIG		19 27.9	−17 47	Irr	1150	−11.0
Antlia		10 01.8	−27 05	dE3	1150	−10.7
WLM	DDO 221	23 59.4	−15 45	Irr	940	−14.0
Tucana		22 38.5	−64 41	dE5	900	−9.6
EGB0427+63	UGC−A92	04 27.4	+63 30	Irr	800	−10.0
M33	NGC 598	01 31.1	+30 24	Sc	795	−18.9
And I		00 43.0	+37 44	dE0	790	−11.7
And III		00 32.6	+36 12	dE6	790	−10.2
IC 1613	DDO 8	01 02.2	+01 51	Irr	765	−14.9
LGS 3		01 01.2	+21 37	Irr/dE	760	−9.7
M31	NGC 224	00 40.0	+40 59	Sb	725	−21.1
M32	NGC 221	00 40.0	+40 36	E2	725	−16.4
NGC 205		00 37.6	+41 25	E5	725	−16.3
NGC 185		00 36.2	+48 04	E3	620	−15.3
NGC 147	DDO 3	00 30.5	+48 14	E4	598	−14.8
And II		01 13.5	+33 09	dE3	587	−11.7
NGC 6822	DDO 209	19 42.1	−14 56	Irr	540	−16.4
Phoenix		01 49.0	−44 42	Irr	390	−9.9
Leo I	DDO 74	10 05.8	+12 33	dE3	270	−12.0
Leo II	DDO 93	11 10.8	+22 26	dE0	230	−10.2
Fornax		02 37.8	−34 44	dE3	131	−13.0
Sextans		10 10.6	−01 24	dE4	90	−10.0
Carina		06 40.4	−50 55	dE4	87	−9.2
Sculptor		00 57.6	−33 58	dE	78	−10.7
Draco	DDO 228	17 19.2	+57 58	dE3	76	−8.6
Ursa Minor	DDO 199	15 08.2	+67 23	dE5	69	−8.9
SMC		00 51.0	−73 06	Irr	58	−16.2
LMC		05 24.0	−69 48	Irr	49	−18.1
Sagittarius		18 51.9	−30 30	dE7	24	−14.0
Galaxy	Milky Way	17 42.4	−28 55	Sbc	8.4	−20.6

ellanic Clouds (MCs): the bigger one, the Large Magellanic Cloud (LMC), is only 49 kpc away and the Small Magellanic Cloud (SMC) is not much farther. Because of this they can be studied in great detail. We have information about nearly every kind of stars and interstellar objects which help us understanding stellar evolution and the extragalactic distance scale. The LMC has a giant H II region, 30 Doradus, a huge complex of massive stars, stars in the process of formation, gas and dust.

There are four moderately bright elliptical galaxies which are companions to M31. Two very close companions are M32 and NGC 205, both of which are seen superimposed on the outer parts of M31. M32 is a nearly circular galaxy with a

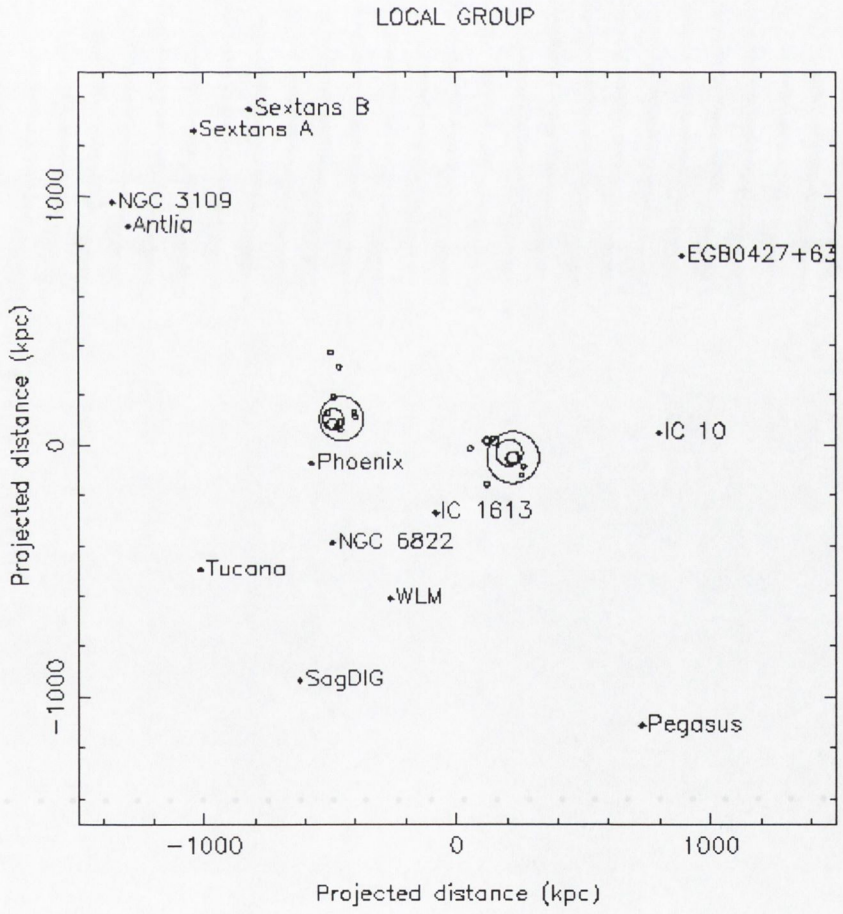

Figure 2.1: Projection of the galaxies in the Local Group onto a convenient plane. The large circle at left is the Milky Way, surrounded by its satellite galaxies; at right is M31 with its satellites. (From Whiting et al. 1997a)

population of exclusively very old stars, whereas NGC 205 is more elongated in shape and contains a small population of young stars, with accompanying dust and gas. The other two companions, NGC 147 and NGC 185, are somewhat fainter and more distant from M31. Besides the few galaxies mentioned here, the Local Group contains a still larger number of dwarf galaxies (see Table 2.1). Figure 2.1 shows a diagram of Local Group galaxies, projected onto a plane (Whiting et al. 1997b).

The Universe is made up of galaxies and over 10^{11} galaxies are visible using modern telescopes. Local Group galaxies are a particular useful sample with which to explore various problems regarding galaxies since we can study members of the Local Group much more thoroughly than more distant objects.

Chapter 3

Known X-ray Properties of Local Group galaxies

3.1 X-ray observations

The optical astronomy has been established for hundreds of years, while other wavelengths of study are products of this century. Radio astronomy started in the 1930s, followed by ultraviolet(UV), infrared(IR) and X-ray astronomy in the 1960s. The gamma-ray astronomy is making progress. Similar as for UV and gamma-ray measurements, X-ray observations must be undertaken using space-borne telescopes. In the early years, the sky was searched for sources of high energy radiation using rocket-borne proportional counters and scintillators. The first X-ray source other than the Sun was detected in 1962, known as Sco X-1 (Giacconi et al. 1962, Gursky et al. 1963), followed by the detection of the Crab Nebula, a well-known young supernova remnant in our galaxy (Clark 1965, Peterson et al. 1966).

By the end of 1970, about 50 cosmic X-ray sources had been discovered, most of them accretion-powered X-ray binaries in the galactic plane. Two of these were identified with stellar optical objects. The diffuse X-ray background was discovered and determined to be uniform to 5–10%. Six supernova remnants had been identified and X-rays had been detected coming from the LMC, the active galaxies M87 and NGC 5128, the Coma Cluster and the quasar 3C273 (*cf.* Charles and Seward 1995).

The first surveying astronomical X-ray satellite, Uhuru, was launched on 12 December 1970 with two sets of conventional proportional counters on board (Giacconi et al. 1971). It was able to detect X-ray sources 10 times fainter than the faintest ones detectable on earlier flights. The 4U (fourth Uhuru) catalogue contains 339 sources (Forman et al 1978).

The study of X-ray properties of normal galaxies as a class was made possible by the Einstein Observatory, which was launched in November 1978 (Giacconi et al. 1979). Before then only 4 Local Group galaxies had been detected in X-rays: the Milky Way, M31, and the Magellanic Clouds. A dozen of Local Group galaxies were observed with Einstein among about 100 galaxies observed in total. The most detailed work on individual X-ray sources in galaxies and their identifications has been done in the Local Group as well.

3.1.1 Einstein observations

Einstein was the first fully imaging X-ray telescope put into space (Bradt et al. 1992), with an angular resolution of a few arcseconds, a field-of-view of tens of arcminutes, and a sensitivity $\sim$ 1000 times greater than any mission before it. The telescope had sensitivity over the approximate energy range 0.2–3.5 keV. The satellite contained a high resolution X-ray telescope and focal plane assembly capable of positioning the focus at one of four instruments: a high resolution imaging detector (HRI), a broader field imaging proportional counter (IPC), a solid state spectrometer (SSS), and a Bragg crystal spectrometer (FPCS). It also contained a monitor proportional counter (MPC) aligned with the telescope, as well as a broad band filter spectrometer (BBFS) and an objective grating spectrometer (OGS) to be used with the imaging detectors.

The IPC had a field of view (FOV) of $75' \times 75'$, with a spatial resolution of $\sim 1'$. The effective detector area was ~ 100 cm^2, and the time resolution was 63 ms. The energy range was 0.4–4.0 keV, and the background count rate was $\sim 10^{-2}$ cts s^{-1}. The HRI had a $25'$ diameter FOV, with a spatial resolution of $2''$ within $5'$ of the axis. The effective area was 20 cm^2 at 0.25 keV; 10 cm^2 at 1 keV; and 5 cm^2 at 2 keV.

The time resolution was 8 ms. The energy range was 0.15–3.0 keV. The background was $\sim 5 \times 10^{-3}$ cts arcmin^{-2} s^{-1}. The HRI had no inherent spectral resolution, but spectral studies could be performed using interchangeable broad band filters and an objective grating.

The Einstein observations of Local Group and other galaxies have been reviewed comprehensively by Helfand (1984) and Fabbiano et al. (1989). Table 3.1 lists the sources in Local Group galaxies detected by the Einstein observatory.

3.1.2 ROSAT observations

Launched in June 1990, ROSAT (Röntgen-Satellite) is the first mission to perform a deep sky survey with an imaging telescope of the whole sky in soft X-rays (0.1–2 keV) and the EUV. It is also used for detailed observations of selected sources, in order to study spatial structure, spectra and time variability. In this Pointing Mode the sensitivity will be at least two times larger than that of former missions.

In the focal plane of the X-ray mirror assembly (XMA) two redundant position sensitive proportional counters (PSPC) are available. These are multiwire proportional counters with a cathode strip readout scheme for position determination. Both spectral and spatial resolution increase with increasing energy. X-rays penetrate into the counter volume through a polypropylene entrance window additionally coated with carbon and lexan (to decrease UV transmission). A filter wheel with four positions is mounted in front of the detector. The open and closed filter wheel positions are used for "standard" observations and for monitoring of particle background; the third position is used for spectral calibrations, while the fourth position contains a boron filter. The insertion of the boron filter into the optical path allows an increase of spectral resolution at lower energies. The full two degree field of view of the XMA can be utilized in conjunction with the PSPC. Table 3.2 gives a summary of the PSPC performance characteristics.

Table 3.1: Einstein sources in Local Group galaxies[†]

Galaxy	Total L_X (ergs s^{-1})	No. of sources	Interlopers	SNR	Binaries		Unidentified
					young Pop I	older population	in galaxies
LMC	6.6×10^{38}	102(52)	$\sim 46(\sim 19)$	32(21)	7(6)	2(2)	$\sim 15(\sim 4)$
SMC	6.1×10^{37}	57	~ 14	~ 12	1	0	~ 30
M31	3.6×10^{39}	117	~ 6	2	~ 26	$\sim$ 23GC+$\sim$ 60	–
M32	5.4×10^{37}	1	–	–	–	1	
M33	1.1×10^{39}	17	~ 3	1	~ 12	0	–
IC 1613	–	0	–	–	–	–	–
NGC 6822	1×10^{37}	2	~ 1	~ 1	–	–	–
NGC 205	$< 9 \times 10^{36}$	0	–	–	–	–	–
Ursa Minor	$\leq 3.2 \times 10^{35}$	3	–	–	–	–	≤ 3
Maffei 1[‡]	1×10^{39}	≤ 3	–	–	–	–	extended
Milky Way	$\sim 3 \times 10^{39}$	~ 125	–	~ 10	~ 40	8GC+$\sim$ 67	–

[†] From Fabbiano et al. (1989).

[‡] This galaxy is no longer regarded as a member of the Local Group.

Table 3.2: ROSAT PSPC Characteristics

Window size	8 cm (diameter of circular aperture)
Field of view	2° (diameter)
Gas mixture	65% argon, 15% methane, 20% xenon
Operating pressure	1.466 bar at 22 °C
Energy resolution	43% at 0.93 keV
Spatial resolution	300 μm ($\sim 25''$) at 1 keV (FWHM)
Entrance window	1 μm polypropylene
Support grid transmission	72% (on average)

The ROSAT high-resolution imager (HRI) is very similar to the Einstein Observatory HRI and comprises two cascaded microchannel plates (MCPs) with a crossed grid position readout system. The detector performance is briefly summarized in Table 3.3. Values of the quantum efficiency and background quoted here are based on in-flight and ground performance of the HRI. Two significant changes from the Einstein instrument that have affected the performance of the detector are: the substitution of CsI for MgF_2 as the detector photocathode, and the introduction of a thin aluminum-coated plastic membrane (the "electrostatic shield") near the front MCP (in addition to the UV/Ion shield which is situated farther in front of the detector).

Table 3.3: ROSAT HRI Characteristics

Field of View	$38'$ (square)
Spatial Resolution	$\sim 4''$ (FWHM)
Quantum Efficiency	30% at 1 keV
Window Transmission	75% at 1 keV
Background	1.0×10^{-3} internal
(counts arcmin^{-2} s^{-1})	$2.1(1.7 - 8.3) \times 10^{-3}$ external†
	$6.9(3.5 - 13.8) \times 10^{-4}$ XRB‡
	3.8×10^{-3} Typical Total
Temporal Resolution	61 μs
Dead Time	0.36 to 1.35 ms

†Depending upon orbital location.

‡Depending upon viewing direction.

3.2 M31

X-rays from M31 (NGC 224) were first seen in the data from a rocket launched in 1973 (Bowyer et al. 1973), which was confirmed by the Uhuru and Ariel V all-sky surveys. The luminosity was calculated as $L_X \sim 2 \times 10^{39}$ ergs s^{-1}. The Einstein IPC revealed 30 bright sources in the outer spiral arms and an unresolved cluster of sources in the nuclear region. The HRI resolved this cluster into 117 individual sources (*cf.* Crampton et al. 1984). Later Trinchieri and Fabbiano (1991) reported 108 point sources in total, using 4 IPC pointings and several HRI pointings. Of these sources, 19 have been identified with globular clusters (Sargent et al. 1977), and 4 more sources could also be associated with globular clusters (Crampton et al. 1984); about 30 sources are associated with the disc and the spiral arms; 2 sources are associated with bright SNRs.

The sources in the spiral arms correlate well with the distribution of neutral hydrogen, so they are likely to be associated with Population I stars. However, most of the X-ray sources in the dominant central cluster are instead likely to belong to an older stellar population. The luminosity of these sources is in the range of Galactic low-mass binaries, and some variability has been reported consistent with the hypothesis of them being powered by accretion onto a compact object (McKechnie et al. 1984).

Supper et al. (1997) reported the result of the first M31 survey with the ROSAT PSPC performed in July 1991. 369 individual sources were detected within the ≈ 6.3 deg^2 field investigated. Their luminosities range from 3×10^{35} ergs s^{-1} to 2×10^{38} ergs s^{-1} (0.1–2.4 keV). Of these sources, 43 have been tentatively identified with foreground sources, 29 with globular clusters, 17 with SNRs, 3 with other galaxies (including M32), and 3 with radio sources. A comparison with the Einstein source list (Trinchieri and Fabbiano, 1991) confirms 65 Einstein sources, 15 of which appear to be variable. In addition, 6 faint possible and 3 bright transients were discovered. 327 ROSAT sources are new whereas 43 Einstein sources are not seen by ROSAT (including the transients).

The ROSAT HRI observation of the central region of M31 revealed 86 sources within $\sim 17'$ of the nucleus of M31 (Primini et al. 1993), 18 of them are identified with globular clusters. Diffuse emission is also detected, the amount is about 6×10^{38} ergs s^{-1} (0.2–4.0 keV) within $5'$ of the nucleus.

3.3 M33

M33 (NGC 589) was observed by Einstein, with both the HRI and the IPC and MPC. The HRI observation (Market and Rallis 1983) detected 8 X-ray sources, most of them associated with Population I tracers. Although the brightest source (the nucleus, namely M33 X-8) was seen to be variable, the simultaneous MPC observations indicated no such variability (Peres et al. 1989), suggesting that the variation existed only below 1.2 keV. No variability was seen with EXOSAT either (Gottwald et al. 1987). In addition to the bright nuclear source and several other bright point-like features seen in the disc and the arms of M33, Trinchieri et al.(1988) also report the detection of low surface brightness, diffuse emission, thought to be the result of the integrated contribution of several lower luminosity sources and possibly diffuse hot gas.

Long et al.(1996) reported recently their results of a long exposure ROSAT PSPC observation of M33. They found 37 sources within $15'$ of the nucleus, most of them associated with Population I tracers, and several of them time-variable. Both spiral arms are very apparent in X-rays. All of the sources seen by Einstein are seen by ROSAT. The brightest source is again the nucleus and accounts for almost 2/3 of the total source flux. The ASCA observations (Takano et al. 1994) are only able to place a tentative 10 percent as an upper limit to the time variability of this source. Takano et al. also found that the nuclear spectrum is significantly softer than typical AGN spectra, and suggest that the nucleus may be a close binary system containing a black hole of 10 $M_{\odot}$.

The diffuse emission detected by Trinchieri et al. (1988) is readily apparent in the ROSAT PSPC observation. Long et al. (1996) found that the diffuse emis-

sion is softer than the faint point sources and the SNRs, and is well fitted with a Bremsstrahlung spectrum with kT $\sim$ 0.4 keV and $log\ N_H \sim 20.6$.

M33 has also been studied with the ROSAT HRI (Schulman and Bregman 1995), revealing 27 sources within 17.5′ of the nucleus, 12 of which had also been detected by Einstein. 3 of the detected sources appear to be coincident with giant H II regions, 7 with SNRs and 2 may be correlated with holes in the neutral hydrogen layer. The diffuse emission is also detected within 11′ of the nucleus of M33, the luminosity is about 10^{39} ergs s^{-1} (0.2–4.0 keV).

Chapter 4

ROSAT observations of Local Group galaxies

4.1 Introduction

To investigate the occurrence of nuclear activity in galaxies to the lowest possible levels, a dedicated search is being carried out with data from the ROSAT HRI, or alternatively PSPC, for nuclear sources in members of the Local Group of galaxies around the Milky Way. The use of the HRI may be particularly useful in order to distinguish any nuclear source from other conceivable sources nearby, like bright SNRs, X-ray binaries, *etc.*

Two Local Group galaxies, M31 and M33, (*cf.* 3.2 and 3.3) have been observed previously with the ROSAT PSPC and HRI at different spatial resolution and correspondingly different areas and different dates. These two galaxies are useful for developing our data analysis techniques through comparison with the results published for them.

Besides 4 of the larger systems, M31, M33, LMC and SMC, many of the Local Group galaxies have been observed with the ROSAT PSPC or HRI or both. Table 4.1 lists those galaxies which are at the centre of the XRT Field of View (FOV). All the data are from the ROSAT data archive at the Max Planck Institute for Extraterrestrial Physics (MPE) in Garching. Some data sets under the same

ROSAT Observation Request (ROR) number are stored as two separate observations at two separate exposure times, and the second part of the observation may have started long after the first part. Apart from the listing above there are three galaxies (namely Tucana, Ursa Minor and Sagittarius) which are also in a PSPC FOV with fairly large offset.

In this chapter, the general data analysis procedures are described, followed by two long exposure HRI observations for M31 and M33, after which the detailed results for each of the above small Local Group galaxies are presented. M32 however follows next in a separate chapter.

Table 4.1: ROSAT observation log of small Local Group galaxies

Name	Other Name	ROR No.	Instrument	Start Date	Exposure (ksec)
M 32	NGC 221	600600	HRI	1994.07.19	12.6
NGC 205	M 110	600816	HRI	1996.08.04	28.1
NGC 147	DDO 3	400744	HRI	1995.01.19	14.7
NGC 185		600743	HRI	1995.01.19	21.0
IC 10		600902	HRI	1995.01.18	32.6+38.5
IC 1613		600689	HRI	1995.01.18	3.8+22.7
WLM	DDO 221	600814	HRI	1996.05.30	66.9+21.4
NGC 6822	DDO 209	600815	HRI	1995.10.19	4.9+52.8
		600148	PSPC	1992.04.28	6.8
Sextans A	DDO 75	600116	HRI	1991.12.10	11.5+18.3
		600139	PSPC	1991.11.23	6.7
NGC 3109	DDO 236	600174	PSPC	1992.05.26	18.5
		600385	PSPC	1992.11.18	13.3
Pegasus	DDO 216	600143	PSPC	1992.06.12	8.8
Fornax		600003	PSPC	1992.01.31	10.6
Sextans		600184	PSPC	1992.05.29	1.9
Carina		600185	PSPC	1992.04.05	8.7
Sculptor		600378	PSPC	1992.07.01	9.8
Draco	DDO 228	200724	PSPC	1992.04.01	5.3

4.2 General X-ray data analysis for ROSAT observations

The ROSAT X-ray telescope (XRT) consists of three focal detectors, two of them are PSPC and the third is HRI. For all of the raw data a standard data processing (SASS) is performed before release. During this process the basic events information for each photon first undergoes various corrections and normalizations. The photon event files containing this information form, together with housekeeping and attitude data, the basic input for all further analysis.

With these data-sets, the Standard Processing constructs images of the observed sky regions, searches the images for point-like sources and determines their positions, and scans the SIMBAD catalogue for possible optical counterparts, *etc.* All these results are distributed to the principal investigators (PIs) and thereafter enter the ROSAT archive.

Of course, the Standard Processing only provides a first treatment of the observational data. Much more detailed analysis has to be done for various scientific objectives. We use EXSAS/MIDAS (Zimmermann et al. 1998) as a basic analysis tool, along with other widely used packages such as XSPEC, FTools *etc.* The following procedures have been used to analyse the X-ray data for the Local Group galaxies:

- Images. Apply dead time correction, vignetting correction, mask to exclude edges of the detector and ribs for the PSPC.

- Background. Different ways to determine the background applied to different tasks: (i) background map smoothed from cheesed image (*i.e.* all detected point-like sources are subtracted), used in source detection and related tasks like upper-limit calculation; (ii) take the average of the outer part of the cheesed image as background, apply same level for whole image area, only used when diffuse emission appears in the central part; (iii) local background, take annuli centered on the source, if not possible, take the area near the source,

used to determine the spectrum for individual source.

- Source detection. We accept sources till a lower minimum likelihood of existence in the maximum-likelihood (ML hereafter) detection, as a trade-off between aiming at completeness and introducing spurious detections. In the ML detection, the likelihood of existence is defined as $-ln(1-P)$, where P is the probability of existence of the source (*cf.* Cruddace et al. 1988, Zimmermann et al. 1998). The start positions for the ML detection are the results from map and local detection. We use the minimum likelihood of existence 6 to 10 which corresponds to 3 to 4 Gaussian σ.

- Astrometry. Find optical counterparts with accurate positions and improve X-ray positioning, usually HRI data will be used if available; considered useful only if any sources are found near the centre of the galaxy.

- Search for diffuse emission. Annuli around centre of the galaxy; also contour plots for image with different smoothing parameters.

- Determination of characteristics of individual sources. Positions, extendedness, flux, and if possible, spectra and/or hardness ratios, and variability.

The following definitions and remarks apply to all data analysis results unless specified:

- Galaxy optical parameters. The coordinates found from with SIMBAD and NED. The distances used are those listed in Table 2.1. The D_{25}, R_{25} and PA are from the RC3 catalogue (de Vaucouleurs et al. 1991).

- Sources detected. Source numbering is arbitrary, mostly in the order of decreasing declination; the coordinates listed are the X-ray results from the ML detection transferred to the equinox J2000.0; the count rate and its error are background, vignetting and dead time corrected, the error is calculated with 1σ errors in counts determined from the ML method, however the source counts quoted in the text are only background corrected; the likelihood of existence

of a source is also quoted as ML; the off-axis angle is the offset to the center of the field of view (FOV).

- Source identification. Searches for counterparts were done within a few arcsecs away from the HRI position and a few tens of arcsecs away from the PSPC position, in view of the FWHM of the PSF (see below). Sources are taken from various catalogues and papers, most can be found in the CDS/SIMBAD database; the names follow those in SIMBAD if available; the coordinates quoted are FK5 if from SIMBAD instead of original ones; the B magnitude and spectral type are also quoted if available. The Hubble Guide Star Catalog (GSC hereafter) version 1.2 is always checked within the HRI FOV and within a quarter of the PSPC FOV (*i.e.* half box size).

- Point Spread Function (PSF, also called point response function as PRF). Defined as to be the (normalized) photon distribution in the focal plane caused by a celestial X-ray point source at infinity.

- X-ray image. The HRI images are formed by binning the Photon Event Tables (PET) at 5 arcsecs, the PSPC images at 15 arcsecs, corresponding to their typical resolution. For contour plots in a large part of FOV, the HRI image is smoothed with 3-pixel size Gaussians; the PSPC image is dead time and vignetting corrected, and smoothed with 2-pixel size Gaussians over larger regions.

- Optical image. Digital Sky Survey (DSS) is used, which contains mostly the POSS; obtained from HEASARC Skyview.

- Hardness Ratios (HRs). Only for PSPC. Often calculated for sources with a small number of counts, which is not suitable to fit a spectral model. Two HRs are defined as:

$$\mathrm{HR}_1 = \frac{\mathrm{B-A}}{\mathrm{B+A}} \qquad \text{and} \qquad \mathrm{HR}_2 = \frac{\mathrm{D-C}}{\mathrm{D+C}}$$

where A(11–41), B(52–201), C(52–90), and D(91–201) are counts summed over a fixed number of pulse height channels as given in parentheses, corresponding

roughly to the energy band A(0.11–0.42 keV), B(0.52–2.02 keV), C(0.52–0.91 keV), and D(0.91–2.02 keV); the errors of the HRs are calculated again from the 1σ error of the counts.

- Variability measurement. Defined as $|L_2 - L_1|/(\sigma_2^2 + \sigma_1^2)^{1/2}$ where σ is the error of L.

- Upper limit. Calculated at 95.4% confidence level, corresponding to 2 Gaussian σ.

4.3 M31 and M33

As discussed in Chapter 3, M31 and M33 are the two Local Group galaxies that were well-studied at X-rays before, besides the Magellanic Clouds. We restrict ourselves to analysis of two long exposure HRI observations for these galaxies.

Searching the ROSAT data archive within $57'$ radius around M31, we find nearly 90 data sets available, spanning 8 years from 1990. Among them about a dozen are observed with the HRI, and most of the PSPC data sets are for the second survey, conducted during 1992 and 1993, with exposure times of only a few thousand seconds. (*cf.* Figure 5.1 for field centres of these observations.)

Primini et al. (1993) and Supper et al. (1997) published the results for an HRI observation in 1990 (ROR 150006) and the first PSPC survey in 1991, respectively. We present here some results from a later HRI observation in January 1996 (ROR 600780) for comparison. This data set has the longest exposure time (85.4 ksec) among those focusing on the central area of M31.

Within about $5'$ of radius from the field center, 61 sources are detected with $ML \geq 10$. Table 4.2 lists their position and count rates. Comparing with the previous HRI detection, 20 more sources are found, most of them are faint ones, though. There are also a few sources that were detected before but have disappeared in this data set.

In the bulge of M31, the diffuse emission is also clearly visible, especially near

Table 4.2: ROSAT HRI point sources of M31 in central area

Source No.	α_{2000} $h\ m\ s$	δ_{2000} $^\circ\ '\ ''$	Count Rate 10^{-3} s^{-1}	ML	Off-axis $'$
1	00 42 35.20	+41 20 07.8	0.49±0.10	22.9	4.6
2	00 42 31.22	+41 19 40.8	3.17±0.21	480.3	4.7
3	00 42 59.72	+41 19 20.7	4.65±0.25	780.1	3.8
4	00 43 09.89	+41 19 02.2	9.62±0.35	2057.5	5.0
5	00 42 52.55	+41 18 55.9	8.52±0.33	1697.7	2.9
6	00 42 40.14	+41 18 48.7	0.43±0.09	26.5	3.0
7	00 42 55.52	+41 18 36.2	0.84±0.12	49.1	2.8
8	00 42 49.21	+41 18 17.7	0.80±0.12	56.7	2.1
9	00 43 03.94	+41 18 05.9	4.16±0.24	656.2	3.5
10	00 42 45.22	+41 17 23.8	1.72±0.16	141.9	1.3
11	00 42 57.70	+41 17 21.0	0.64±0.11	37.1	2.2
12	00 42 39.77	+41 17 10.5	0.45±0.10	15.6	1.8
13	00 42 26.35	+41 16 56.6	1.81±0.16	233.5	4.1
14	00 42 42.64	+41 16 53.6	1.49±0.19	22.9	1.2
15	00 42 38.51	+41 16 46.7	0.87±0.15	10.8	1.9
16	00 42 45.73	+41 16 44.9	2.02±0.21	30.4	0.7
17	00 42 49.66	+41 16 36.5	1.25±0.17	22.3	0.5
18	00 42 35.45	+41 16 38.0	0.33±0.08	16.9	2.4
19	00 42 43.77	+41 16 30.6	5.53±0.29	409.0	0.9
20	00 42 47.13	+41 16 27.7	16.76±0.47	2479.6	0.3
21	00 42 31.06	+41 16 22.2	6.12±0.28	1078.5	3.2
22	00 42 33.78	+41 16 20.6	1.44±0.16	101.3	2.7
23	00 42 50.77	+41 16 20.6	1.05±0.16	21.8	0.5
24	00 42 41.14	+41 16 13.9	1.70±0.20	25.1	1.3
25†	00 42 44.73	+41 16 11.7	17.56±0.48	1521.3	0.6
26	00 42 59.90	+41 16 06.5	3.14±0.21	421.9	2.2
27	00 42 38.54	+41 16 03.8	47.32±0.76	13294.2	1.8
28	00 42 54.98	+41 16 03.6	7.90±0.32	1395.0	1.3
29	00 42 50.71	+41 15 57.5	1.07±0.16	19.6	0.6
30	00 42 42.68	+41 15 48.8	6.31±0.30	326.4	1.1
31	00 42 39.94	+41 15 47.7	6.23±0.30	645.9	1.6
32	00 42 45.96	+41 15 44.8	1.88±0.20	33.4	0.6
33	00 42 36.52	+41 15 43.0	0.91±0.16	11.7	2.2
34	00 42 52.58	+41 15 40.0	13.25±0.41	2625.1	1.0
35	00 42 49.17	+41 15 32.8	1.53±0.18	16.0	0.7
36	00 42 25.16	+41 15 36.4	10.24±0.36	2051.0	4.3
37	00 42 22.90	+41 15 35.6	3.02±0.20	427.7	4.8
38	00 42 38.40	+41 15 31.4	1.48±0.18	24.7	1.9
39	00 42 58.42	+41 15 29.3	1.73±0.16	164.1	2.1
40	00 43 03.23	+41 15 25.9	3.86±0.23	405.8	3.0
41	00 42 45.08	+41 15 26.1	1.90±0.20	32.0	0.9
42	00 42 25.33	+41 15 34.9	5.97±0.28	1224.5	4.3
43	00 42 48.43	+41 15 23.0	12.33±0.41	1537.9	0.8
44	00 42 40.83	+41 15 23.1	1.73±0.20	26.7	1.6
45	00 42 42.95	+41 15 13.9	1.81±0.19	40.9	1.4
46	00 42 41.16	+41 15 07.7	1.01±0.17	14.3	1.7
47	00 42 45.84	+41 15 01.0	0.91±0.16	12.6	1.3
48	00 43 10.72	+41 14 51.1	15.27±0.44	3660.1	4.5
49	00 42 44.23	+41 14 51.9	1.00±0.17	11.3	1.5
50	00 42 42.37	+41 14 45.1	2.01±0.18	140.3	1.8
51	00 42 44.42	+41 14 46.9	0.58±0.12	11.3	1.6
52	00 42 39.45	+41 14 28.6	1.65±0.16	148.1	2.4
53	00 42 46.94	+41 14 13.6	0.26±0.08	11.7	2.0
54	00 42 39.74	+41 14 21.9	0.28±0.08	10.9	2.4
55	00 42 44.97	+41 14 06.8	1.06±0.13	101.7	2.2
56	00 43 01.14	+41 13 51.7	0.58±0.10	39.5	3.4
57	00 43 01.09	+41 13 51.2	0.66±0.11	43.3	3.4
58	00 42 36.42	+41 13 50.5	0.54±0.11	21.3	3.2
59	00 42 40.70	+41 13 27.5	1.50±0.15	139.9	3.1
60	00 42 32.09	+41 13 13.7	3.84±0.23	510.5	4.2
61	00 42 44.85	+41 11 37.1	3.79±0.23	608.4	4.6

† Possible nuclear source.

the nuclear source (No.25). (See Figure 4.1.) These data do even not resolve the source which was found previously in 150006 between No.25, 19 and 20. The nuclear source has a count rate of $17.56 \pm 0.48 \times 10^{-3}$ s^{-1}, which is obviously contaminated by the diffuse emission because the source position is clearly away from the peak (Figure 4.1). We restrict the cut radius as 9″ from the peak position (Gaussian

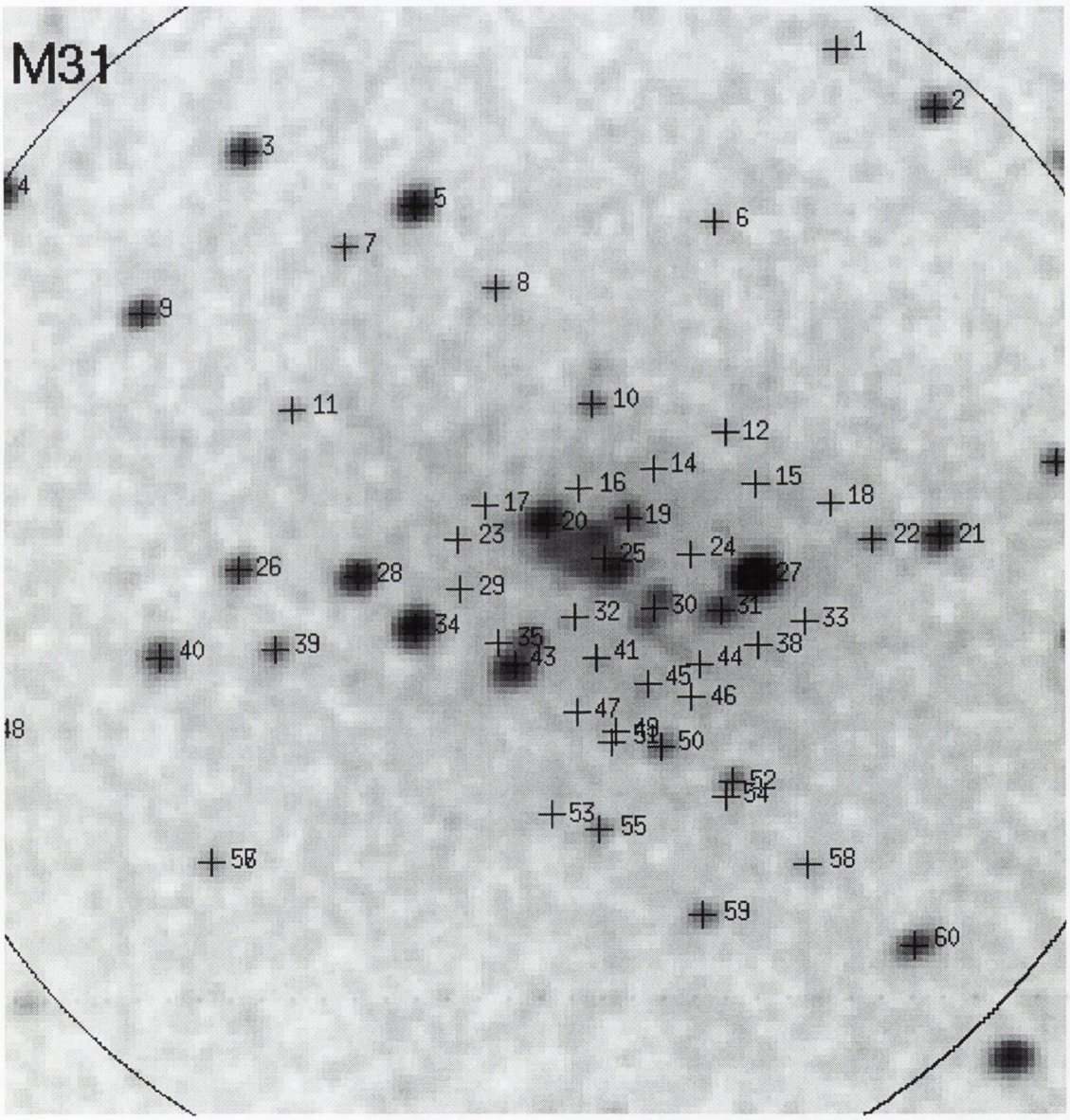

Figure 4.1: ROSAT HRI image of M31 on a field of 8.5′ × 8.5′ and centered at the HRI field centre. The image has 3″ × 3″ pixels and has been smoothed with 1-pixel size Gaussians. The logarithm of intensity is displayed. The source numbers are as in Table 4.2.

center), the count rate will be $7.72 \pm 0.32 \times 10^{-3}$ s^{-1}, which is comparable with the count rate ($6.60 \pm 0.49 \times 10^{-3}$ s^{-1}) derived by the same way from the data observed 6 years ago (ROR 150006h). The variability measurement is 1.5.

The source search for M33 from the ROSAT HRI archive data (ID 600020h), observed in 1992, reveals 20 sources with $ML \geq 10$. 2 of them are resolved from the nuclear source which is thought to be extended. All of the remaining 18 sources are also detected by Schulman and Bregman (1995, Table 1). Among 9 undetected sources that had been reported by Schulman and Bregman, 4 have lower ML levels between 10 and 6.

4.4 NGC 147 and 185

NGC 147 and NGC 185 are two elliptical galaxies that are situated about 100 kpc from M31. NGC 147 has a predominantly old stellar population $\gtrsim$ 12 Gyr and 4 known globular clusters (Ford 1977). Most of the stars in NGC 185 are also old, but it probably contains a SNR (Gallagher 1984) and some OB stars. There are 6 globular clusters in the field. In the X-ray band, Brandt et al. (1997) have reported the results of ROSAT HRI observations which were carried out in January 1995.

Table 4.3: Possible point sources within ROSAT HRI field of NGC 147

Source No.	α_{2000} h m s	δ_{2000} $^\circ$ $'$ $''$	Count Rate 10^{-3} s^{-1}	ML	Off-axis $'$
1	00 32 43.63	48 39 10.9	0.92±0.34	7.2	9.8
2	00 34 35.21	48 37 50.0	3.15±0.92	7.6	15.6
3	00 32 58.79	48 37 25.2	0.58±0.24	7.1	7.2
4	00 32 10.76	48 33 40.9	1.28±0.42	8.5	10.6
5	00 34 46.41	48 32 25.5	2.27±0.68	8.5	15.6
6	00 32 28.28	48 31 55.4	2.61±0.46	62.1	7.4
7	00 33 39.64	48 30 10.7	0.57±0.23	8.4	4.6
8	00 33 05.45	48 28 37.8	0.70±0.27	7.0	2.2
9	00 32 32.48	48 27 44.9	0.66±0.27	7.8	7.1
10	00 32 54.62	48 17 06.0	2.29±0.61	11.6	13.8

The total exposure time for this NGC 147 ROSAT HRI observation was about 14.7 ksec. We detect 11 sources within 16′ from the field centre with $ML \geq 7$, among which are 2 sources with $ML \geq 10$. Table 4.3 lists all source positions with

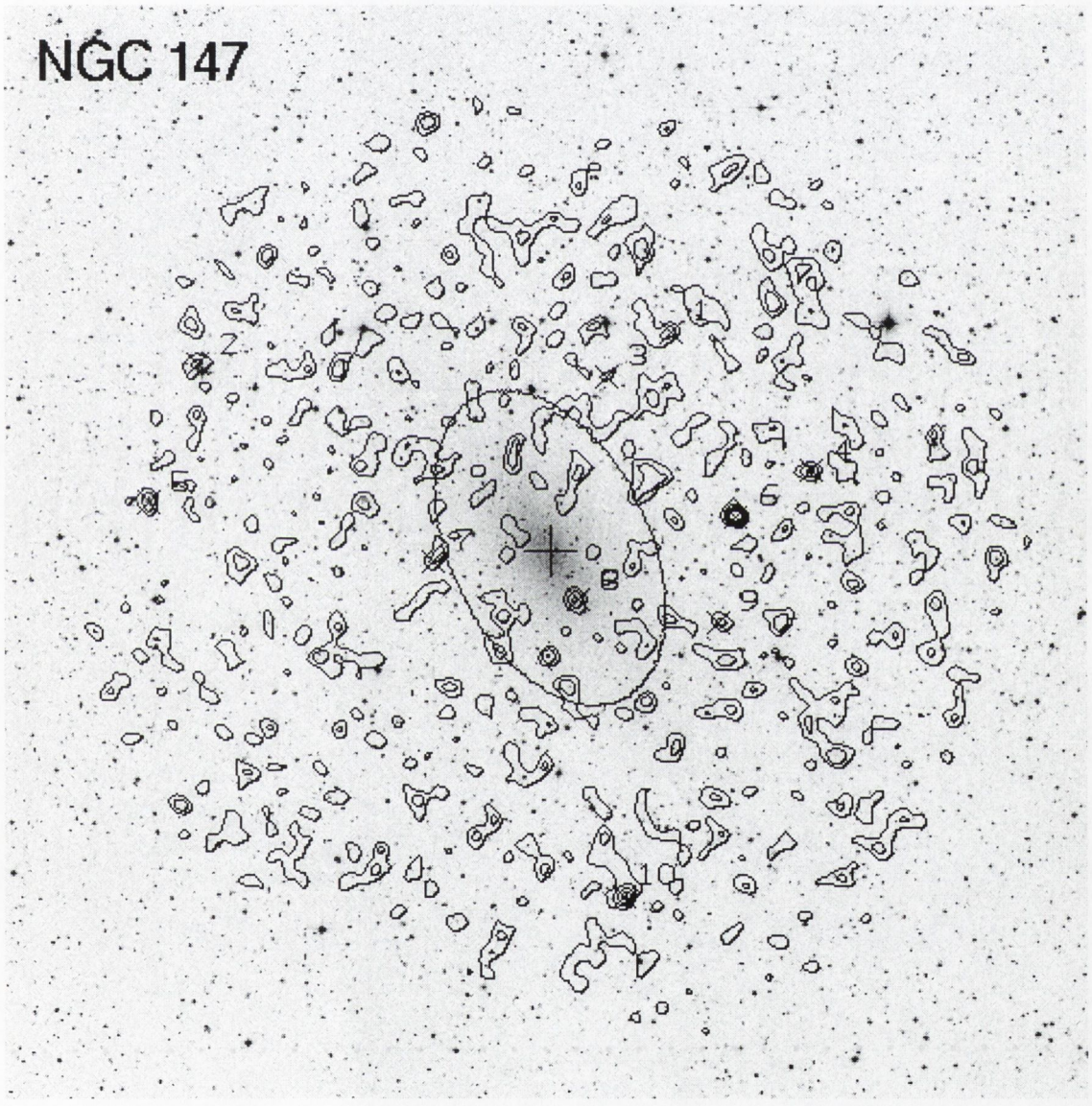

Figure 4.2: ROSAT HRI contour plot of NGC 147 overlaid on optical image from the POSS. The centre of the galaxy is marked with a cross and the D_{25} ellipse (from the RC3 catalogue) is drawn in. The background level in the HRI image is ~ 0.4 cts pix^{-1}. The contour levels are 0.48, 0.56, 0.64, 0.72 and 0.8 cts pix^{-1}. The HRI image has $5'' \times 5''$ pixels and is smoothed with a 3-pixel size Gaussians.

their count rates and Maximum-Likelihood levels.

When we overlay the X-ray image on the optical one (DSS), we find that source No.8 lies within the D_{25} ellipse of the galaxy, but there is no source coincident with the centre (Figure 4.2). We scanned SIMBAD and the Guide Star Catalogue (GSC), but no catalogued optical object was found at the position of any of these X-ray sources, and none of the known globular clusters either. Nevertheless, the brightest X-ray source in the HRI region, No.6, may have a much fainter ($\gg 15^m$) optical counterpart than would be included in the GSC, as there is a visible spot in the Digital Sky Survey.

From constructing a radial brightness profile for the known nuclear position, we find no evidence for diffuse emission centred on NGC 147. Most of the X-ray sources are probably unrelated foreground or background sources. The upper limit for the centre of the galaxy is about $0.22 \times 10^{-3}\ s^{-1}$, which corresponds to a flux of 2.1×10^{-14} ergs cm^{-2} s^{-1} and a luminosity of 0.8×10^{36} ergs s^{-1} (0.1–2.5 keV) at the distance of 598 kpc, assuming a power law model with photon index of 2 and Galactic column 1.2×10^{21} cm^{-2}.

Table 4.4: Possible point sources within ROSAT HRI field of NGC 185

Source No.	α_{2000} $h\ m\ s$	δ_{2000} $^\circ\ '\ ''$	Count Rate 10^{-3} s^{-1}	ML	Off-axis $'$
1	00 40 39.49	48 32 07.7	1.58±0.50	7.2	14.5
2	00 40 25.05	48 26 44.0	2.69±0.59	16.4	16.0
3	00 39 02.24	48 24 13.5	1.39±0.28	39.3	3.9
4	00 38 21.80	48 24 09.5	1.11±0.27	25.0	7.0
5	00 39 03.87	48 23 22.3	1.23±0.41	7.2	13.2
6	00 38 27.76	48 17 55.1	0.52±0.19	8.1	5.5
7	00 39 24.98	48 15 41.4	0.43±0.18	7.1	6.6
8	00 38 41.77	48 13 49.6	0.60±0.21	8.8	7.1

NGC 185 was observed for 20.1 ksec during the same dates as NGC 147. Using the same method we detect 8 X-ray sources which are listed in Table 4.4, among which 3 sources with ML$\geq$ 10. One source which can be seen in the left (East) of the raw image is not detected because it is located at the very edge of the detector and

is masked out in the detection routine. Figure 4.3 shows the HRI contours overlaid on the optical image.

Compared with the optical image, all sources lay in the outer area of the galaxy; none of them is coincident with known globular clusters or stars *etc.* from the SIM-

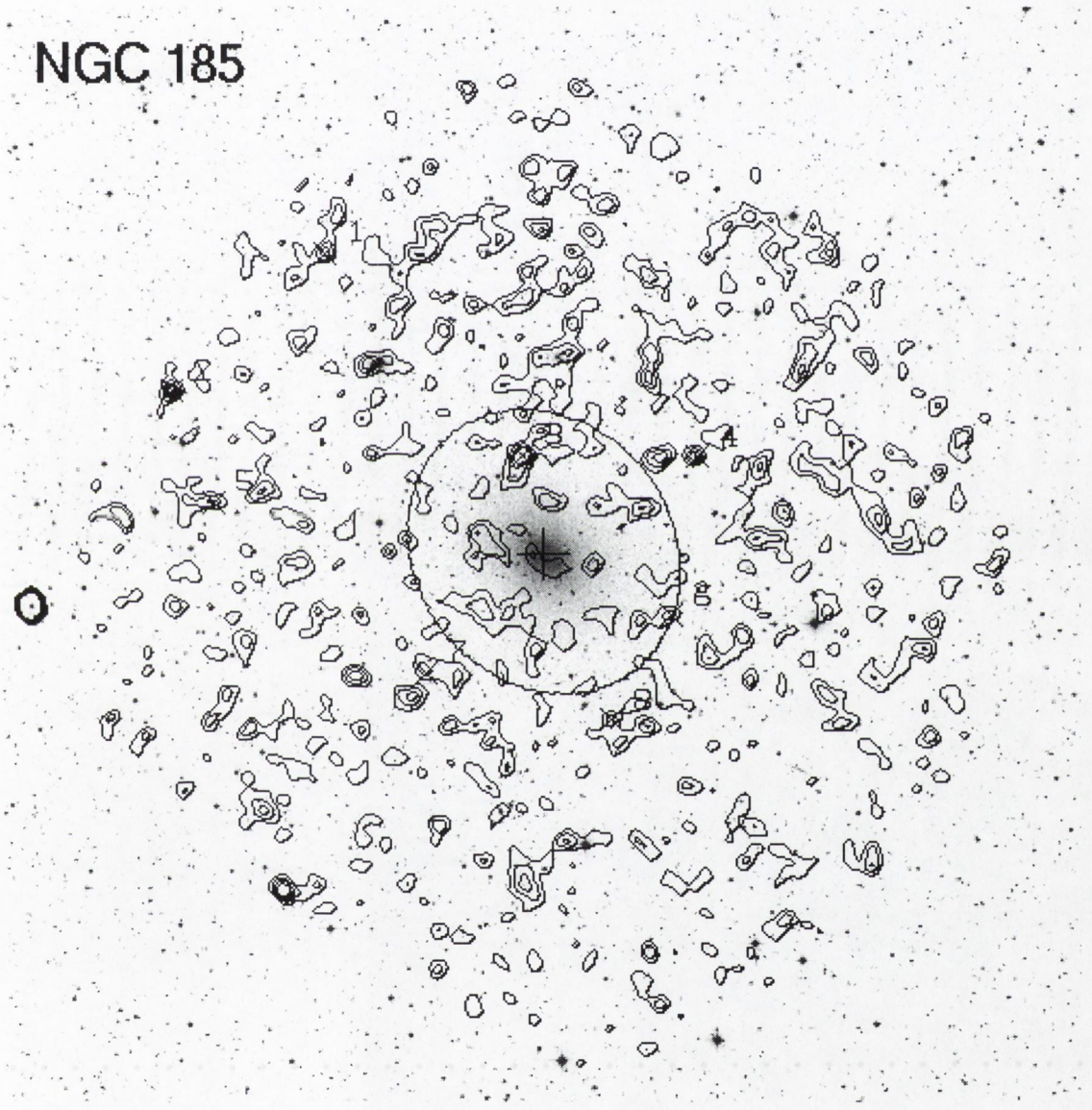

Figure 4.3: ROSAT HRI contour plot of NGC 185 overlaid on optical image covering whole HRI area. The centre of the galaxy is marked with a cross and the D_{25} ellipse (from the RC3 catalogue) are marked with cross and solid ellipse is drawn in. The background level in HRI image is ~ 0.6 cts pix^{-1}. The contour levels are 0.68, 0.76, 0.84 and 0.92 cts pix^{-1}. The HRI image has $5'' \times 5''$ pixels and is smoothed with 3-pixel size Gaussians.

BAD catalogue. However, some of them are probably coincident with fainter counterparts. Near Nos. 3 and 8, there are objects visible in the image of the POSS survey. The one near No.3 is catalogued in the GSC 1.2 as a star (GSC 0325300517, $\alpha_{2000} = 0^h39^m2.60^s$, $\delta_{2000} = 48°24'10.8''$, Pmag=13.51). The other one is about $10''$ from source No.8, with magnitude > 15.

Around the central position, there are lower contours which may be a hint of diffuse emission. However, from constructing a radial brightness profile for the nuclear position, we find no clear evidence for diffuse emission centred on NGC 147. The upper limit for the centre of the galaxy is about 0.41×10^{-3} s^{-1}. Using the same model as for NGC 147, this corresponds to a flux of 3.9×10^{-14} ergs cm^{-2} s^{-1} and a luminosity of 1.5×10^{36} ergs s^{-1} (0.1–2.5 keV) at the distance of 620 kpc.

Comparing the upper limits with those derived by Brandt et al. (1997), our value for NGC 185 is similar to their 0.46×10^{-3} s^{-1}, but for NGC 147, is only one-third of their 0.60×10^{-3} s^{-1}. We checked at other central positions near the ones from various catalogues (SIMBAD and NED), and at such positions closeby the upper limit count rates may reach upto 4.1×10^{-3} s^{-1}, thus differences like these can easily occur between different analyses.

4.5 IC 1613

IC 1613 is a dwarf irregular (dI) galaxy which is among a few such galaxies observed with Einstein. The X-ray emission associated with this galaxy is mainly from a single source (namely IC 1613 X-1) which is about $5.6'$ away from the centre of the galaxy and probably to be identified with a cluster of galaxies (Eskridge 1995). The Einstein IPC received a flux of $f_X = 2.20 \times 10^{-12}$ ergs cm^{-2} s^{-1} (0.2–4.0 keV and for the Bremsstrahlung model with kT = 5 keV).

The ROSAT HRI observation was carried out during June and July 1995. An earlier HRI observation in January 1995 has only 3.8 ksecs, which we do not use here. Within the HRI field of the second observation which has 22.7 ksec of exposure time, we detect 18 sources with $ML \geq 7$ (among these 5 sources with $ML \geq 10$).

Table 4.5: Point sources within ROSAT HRI field of IC 1613

Source No.	α_{2000} $h\ m\ s$	δ_{2000} $^\circ\ '\ ''$	Count Rate 10^{-3} s^{-1}	ML	Off-axis $'$
1	01 04 47.96	+02 19 29.7	1.51±0.46	7.7	15.7
2	01 04 50.96	+02 12 59.5	0.74±0.25	8.2	9.2
3	01 04 49.95	+02 10 31.9	0.54±0.20	8.3	7.1
4	01 05 02.46	+02 08 42.5	2.11±0.33	83.5	4.5
5	01 05 00.01	+02 02 45.9	0.64±0.22	7.7	1.6
6	01 05 01.46	+02 02 44.5	0.39±0.15	8.7	1.5
7	01 04 52.27	+02 02 25.3	0.46±0.17	9.7	3.1
8	01 05 02.07	+02 02 05.2	0.63±0.20	12.9	2.1
9	01 05 04.72	+02 01 53.9	0.36±0.15	7.5	2.4
10	01 05 00.35	+02 01 49.1	0.37±0.15	7.9	2.4
11	01 05 01.79	+02 01 35.4	1.27±0.31	8.3	2.6
12	01 05 01.50	+02 01 24.1	1.25±0.30	9.5	2.8
13	01 04 40.80	+02 01 07.7	1.98±0.32	68.2	6.2
14	01 04 10.22	+01 59 21.9	1.67±0.43	12.9	13.9
15	01 05 16.06	+01 59 12.2	1.23±0.27	29.2	6.1
16	01 05 43.30	+01 58 39.2	0.92±0.30	8.4	11.6
17	01 05 14.96	+01 57 49.9	0.67±0.22	9.7	7.1
18	01 04 11.04	+01 55 36.2	1.67±0.50	7.9	15.4

Table 4.5 lists all sources detected within the HRI field with their count rates. To compare with the POSS survey, the sources Nos. 1–4 are located within the boundaries of the optical galaxy, but have no obvious optical counterparts. Source No.15 is situated in the outer area, probably coincident with an optical object listed in the Guide Star Catalogue (GSC 0001900392, $\alpha_{2000} = 1^h5^m15.94^s$, $\delta_{2000} = +1^\circ59'14.7''$, Pmag=11.42) that is only 4 arcsec away from the X-ray position. Source No.4 is not far from the optical positions of IC 1613 as given by SIMBAD and NED, and has been identified as a supernova remnant (SNR) by Lozinskaya et al. (1998). The count rate of this SNR is $(2.1 \pm 0.3) \times 10^{-3}$ s^{-1}. For the Galactic column density of $N_H = 2.8 \times 10^{20}$ cm^{-2}, a power law model with photon index = 2.0 gives an unabsorbed flux $f_X = 1.23 \pm 0.18 \times 10^{-14}$ ergs cm^{-2} s^{-1} and a luminosity $L_X = 8.6 \pm 1.2 \times 10^{36}$ ergs s^{-1} (0.1–2.4 keV) at the distance of 765 kpc.

The Einstein source IC 1613 X-1 is also detected with the ROSAT HRI. Our HRI image (Figure 4.4) shows that most of the X–1 region has been resolved into individual sources which are listed in Table 4.5 as Nos. 5–12. However the central part of X–1 has not been resolved completely and is indeed reminiscent of X-ray

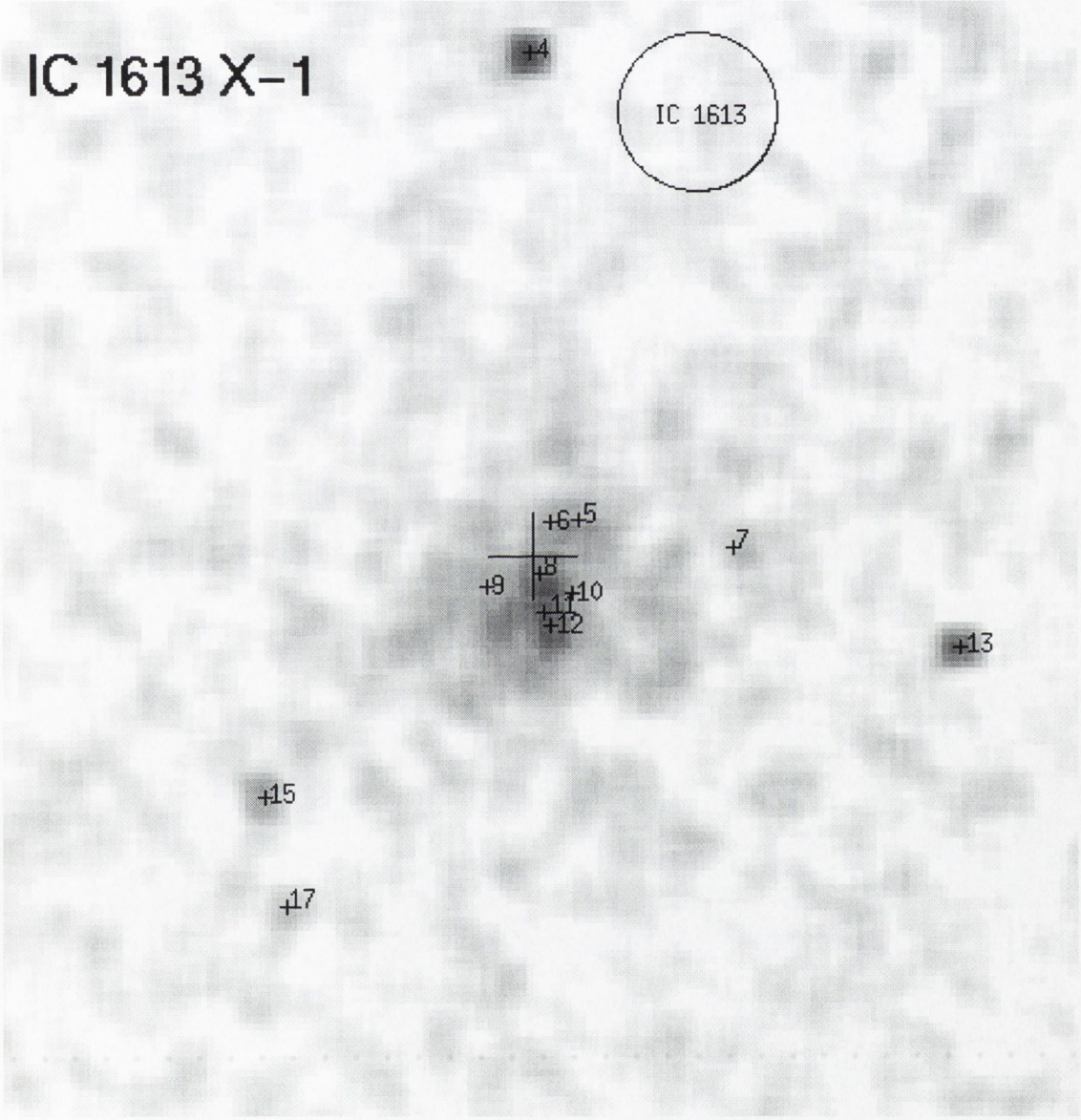

Figure 4.4: ROSAT HRI image of IC1613 X–1 on a field of $14' \times 14'$ and centered at the X–1 position, marked with a big cross. The image has $5'' \times 5''$ pixels and has been smoothed with a 2-pixel size Gaussians. IC 1613 itself is located North-West of X–1 where the big circle indicates its optical position in the NED (*cf.* Palumbo et al. 1988). The arbitrary radius of the circle $1'$.

emission from a cluster of galaxies. We integrate the counts within 3.5′ radius, that gives a count rate of 0.0312±0.0012 s^{-1}. Using a Bremsstrahlung model with kT = 5 keV, we get an unabsorbed flux $f_X = 1.51 \pm 0.06 \times 10^{-12}$ ergs cm^{-2} s^{-1} (0.1–2.4 keV).

We also derived upper limits to the X-ray flux for several optical positions of IC 1613 in various catalogues (from SIMBAD and NED). The upper limit count rate is from 1.9×10^{-4} to 4.1×10^{-4} s^{-1}. Using the same conversion factor as above the flux $f_X \sim (1.1 - 2.4) \times 10^{-14}$ ergs cm^{-2} s^{-1} in the 0.1–2.4 keV band, the luminosity $L_X = (0.8 - 1.7) \times 10^{36}$ ergs s^{-1}.

4.6 NGC 6822

NGC 6822 was previously observed with Einstein (Markert and Donahue 1985). Eskridge and White (1997) summarized the Einstein HRI and ROSAT PSPC results and gave details of the source in the bar of the galaxy. This source coincides with the emission-line object Ho 12. With only 75 ROSAT PSPC counts, a RS model fit is attempted that gives kT∼0.56 keV, while a BB model gives kT∼0.06 keV. They argue that this object may be either an HII region or a SNR, but the variability of the X-ray source over 13 years indicates that the X-rays are not due to direct emission from a SNR.

Our own PSPC data analysis yields 15 sources with $ML \geq 10$, listed in Table 4.6. The brightest source (No.15) may be associated with a bright star, HR 7496 (F5IV, 5.95^m) with coordinates ($\alpha_{2000} = 19^h43^m33.53^s$, $\delta_{2000} = -15°28'12.4''$), which is only a few arc-seconds away. This source is a supersoft source with $HR_1 < 0$. No.3 is partially obscured by the window support structure, its count rate may be underestimated. It is not far (about 7″) from the star SAO 162956 (G5, 10.45^m).

The source on the bar of NGC 6822 mentioned above is No.10. Its 80 counts is too little to fit any spectral model. We calculate the hardness ratios of all the detected sources and also list these in Table 4.6.

The ROSAT HRI observation was carried out on October 1995 and October

Table 4.6: Sources and count rates within ROSAT PSPC field of NGC 6822

Src No.	α_{2000} h m s	δ_{2000} $^\circ$ $'$ $''$	Cnt Rate 10^{-3} s^{-1}	HR_1	HR_2	ML	Off-axis$'$
1	19 43 13.31	-14 15 49.4	22.0±4.2	0.72±0.12	0.11±0.15	16.9	40.9
2	19 45 46.55	-14 18 26.6	14.1±3.0	0.54±0.14	0.56±0.16	13.4	31.8
3	19 45 35.89	-14 27 46.7	88.3±4.2	0.90±0.02	0.24±0.05	966.3	22.2
4	19 45 05.85	-14 36 38.7	9.5±1.3	0.75±0.13	0.25±0.15	100.0	11.5
5	19 44 20.32	-14 37 57.7	2.4±0.8	0.75±0.37	0.38±0.30	10.9	13.5
6	19 45 21.97	-14 40 20.7	8.0±1.2	0.92±0.10	-0.01±0.15	95.2	9.7
7	19 44 59.62	-14 42 10.9	1.9±0.6	0.64±0.39	0.14±0.34	11.7	5.8
8	19 44 27.42	-14 43 15.8	3.9±0.9	0.87±0.22	-0.14±0.22	37.7	8.7
9	19 47 47.81	-14 48 26.0	11.3±2.8	0.57±0.27	0.28±0.23	11.9	41.1
10	19 44 56.73	-14 48 27.5	12.3±1.4	0.74±0.10	-0.08±0.13	184.6	0.5
11	19 43 58.94	-14 48 36.5	4.7±1.0	0.55±0.22	0.14±0.22	30.8	14.2
12	19 43 16.65	-14 54 37.2	8.9±1.8	0.77±0.14	0.31±0.15	21.5	25.3
13	19 47 59.04	-15 03 10.5	28.7±5.7	0.21±0.20	-0.17±0.18	13.4	46.4
14	19 45 48.30	-15 21 41.1	15.9±2.9	0.13±0.17	0.13±0.23	24.9	35.8
15	19 43 33.69	-15 28 08.2	153.4±7.4	-0.24±0.05	-0.16±0.08	521.7	45.0

1996 with exposure times 4.9 ksec and 52.8 ksec, respectively. We concentrate on the latter data set, where 7 sources are detected with $ML \geq 10$ within 16 arcmin from the field centre (Table 4.7). The source No.6 is on the bar of NGC 6822, with about 178 counts. Its position ($19^h44^m56.5^s, -14°48'30''$) is consistent with Einstein HRI's detection ($19^h44^m56.7s, -14°48'31''$).

The first HRI observation has about 1/10 exposure time of the second one. 3 sources are found with $ML \geq 10$ (see Table 4.7), 2 of which are also seen in the second observation with similar count rates. The third one (No.8 in Table 4.7 is obviously variable during one year as it is still not detected in the second observation down to ML=6. It did appear in PSPC field (in April 1992) with a count rate at the same level, as seen in the second HRI field.

There are no obvious optical counterparts for X-ray sources detected in either HRI field. However, close to central main source on the bar of NGC 6822, at about 23″ NW, a source with 22 net counts and likelihood of existence of 8.9 is

Table 4.7: Sources in two ROSAT HRI observations of NGC 6822

Src No.	α_{2000} $h\ m\ s$	δ_{2000} $^\circ\ '\ ''$	Count Rate 10^{-3} s^{-1} (I)	(II)	ML (I)	(II)	Off-axis′	Src* No.
1	19 44 20.34	-14 38 03.0	1.03±0.22		17.7		11.3	5
2	19 45 22.49	-14 40 20.2	3.63±0.29	5.14±1.10	248.2	37.8	8.4	6
3	19 44 59.51	-14 42 08.0	0.44±0.11		19.9		3.6	7
4	19 44 27.05	-14 43 14.8	0.89±0.16		40.4		7.2	8
5	19 44 43.53	-14 47 52.6	0.61±0.12		32.9		3.6	
6	19 44 56.46	-14 48 30.3	3.56±0.27	2.94±0.88	284.6	10.0	2.9	10
7†	19 44 55.44	-14 48 12.2	0.43±0.12		8.9		2.6	10
8	19 45 06.06	-14 36 35.0		2.38±0.82		10.8	9.4	4

* PSPC source No., see Table 4.6.

† Possible nuclear source.

found as a possible nuclear source. Its position (Table 4.7, No.7) is very close to those given by SIMBAD ($\alpha_{2000} = 19^h44^m56.2^s$, $\delta_{2000} = -14^\circ48'4''$) and NED ($\alpha_{2000} = 19^h44^m56.14^s$, $\delta_{2000} = -14^\circ48'5.5''$, from Gallouët et al. (1975), mean error $4''$). Figure 4.5a shows the contour plot of the central $4' \times 4'$ area.

In the PSPC data, this source has not been resolved from the bright source nearby because of the short distance between two. The PSPC contour plot of the main source (No.10 in Table 4.6) does not show any sign of this additional source (see Figure 4.5b), and the azimuthal profile constructed from the Photon Events Table does not show a higher intensity for the first quadrant either.

The hard band image (0.5–2.0 keV) for the PSPC has also been checked to reduce the background and in the view of possible spectral differences between the two HRI sources. Nevertheless, the contour plot (Figure 4.5c) shows a little sign of extension to the NW position but otherwise no sign of the additional source is found. On the other hand, in the soft band (0.1–0.4 keV) (Figure 4.5d) even the main source is not found. The contour plot shows that there might be some emission from a position SE to the main source.

The HRI data have only few energy channels with, unfortunately, high spatial and temporal gain variations. Wilson et al. (1992) and Matt et al. (1994) tried to use hardness B/A (or softness A/B) defined by the channels A(1–5) and B(6–11)

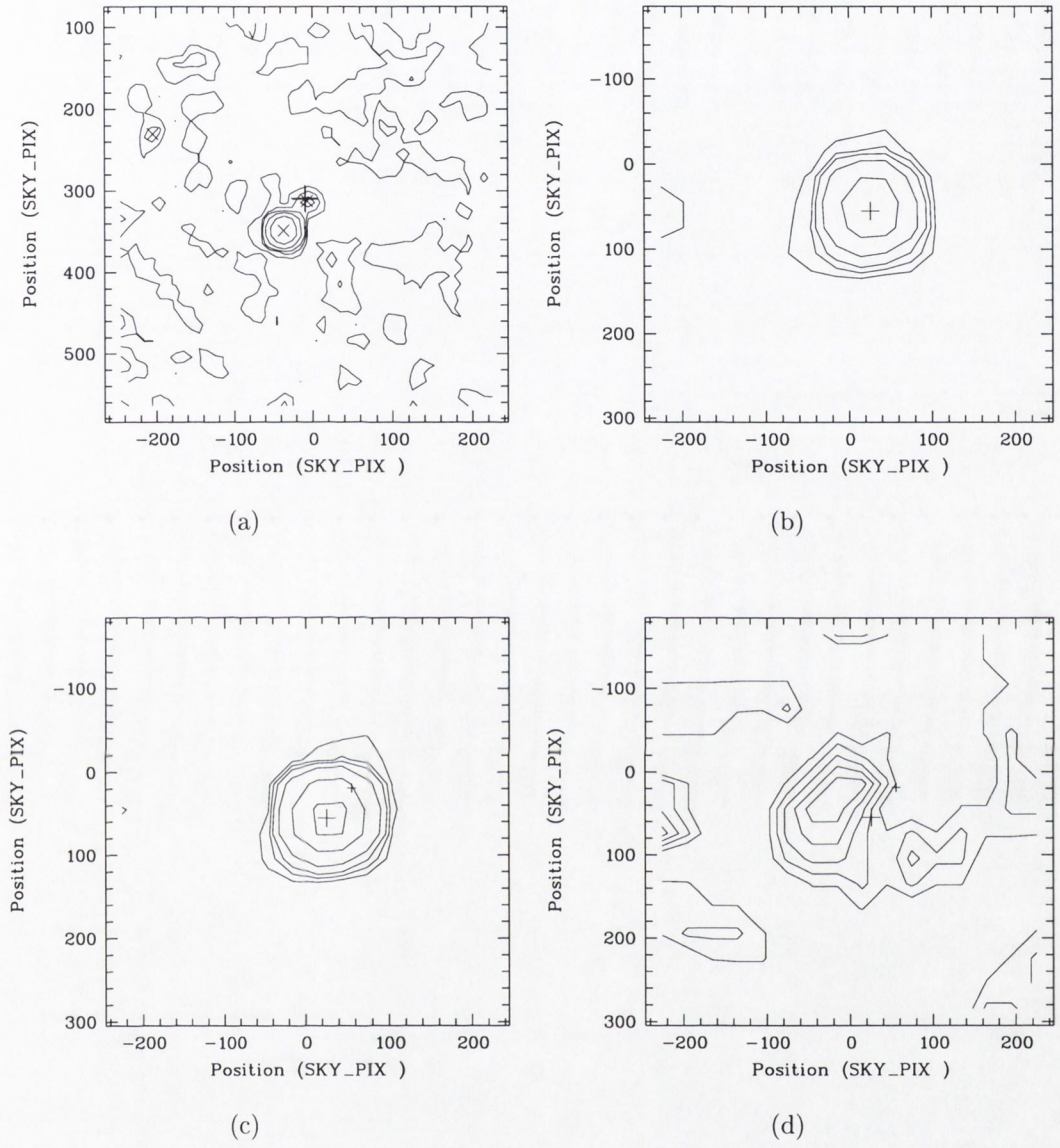

Figure 4.5: ROSAT contour plots of NGC 6822's central $4' \times 4'$ area. (a) Second HRI observation. The background level is ~ 1.7 cts pix^{-1}, and the contour levels are 2.1, 2.9, 3.7, 5.7 and 9.7 cts pix^{-1}. The big crosses at the centre are SIMBAD and NED positions of the galaxy. The X-ray sources with $ML \geq 6$ are marked with "×". (b) PSPC broad band. The background level is ~ 0.3 cts pix^{-1}, and the contour levels are 0.8, 1.3, 1.8, 2.8, and 5.3 cts pix^{-1}. (c) PSPC hard band (0.5–2.0 keV). The background level is ~ 0.12 cts pix^{-1}, and the contour levels are 0.47, 0.82, 1.17, 1.87, 3.62 and6.0 cts pix^{-1}. (d) PSPC soft band (0.1–0.4 keV). The background level is ~ 0.22 cts pix^{-1}, and the contour levels are 0.32 to 1.0 cts pix^{-1} in a step of 0.10 cts pix^{-1}. The big cross is marked as the ML position of the PSPC source in broad band, and the small cross as the relative position of the possible nuclear source detected in the HRI field. The HRI image has $5'' \times 5''$ pixels and the PSPC images have $15'' \times 15''$ pixels. Each image has been smoothed with a 1-pixel size Gaussians.

or A(1–4) and B(5–15). We use the latter choice and find that the B/A values are 2.32±0.60 and 1.68±1.72 for the main source and the possible nuclear source respectively.

The observed count rate predicts an unabsorbed flux for this possible nuclear source of $f_X \sim 3.69 \times 10^{-14}$ ergs cm^{-2} s^{-1} (0.1–2.4 keV), assuming a power law model with photon index of 2.0 and Galactic $N_H = 9.5 \times 10^{20}$ cm^{-2}. For the distance of NGC 6822 (540 kpc), the luminosity becomes $L_X = 1.29 \times 10^{36}$ ergs s^{-1}.

4.7 WLM

The WLM dwarf galaxy was first discovered by Wolf on a plate taken at Heidelberg by Lorenz in 1909 with a 6 inch camera. This galaxy was rediscovered by Melotte during an inspection of the Franklin-Adams Chart Plates, and he comments that the system had previously been marked on the same plate by Lundmark. By common usage, the galaxy is named Wolf-Lundmark-Melotte.

ROSAT observed the WLM galaxy with the HRI for totally about 88 ksec in 1996 (ROR 600814) and the data are processed and archived in two data sets. One includes 66.9 ksec exposure carried out from 30 May to 1 July and the other includes 21.5 ksec exposure from 2 to 4 December. With the first (and the longer) data set, 12 sources (with $ML \geq 10$) are detected within 16′ from the centre. Table 4.8 lists positions and count-rates of these sources. Source No.11 is identified as a radio cluster PKS 2359-159 (Parma et al. 1991). Among other sources, only source No.5 may have an optical counterpart which is a star catalogued in the GSC 1.2 (GSC 0583800179). Its coordinates ($\alpha_{2000} = 0^h1^m5.9^s, \delta_{2000} = -15°20'44''$) are only about 4″ away from the X-ray position. It is not suitable for astrometric purposes because of its large off-axis position of 14.6′.

There are only 5 sources detected with the second data set, among which 1 is not seen at $ML \geq 10$ in the first observation (see Table 4.8, No.13). When setting 6 as the minimum ML, more sources can be found and their count rates are shown in the table, but still 5 sources seen in the 1st observation remain undetected in the 2nd

Table 4.8: Sources and Count Rates within ROSAT HRI field of WLM

Src No.	α_{2000} h m s	δ_{2000} $^\circ$ $'$ $''$	Count Rate 10^{-3} s^{-1} (I)	(II)	ML (I)	(II)	Off-axis $'$
1	00 02 19.75	-15 14 37.1	2.67±0.30	1.56±0.51	66.6	6.2	14.6
2	00 02 44.72	-15 17 35.5	1.87±0.29	-	29.9	-	15.5
3	00 01 16.37	-15 19 45.1	1.01±0.22	-	15.1	-	13.0
4	00 01 38.44	-15 20 40.8	0.45±0.12	-	10.7	-	8.8
5	00 01 05.92	-15 20 40.7	1.81±0.28	2.54±0.58	31.7	14.3	14.6
6	00 02 20.48	-15 23 11.8	0.73±0.13	0.52±0.20	36.2	7.5	7.4
7	00 01 35.56	-15 27 52.4	1.57±0.17	2.39±0.36	157.5	82.1	5.3
8†	00 01 58.24	-15 27 56.7	0.48±0.11	0.59±0.19	18.1	13.5	0.3
9	00 02 31.63	-15 35 48.1	0.76±0.16	-	18.8	-	11.2
10	00 01 51.33	-15 40 02.6	0.77±0.18	-	13.5	-	11.9
11	00 01 41.59	-15 40 44.0	18.33±0.67	16.06±1.15	670.8	171.3	13.1
12	00 02 19.62	-15 19 45.6	0.51±0.14	1.18±0.32	10.2	12.8	10.0
13	00 01 37.05	-15 31 35.6	0.26±0.08	0.70±0.22	9.6	11.7	6.0

† Possible nuclear source.

due to either the shorter exposure time ($\sim 1/3$) or these sources having decreased in brightness. Thus, most of the sources are variable within half a year.

These is only one globular cluster near this galaxy, there is no sign of any X-ray source being associated with it.

Among the detected sources, one is on the bar of WLM. Although there is no obvious optical nuclear source in WLM, this X-ray source (No.8) is close the centre position given by SIMBAD which is $\alpha_{2000} = 0^h1^m58.0^s$, $\delta_{2000} = -15°27'50''$. (See Figure 4.6.) Its count rate of 0.59×10^{-3} s^{-1} will give a (0.1–2.4 keV) flux of $f_X = 3.23 \times 10^{-14}$ ergs cm^{-2} s^{-1}, assumming a power law model with photon index $\Gamma = 2.0$ and Galactic column $N_H = 2.2 \times 10^{20}$ cm^{-2}. If this faint X-ray source is associated with the galaxy, at the distance of about 940 kpc, the luminosity $L_X = 3.4 \times 10^{36}$ ergs s^{-1}. Although some other sources are clearly various between two observations, this central source has nearly the same brightness, the variability measurement is 0.5.

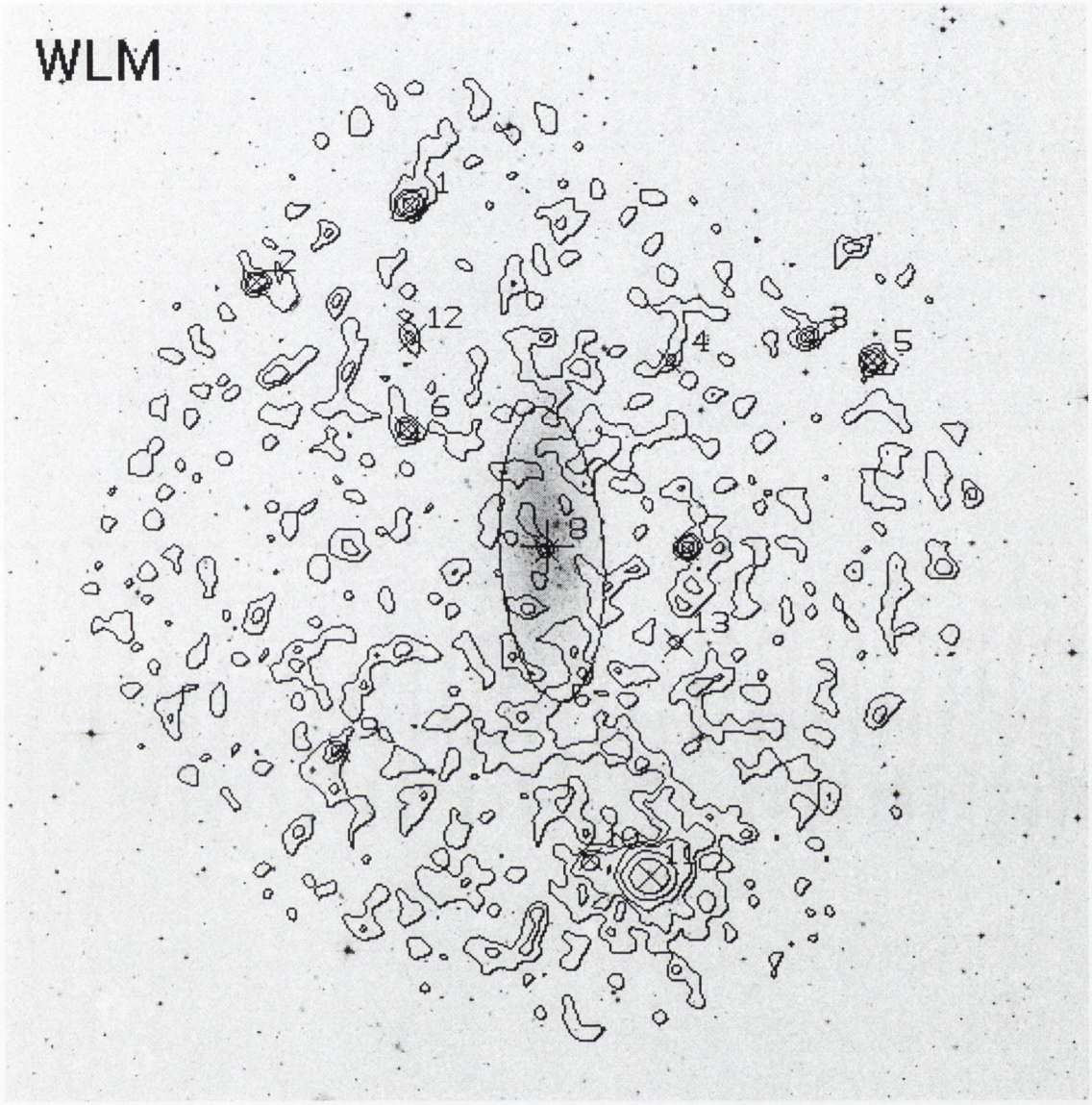

Figure 4.6: ROSAT HRI contour plot of WLM overlaid on optical image. The centre of the galaxy (from the SIMBAD) is marked with a cross and the D_{25} ellipse is taken from the RC3 catalogue. The background level of the HRI image is ~ 1.73 cts pix^{-1}. The contour levels are 1.84, 2.06, 2.28, 2.83 and 3.93 cts pix^{-1}. The HRI image has $5'' \times 5''$ pixels and is smoothed with a 3-pixel size Gaussians.

4.8 NGC 205

Besides M32, NGC 205 is another close companion of M31. This small elliptical galaxy shows a dozen bright early type stars and several dust clouds in its central area, and is one of three small Local Group galaxies that Mateo (1998) considers to

possess a nucleus.

NGC 205 was observed with the Einstein HRI in January 1975 for about 23.7 ksec (Markert and Donahue 1985). No X-ray source was detected, giving an upper limit $L_X < 9 \times 10^{36}$ ergs s^{-1} (0.2–4.0 keV).

The ROSAT HRI observation of NGC 205 was carried out in August 1996 with 28.1 ksec of exposure time (ROR ID 600816). There are 2 PSPC pointings in the first ROSAT M31 survey (ROR IDs 600067, 600068) which cover the area of NGC 205; both of them are in the outer field of the PSPC at about 40′ off-axis angle. We checked these two PSPC frames, there are no sources which are associated with NGC 205.

Table 4.9: Sources within ROSAT HRI field of NGC 205

Source No.	α_{2000} $h\ m\ s$	δ_{2000} $^\circ\ '\ ''$	Count Rate 10^{-3} s^{-1}	ML	Off-axis $'$	Notes
1	00 39 47.11	+41 56 58.4	4.10±0.86	12.1	16.7	
2	00 38 58.93	+41 50 17.2	2.68±0.60	13.7	17.4	
3	00 38 56.12	+41 47 54.5	4.86±1.02	11.5	16.8	
4	00 39 52.02	+41 45 17.8	1.16±0.26	21.5	6.4	3
5	00 40 01.49	+41 45 12.0	0.74±0.20	15.8	5.0	
6	00 40 58.22	+41 43 54.1	0.84±0.22	16.2	7.7	1
7	00 40 46.37	+41 40 52.7	0.64±0.19	15.0	5.1	
8	00 40 07.94	+41 40 14.6	0.86±0.20	28.9	2.4	
9	00 41 43.70	+41 34 18.2	14.57±0.95	272.4	17.3	1,2
10	00 40 53.40	+41 32 24.2	1.41±0.32	16.7	11.0	2
11	00 39 47.77	+41 31 48.1	1.59±0.36	15.5	11.3	
12	00 40 14.55	+41 29 38.4	1.58±0.36	15.7	11.8	
13	00 40 27.23	+41 29 11.8	1.54±0.37	13.2	12.3	2,3
14	00 39 43.50	+41 24 55.7	6.54±1.06	22.1	17.8	

Note: 1. With optical counterpart; 2. also detected in M31 PSPC survey; 3. with possible optical counterpart.

The brightest X-ray source in the HRI field is located at the edge with an off-axis angle of 17.3′, which is easily identified as a globular cluster, Bol 45. Apart from this, 13 sources are detected with $ML \geq 10$ (Table 4.9 and Figure 4.7); 3 out of these may have optical counterparts as well. Table 4.10 lists all 4 possible counterparts.

Table 4.10: Possible optical counterparts within ROSAT HRI field of NGC 205

Name	α_{2000} h m s	δ_{2000} $\circ$ $\prime$ $\prime\prime$	P_mag	Offset
GSC 2792_01681	00 39 52.01	+41 45 10.6	14.3	7″ from #4
SAO 36570	00 40 57.91	+41 43 51.6	9.4	4″ from #6
Bol 45	00 41 43.25	+41 34 20.6	15.8	6″ from #9
Bol 7	00 40 27.60	+41 29 10.7	18.0	4″ from #13

The 2 globular clusters listed (Bol 45 and Bol 7) are more likely associated with M31. At the positions of several globular clusters which may belong to NGC 205 (Battistini et al. 1987, Hubble 1932), no source was found.

Source No.8 is the only one located within the D_{25} area of NGC 205, but there is no sign of an optical counterpart. Two possible sources with $6.0 \leq ML < 10$ are found near the centre, but still $\sim 1.4'$ away from it. However, from the different smoothed images and contour plots, there seems to be some diffuse emission in the central area (*cf.* Figure 4.7). The upper limits are calculated for several central positions. A typical value is found for the Palumbo's position ($\alpha_{2000} = 0^h40^m22.0^s$, $\delta_{2000} = +41°41'25.8''$, mean error $0.7''$, Palumbo et al. (1988)), about 8 net counts are collected within $15''$ around a position that moved $8''$ to the West from the optical position of this galaxy (see also Section 6.2.1. The upper limit count rate is 4.2×10^{-4} s^{-1}. Using a power law model with photon index = 2.0 and Galactic $N_H = 6.74 \times 10^{20}$ cm^{-2}, the unabsorbed (0.1-2.4 keV) flux and luminosity are $f_X < 3.3 \times 10^{-14}$ ergs cm^{-2} s^{-1} and $L_X < 2.1 \times 10^{36}$ ergs s^{-1} at the distance of 725 kpc.

4.9 Sextans A

The ROSAT has observed Sextans A with both the PSPC and HRI detectors. The PSPC observation (ROR 600139) was carried out from 23 November to 2 December 1991 with an exposure time of 6.7 ksec. Table 4.11 lists 18 sources detected with $ML \geq 10$. Source No.16 can be identified as a star, HD 88682 ($\alpha_{2000} = 10^h13^m31.30^s$,

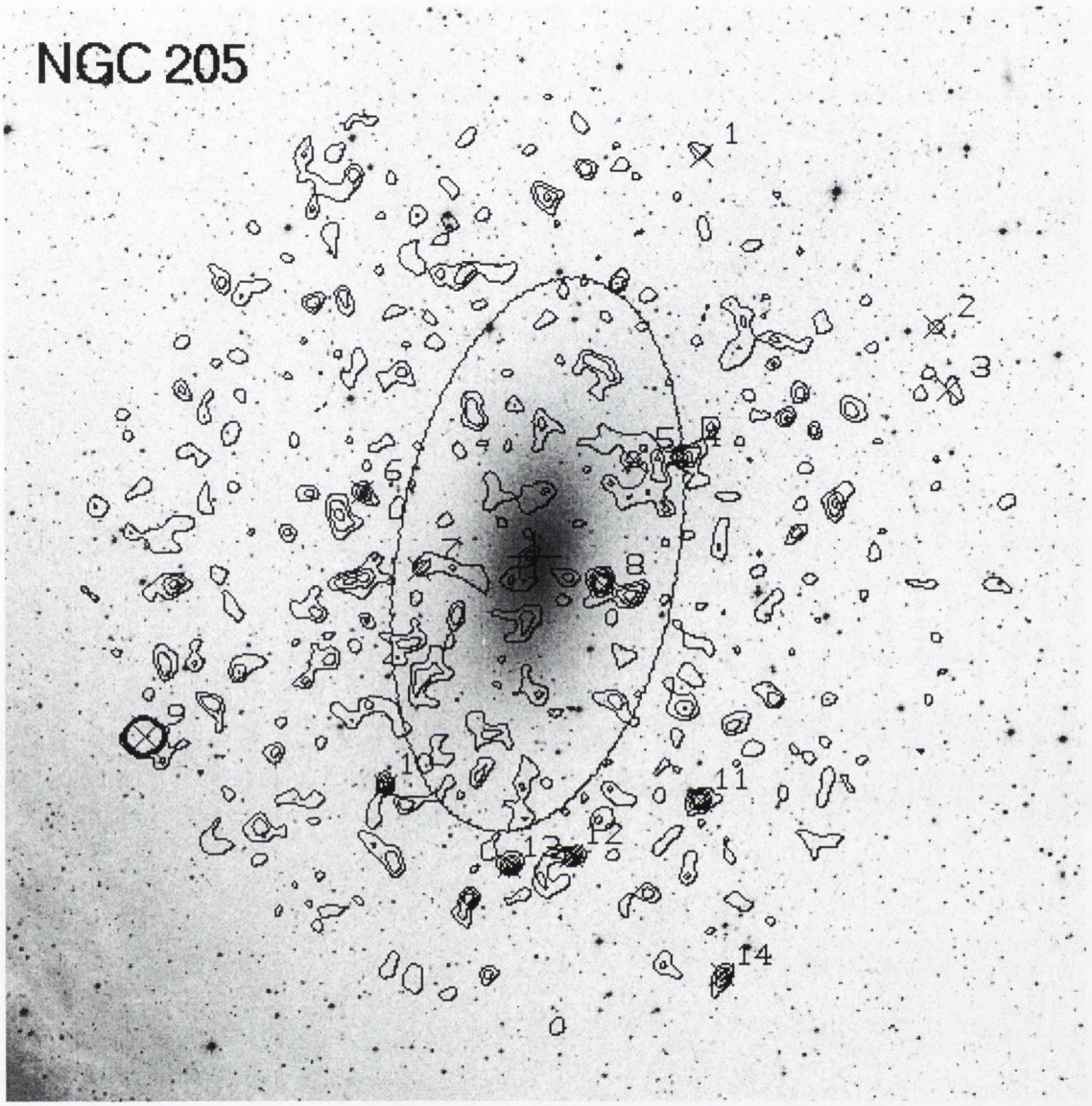

Figure 4.7: ROSAT HRI contour plot of NGC 205 overlaid on optical image covering the whole HRI area. The centre of the galaxy (Palumbo et al. 1988) is marked with a cross and the D_{25} ellipse is taken from RC3 catalogue. The background of the HRI image is ~ 1.06 cts pix^{-1}. The contour levels are 1.17, 1.28, 1.39 and 1.50 cts pix^{-1}. The HRI image has $5'' \times 5''$ pixels and is smoothed with a 3-pixel size Gaussians.

$\delta_{2000} = -5°5'14.4'')$, which has spectral type F2 and magnitude $m_B = 7.9$. Figure 4.8 shows the contour plot of the central $40' \times 40'$ area.

The two HRI observations were carried out on 10 December 1991 and 22 May 1992 with exposures of 11.5 and 18.3 ksec respectively. Table 4.12 lists all sources detected with $ML \geq 10$ in either data set. The sources that are also detected with

Table 4.11: Sources and count rates within ROSAT PSPC field of Sextans A

Source No.	α_{2000} $h\ m\ s$	δ_{2000} $^\circ\ '\ ''$	Count Rates 10^{-3} s^{-1}	ML	Off-axis $'$	HRI† source
1	10 10 07.84	-04 04 15.6	22.1±3.7	25.1	39.6	
2	10 11 30.13	-04 23 18.8	6.7±1.4	24.4	19.4	
3	10 11 29.71	-04 29 47.5	3.3±1.0	13.3	13.5	
4	10 11 10.76	-04 31 15.6	3.3±0.9	16.3	10.4	
5	10 10 11.53	-04 33 34.3	5.4±1.1	32.4	14.9	
6	10 09 56.38	-04 37 32.9	4.9±1.2	16.2	16.9	
7	10 11 32.40	-04 38 43.1	4.0±0.9	26.4	7.9	3
8	10 11 24.68	-04 42 20.0	26.5±2.1	406.2	5.6	4
9	10 11 07.82	-04 47 40.7	5.3±1.0	41.3	6.4	6
10	10 10 35.51	-04 47 46.8	12.7±1.5	155.1	9.3	7
11	10 11 02.22	-04 48 37.1	2.9±0.8	15.3	7.2	
12	10 11 42.33	-04 49 23.2	4.6±1.1	21.9	12.8	
13	10 13 20.85	-04 55 42.3	10.5±2.7	10.8	37.3	
14	10 10 25.86	-04 55 53.2	4.7±1.3	11.2	17.1	
15	10 13 55.18	-04 56 30.7	26.3±5.3	21.3	45.6	
16	10 13 31.24	-05 05 14.1	138.6±7.1	466.8	44.1	
17	10 11 27.09	-05 05 51.0	47.7±3.5	220.8	25.2	
18	10 09 03.72	-05 16 44.4	67.8±5.9	116.6	46.1	

† see Table 4.12.

PSPC are listed in Table 4.11. The brightest source in the HRI field (No.4, see Figure 4.9) is at the edge of the galaxy, but no optical object can be seen on the

Table 4.12: Sources and count rates within ROSAT HRI field of Sextans A

Source No.	α_{2000} $h\ m\ s$	δ_{2000} $^\circ\ '\ ''$	Count Rate 10^{-3} s^{-1} (I)	(II)	ML (I)	(II)	Off-axis $'$
1	10 10 51.13	-04 34 15.9	1.0±0.4	-	11.4	<6.0	7.7
2	10 10 37.70	-04 35 09.4	-	1.2±0.3	<6.0	15.6	8.8
3	10 11 33.14	-04 38 41.7	1.9±0.5	0.7±0.2	22.4	9.0	8.1
4	10 11 24.85	-04 42 19.9	8.0±0.9	8.6±0.7	269.2	478.6	5.7
5	10 11 06.19	-04 44 12.5	0.8±0.3	0.5±0.2	12.0	11.9	3.0
6	10 11 07.92	-04 47 43.3	2.0±0.5	1.6±0.3	39.0	47.6	6.5
7	10 10 35.47	-04 47 53.9	2.4±0.5	5.4±0.6	32.5	160.7	9.3

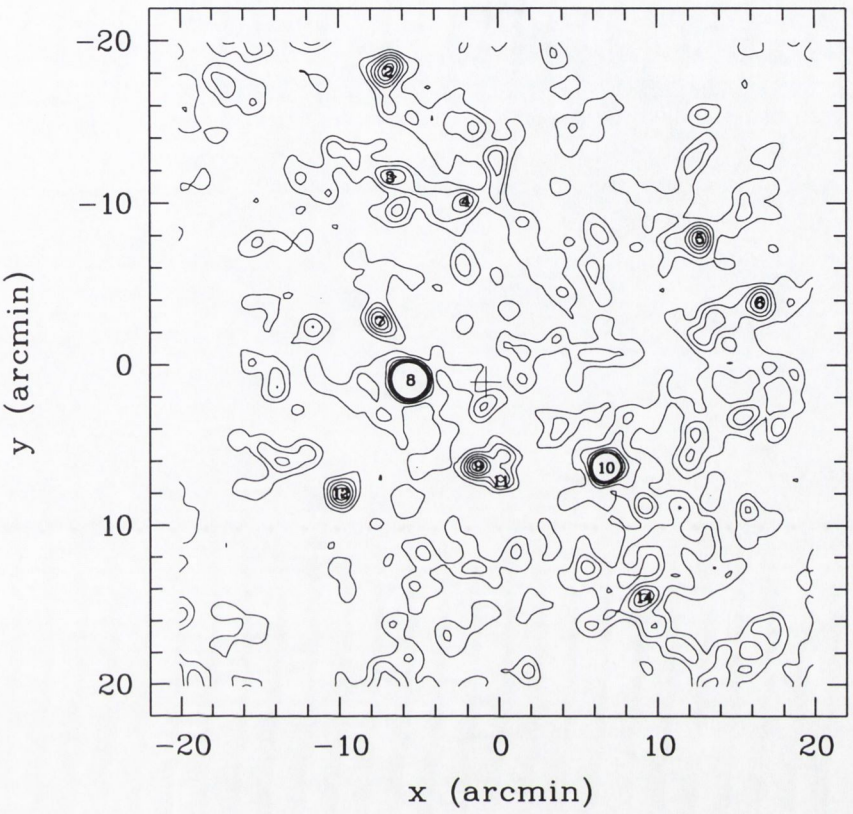

Figure 4.8: ROSAT PSPC contour plot of Sextans A, central $40' \times 40'$ area. The PSPC image has $15'' \times 15''$ pixels and smoothed with 2-pixel size Gaussian. The background is ~ 0.35 cts pix^{-1}. The contour levels start with 0.50 cts pix^{-1} and increase by 0.15 cts pix^{-1}. The SIMBAD position of the galaxy is marked with a cross and the X-ray sources are marked with source numbers (see Table 4.11).

DSS for this source, nor for others. As of the position, No.5 is the most likely one to be associated with the galaxy, but it is not in the central area and it is too weak to be seen as a source in the relatively short PSPC observation. However the contour plot does show the higher counts at the position (Figure 4.8).

From the PSPC observation, we calculate the upper limits at several catalogued optical positions for this galaxy. The biggest value is from the RC3 position, the upper limit count rate is 1.3×10^{-3} s^{-1}. Assuming power a law model with photon index = 2.0 and Galactic column $N_H = 3.85 \times 10^{20}$ cm^{-2}, the unabsorbed flux and luminosity are $f_X < 2.8 \times 10^{-14}$ ergs cm^{-2} s^{-1} and $L_X < 5.8 \times 10^{36}$ ergs s^{-1} (0.1–2.4 keV), at the distance of 1.3 Mpc. For comparison, the upper limit count rate

Figure 4.9: ROSAT HRI contour plot of Sextans A overlaid on optical image covering whole HRI area. The position of the galaxy from SIMBAD is marked with a cross. The background level in HRI image is ~ 0.5 cts pix^{-1}. The contour levels are 0.6, 0.7, 0.8 and 0.9 cts pix^{-1}. The HRI image has $5'' \times 5''$ pixels and is smoothed with a 3-pixel size Gaussians.

of the second deeper HRI observation is 0.21×10^{-3} s^{-1}. Using the same model, $f_X < 1.4 \times 10^{-14}$ ergs cm^{-2} s^{-1}, $L_X < 2.8 \times 10^{36}$ ergs s^{-1} (0.1–2.4 keV).

4.10 Fornax

The Fornax dwarf is the brightest dwarf spheroidal galaxy among the satellites of our Galaxy. Kinematic study suggests that the central mass-to-light ratio is 12.3 (Mateo et al. 1991). The core radius for a King model fit is $16.7' \pm 1.8'$ (Eskridge 1988). The stellar population of dwarf spheroidals can have an intermediate age component as well as the older globular cluster type population. Fornax is believed to lie in the middle of the range, having a 25% intermediate age component.

The first X-ray observation of Fornax was carried out with the ROSAT PSPC in February 1992. With an exposure time of 10.6 ksec, Gizis et al. (1993) detected

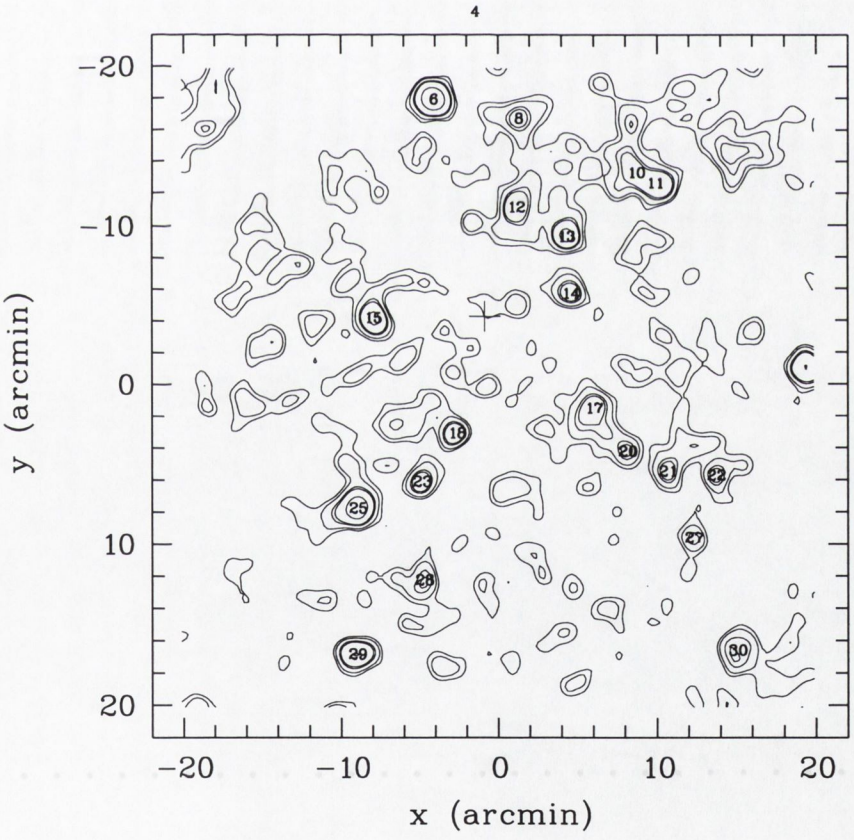

Figure 4.10: ROSAT PSPC contour plot of Fornax, central $40' \times 40'$ area. The PSPC image has $15'' \times 15''$ pixels and smoothed with 2-pixel size Gaussians. The background level is ~ 0.83 cts pix^{-1}. The contour levels are 0.97, 1.11, 1.39, 1.53 and 2.37 cts pix^{-1}. The SIMBAD position of the galaxy is marked with a cross and the X-ray sources are marked with source numbers (see Table 4.13.)

18 discrete sources in the field but they argue that those sources are attributable to the expected extragalactic background.

Table 4.13: Sources within ROSAT PSPC field of Fornax

Source No.	α_{2000} $h\ m\ s$	δ_{2000} $^\circ\ '\ ''$	Count Rate 10^{-3} s^{-1}	ML	Off-axis $'$
1	02 38 28.26	-33 56 55.9	20.01±3.31	23.1	38.7
2	02 41 48.48	-34 00 50.0	10.90±2.41	13.3	38.3
3	02 41 10.37	-34 05 31.3	6.77±1.62	12.1	30.0
4	02 40 02.20	-34 07 44.0	5.34±1.22	15.4	23.5
5	02 41 15.82	-34 09 48.5	7.52±1.61	15.8	27.1
6	02 40 15.05	-34 13 15.6	12.15±1.40	90.0	18.4
7	02 39 49.00	-34 14 28.6	3.95±0.94	15.5	16.8
8	02 42 08.99	-34 15 25.7	18.19±3.00	15.4	31.8
9	02 39 13.27	-34 17 53.2	8.36±1.45	17.4	15.9
10	02 39 07.59	-34 18 32.3	8.54±1.37	29.2	16.0
11	02 39 49.65	-34 20 02.5	5.23±0.91	40.2	11.2
12	02 39 34.36	-34 21 54.1	6.90±0.96	83.5	10.2
13	02 39 33.03	-34 25 29.9	4.13±0.80	33.5	7.3
14	02 40 33.73	-34 27 01.0	6.31±0.95	62.7	9.0
15	02 37 25.81	-34 30 10.1	12.60±2.02	30.1	30.8
16	02 39 25.95	-34 32 42.6	6.05±1.05	23.5	6.2
17	02 40 07.94	-34 34 16.2	4.54±0.81	40.4	4.0
18	02 36 58.65	-34 34 51.9	14.23±2.35	28.2	36.5
19	02 39 15.65	-34 35 25.2	3.37±0.73	25.7	9.2
20	02 39 03.47	-34 36 39.1	3.91±0.82	24.4	12.0
21	02 38 48.62	-34 36 54.1	3.73±0.83	20.8	14.8
22	02 40 18.80	-34 37 17.7	4.31±0.77	45.3	7.8
23	02 40 38.71	-34 38 56.9	10.07±1.17	107.6	11.8
24	02 42 07.62	-34 39 47.8	33.92±2.53	192.9	28.6
25	02 38 55.38	-34 40 47.5	3.06±0.80	13.7	15.6
26	02 40 18.11	-34 43 26.0	3.98±0.95	12.0	13.1
27	02 40 39.01	-34 48 01.2	7.83±1.20	42.8	19.1
28	02 38 41.89	-34 47 46.3	6.26±1.34	14.9	22.4
29	02 36 56.26	-34 51 16.3	13.09±2.97	13.1	41.9
30	02 42 31.90	-35 07 28.6	15.06±3.71	12.0	48.5

We re-examined data and get 30 sources with $ML \geq 10$ (Table 4.13). After searching various catalogues, we found only for No.22 a possible optical counterpart, GSC 0701400651, which is a 13.9^m non-stellar object ($\alpha_{2000} = 2^h40^m19^s, \delta_{2000} = -34°37'20.2''$). No.24 is the brightest source in the field with about 280 counts.

Tinney et al. (1997) present the first sample of QSOs behind the 3 dwarf spheroidal galaxies, Fornax, Carina and Sculptor. For Fornax, 2 QSOs, which are QJ0240–3443A (QJ0240–3443B) and QJ0240–3438 can be identified as X-ray sources, Nos.17 and 23 respectively.

Within the central area of the galaxy around the position given by NED and SIMBAD of the galaxy, there is no clear sign of diffuse emission (see contours in Figure 4.10), as Gizis et al. (1993) had concluded already. The upper limit count-rate is calculated as 1.4×10^{-3} s^{-1} for the position given by SIMBAD. Using a power law model with photon index = 2.0 and Galactic column $N_H = 2.87 \times 10^{20}$ cm^{-2}, it predicts an unabsorbed flux of $f_X < 2.6 \times 10^{-14}$ ergs cm^{-2} s^{-1} (0.1-2.4 keV). At the distance of the galaxy of 131 kpc, the luminosity $L_X < 5.3 \times 10^{34}$ ergs s^{-1}.

4.11 NGC 3109

There are two data sets in the ROSAT data archive about NGC 3109. Both are PSPC including the galaxy in the center of the field of view. The first observation was carried out between 26 May and 10 June 1992 with 18.5 ksec exposure time. 55 sources detected with $ML \geq 10$ are listed in Table 4.14. There is no source near the SIMBAD sources in the area. The brightest source is at the edge of the field (No.23) with about 2300 counts. It is a supersoft source with $HR_1 = -0.92 \pm 0.01$ and $HR_2 = 0.39 \pm 0.24$.

There are a few source around the $D_{25}(= 19.1')$ isophote ($R_{25} = 5.1$, $PA = 93°$), but none of them is located at central position. At the SIMBAD position, the upper limit count rate is 0.82×10^{-3} s^{-1}. Using the power law model with photon index =2.0 and Galactic column $N_H = 4.23 \times 10^{20}$ cm^{-2}, we get the unabsorbed flux $f_X = 1.9 \times 10^{-14}$ ergs cm^{-2} s^{-1} (0.1–2.4 keV) and luminosity $L_X = 3.6 \times 10^{36}$ ergs s^{-1}

Table 4.14: Sources and count rates within ROSAT PSPC field of NGC 3109: I

Source No.	α_{2000} $h\ m\ s$	δ_{2000} $^\circ\ '\ ''$	Count Rate 10^{-3} s^{-1}	ML	Off-axis $'$	Source in II[†]
1	10 03 43.98	-25 31 21.6	16.4±2.7	13.8	39.1	
2	10 04 12.39	-25 35 54.5	8.9±1.9	13.4	36.7	
3	10 05 35.53	-25 41 42.5	21.7±3.3	15.2	43.5	
4	10 05 32.17	-25 41 37.6	15.9±2.8	14.4	42.9	
5	10 04 58.33	-25 44 54.3	16.6±1.6	91.1	35.1	3
6	10 02 03.24	-25 47 39.7	2.8±0.7	10.7	26.2	
7	10 03 01.13	-25 51 20.7	4.1±0.6	46.6	18.3	5
8	10 02 57.72	-25 54 30.0	2.2±0.5	21.5	15.3	6
9	10 02 36.01	-25 56 28.1	4.3±0.6	58.6	14.9	
10	10 03 14.86	-25 56 57.5	1.5±0.4	14.5	12.8	7
11	10 04 49.96	-25 58 16.2	7.6±1.0	54.5	25.7	8
12	10 01 13.69	-25 58 28.2	5.6±1.2	13.0	27.8	
13	10 03 15.19	-25 58 43.7	1.5±0.4	15.2	11.0	
14	10 03 31.16	-25 58 47.5	3.0±0.5	42.1	12.1	
15	10 02 51.83	-25 59 34.2	1.2±0.4	10.8	10.6	
16	10 02 29.38	-26 00 02.1	2.0±0.4	21.4	12.8	
17	10 03 20.47	-26 00 25.1	1.9±0.4	25.4	9.6	
18	10 03 05.08	-26 00 50.0	2.3±0.5	26.2	8.8	9
19	10 02 50.57	-26 01 07.2	4.4±0.6	82.0	9.3	10
20	10 01 12.89	-26 02 43.6	6.6±1.2	16.0	26.6	
21	10 02 32.49	-26 02 34.9	5.5±0.6	126.1	10.5	12
22	10 02 18.82	-26 03 33.0	2.8±0.5	34.6	12.4	13
23	09 59 38.02	-26 04 29.4	224.4±5.4	1841.3	47.2	14
24	10 01 48.76	-26 04 45.6	1.9±0.5	12.0	18.3	15
25	10 02 03.27	-26 05 03.5	2.1±0.5	12.9	15.1	
26	10 03 17.72	-26 07 12.0	24.0±1.2	1324.6	3.4	19
27	10 03 41.84	-26 09 05.0	4.4±0.6	113.1	7.8	21
28	10 02 59.64	-26 10 11.2	8.3±0.7	303.5	1.8	22
29	10 02 14.82	-26 10 51.2	2.5±0.5	19.2	11.8	23
30	10 03 49.21	-26 11 13.5	1.2±0.3	11.6	9.6	
31	10 03 56.60	-26 11 08.4	1.6±0.4	11.8	11.2	
32	10 03 36.56	-26 11 42.6	1.3±0.4	15.7	6.9	
33	10 02 58.77	-26 11 55.0	4.0±0.5	101.1	3.0	24
34	10 02 42.03	-26 12 16.4	4.1±0.5	105.9	6.2	25
35	10 03 45.03	-26 12 34.1	1.9±0.4	18.9	9.0	
36	10 04 25.00	-26 12 47.8	6.5±0.8	71.5	17.7	26
37	10 03 22.95	-26 13 25.1	1.5±0.4	20.3	5.2	
38	10 05 55.87	-26 13 24.2	8.9±1.6	22.1	38.0	
39	10 03 28.68	-26 13 44.0	2.1±0.4	35.3	6.4	27
40	10 02 20.19	-26 14 03.3	2.3±0.5	30.7	11.4	28
41	10 04 57.93	-26 14 14.7	3.4±0.8	11.8	25.3	
42	10 05 34.07	-26 16 02.6	11.7±1.9	19.6	33.6	
43	10 02 34.32	-26 20 06.1	3.5±0.6	26.8	12.8	
44	10 05 04.04	-26 19 48.0	6.7±0.0	22.3	28.1	
45	10 03 40.56	-26 20 28.2	1.5±0.4	13.5	13.2	
46	10 04 48.39	-26 20 32.0	13.2±1.2	112.6	25.2	30
47	10 01 08.48	-26 20 28.3	3.9±1.0	11.5	28.8	
48	10 02 48.30	-26 21 44.2	2.0±0.4	22.1	12.9	
49	10 03 44.18	-26 22 18.7	1.6±0.5	10.6	15.2	
50	10 02 30.92	-26 22 28.7	4.7±0.7	55.8	15.2	31
51	10 03 05.61	-26 22 41.5	1.7±0.4	19.4	13.1	
52	10 01 09.89	-26 26 16.9	4.3±1.1	10.7	31.1	
53	10 02 25.15	-26 26 37.8	1.7±0.5	10.6	19.5	
54	10 01 13.85	-26 37 17.8	13.1±1.9	25.3	37.6	
55	10 03 24.23	-26 43 21.8	7.7±1.2	36.9	34.0	34

[†] Also detected in the 2nd data set. See Table 4.15 for source Nos.

Table 4.15: Sources and count rates within ROSAT PSPC field of NGC 3109: II

Source No.	α_{2000} $h\ m\ s$	δ_{2000} $^\circ\ '\ ''$	Count Rates 10^{-3} s^{-1}	ML	Off-axis $'$
1	10 01 42.92	-25 26 15.5	21.7±3.9	12.7	47.3
2	10 04 32.69	-25 36 33.8	18.6±3.1	12.3	38.2
3	10 05 00.27	-25 44 32.0	9.8±1.7	22.7	35.7
4	10 04 15.23	-25 45 31.7	7.9±1.6	12.6	28.5
5	10 03 00.34	-25 51 18.0	3.0±0.7	22.4	18.4
6	10 02 58.15	-25 54 17.4	2.3±0.6	16.5	15.4
7	10 03 14.86	-25 56 54.1	2.4±0.5	21.6	12.8
8	10 04 49.70	-25 58 28.2	6.3±1.1	25.0	25.6
9	10 03 05.20	-26 00 58.3	1.9±0.5	15.1	8.6
10	10 02 50.19	-26 01 06.4	2.0±0.5	19.2	9.3
11	10 05 42.96	-26 01 11.8	14.1±2.3	25.0	36.0
12	10 02 32.63	-26 02 36.9	9.8±1.0	218.3	10.4
13	10 02 18.86	-26 03 14.8	2.6±0.6	29.3	12.6
14	09 59 37.90	-26 04 17.5	238.7±6.4	1662.4	47.3
15	10 01 51.37	-26 04 26.5	3.2±0.7	19.2	17.8
16	10 03 51.87	-26 04 45.5	3.3±0.6	38.9	11.1
17	10 05 16.60	-26 06 11.4	4.3±1.1	10.4	29.2
18	10 03 49.65	-26 06 34.8	1.8±0.5	14.7	10.0
19	10 03 17.97	-26 07 09.7	19.5±1.3	658.6	3.4
20	10 06 26.95	-26 07 28.8	17.4±2.7	29.1	44.9
21	10 03 41.86	-26 08 58.4	3.6±0.6	54.7	7.8
22	10 02 59.91	-26 10 03.2	7.3±0.8	169.0	1.7
23	10 02 13.23	-26 10 49.9	1.9±0.5	12.8	12.2
24	10 02 59.13	-26 11 51.6	3.4±0.6	53.0	2.9
25	10 02 42.07	-26 12 08.1	4.6±0.7	83.4	6.2
26	10 04 24.68	-26 12 26.9	3.3±0.7	18.1	17.6
27	10 03 28.93	-26 13 36.4	1.9±0.5	18.8	6.3
28	10 02 20.50	-26 13 56.6	2.5±0.6	24.6	11.3
29	10 00 25.91	-26 16 11.1	7.3±1.6	14.3	36.8
30	10 04 50.91	-26 20 25.4	13.8±1.6	65.9	25.6
31	10 02 30.65	-26 22 17.9	4.9±0.8	32.7	15.1
32	10 03 23.22	-26 29 54.2	7.2±1.0	52.5	20.6
33	10 02 52.12	-26 41 45.3	8.8±1.9	13.1	32.3
34	10 03 25.30	-26 43 22.0	11.8±2.1	19.8	34.0
35	10 01 15.83	-26 44 06.3	18.3±3.1	21.3	42.6
36	10 04 16.98	-26 51 31.0	19.8±3.6	16.1	44.7

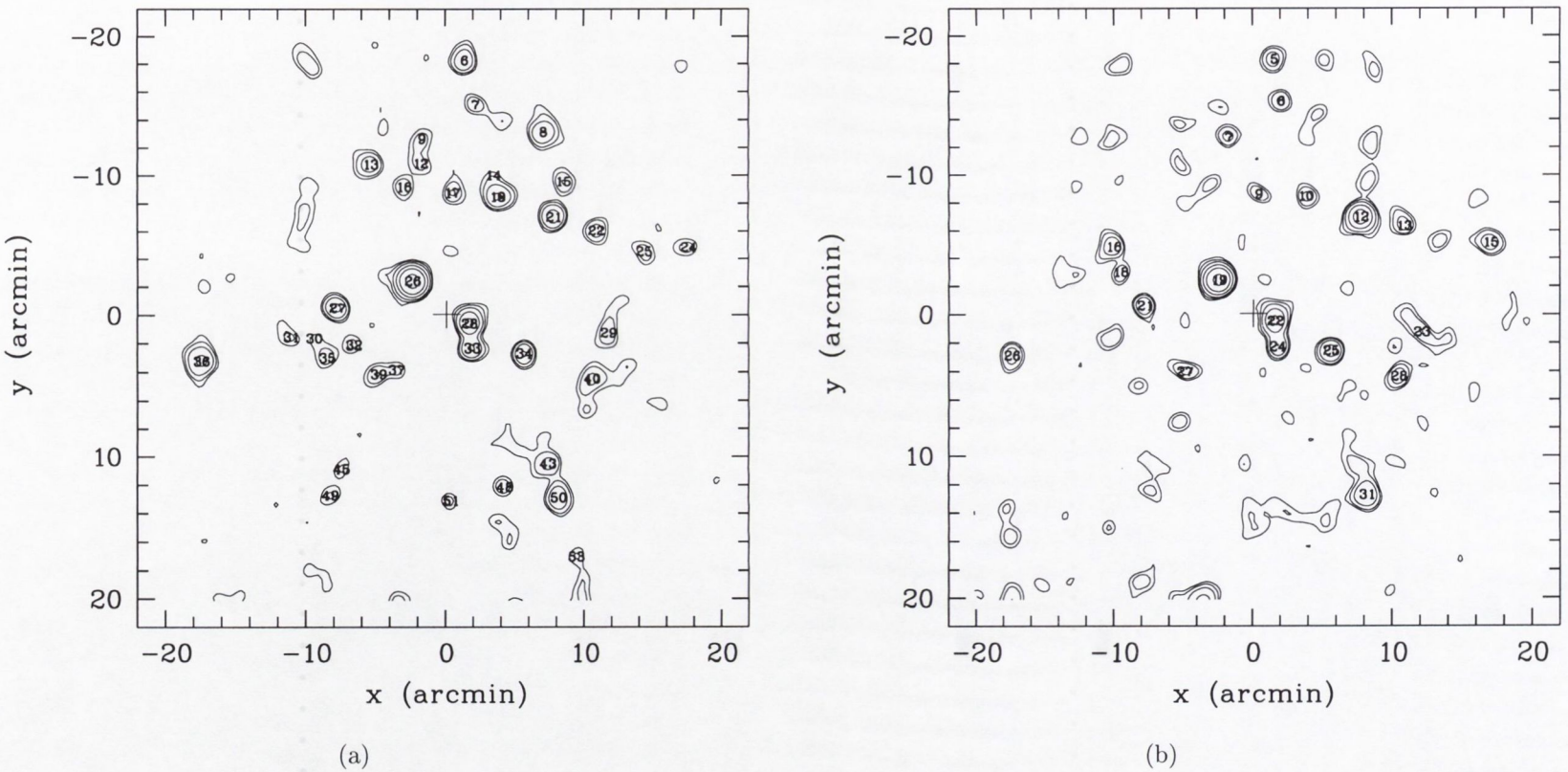

Figure 4.11: ROSAT PSPC contour plots of NGC 3109, central $40' \times 40'$ area. The PSPC images have $15'' \times 15''$ pixels and smoothed with 2-pixel size Gaussians. (a) The first observation. The background level is ~ 0.87 cts pix^{-1}. The contour levels are 1.27, 1.47, 1.87, 2.87, 4.87 and 10.8 cts pix^{-1}. (b) The second observation. The background is ~ 0.75 cts pix^{-1}. The contour levels are 1.01, 1.14, 1.40, 2.05, 3.35 and 7.25 cts pix^{-1}. The SIMBAD position of the galaxy is marked with a cross and the X-ray sources are marked with source numbers (see Tables 4.14 and 4.15).

at the distance of 1.26 Mpc.

The second observation was carried out on 18 November 1992. It pointed at the same area as the first one and, because of less exposure time (13.3 ksec), less sources are detected. Table 4.15 lists all 36 sources of which 23 sources have been seen as marked in the first data set (Table 4.14). They are no changes as regards the region at the optical position of NGC 3109.

4.12 Pegasus

Pegasus was observed with the ROSAT PSPC in June 1992 for about 8.8 ksec (ROR 600143). 23 sources are detected with $ML \geq 10$ (Table 4.16). Searching SIMBAD

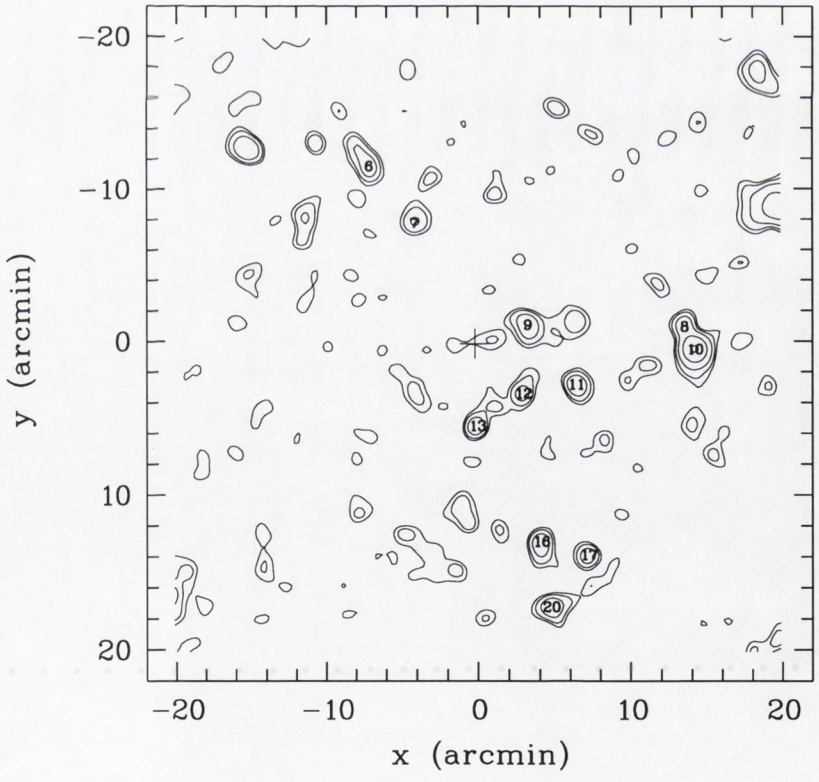

Figure 4.12: ROSAT PSPC contour plot of Pegasus, central $40' \times 40'$ area. The PSPC image has $15'' \times 15''$ pixels and smoothed with 2-pixel size Gaussians. The background level is ~ 0.44 cts pix^{-1}. The contour levels are 0.66, 0.77, 0.99, 1.54 and 2.64 cts pix^{-1}. The SIMBAD position of the galaxy is marked with a cross and the X-ray sources are marked with source numbers (see Table 4.16).

Table 4.16: Sources and count rates within ROSAT PSPC field of Pegasus

Source No.	α_{2000} $h\ m\ s$	δ_{2000} $^\circ\ '\ ''$	Count Rates 10^{-3} s^{-1}	ML	Off-axis $'$
1	23 27 35.73	+15 32 26.0	24.8±0.0	28.1	49.4
2	23 28 18.91	+15 29 51.4	43.5±4.2	86.6	45.0
3	23 27 24.09	+15 24 57.0	159.8±6.4	782.3	43.3
4	23 25 47.16	+15 08 12.3	37.8±5.6	12.1	46.4
5	23 27 17.56	+15 02 31.1	5.5±1.3	15.7	25.4
6	23 29 03.33	+14 56 29.4	3.8±0.9	20.0	13.6
7	23 28 50.93	+14 52 45.2	2.2±0.7	11.2	8.8
8	23 27 37.97	+14 45 56.4	3.8±0.8	29.2	13.5
9	23 28 20.52	+14 46 03.8	4.4±0.9	22.5	3.3
10	23 27 35.05	+14 44 27.7	10.6±1.3	103.9	14.2
11	23 28 07.38	+14 42 11.2	3.6±0.8	33.7	6.9
12	23 28 21.62	+14 41 35.2	2.9±0.7	25.0	4.5
13	23 28 33.86	+14 39 29.2	3.2±0.7	31.5	5.5
14	23 30 43.52	+14 38 00.0	11.8±2.1	25.8	32.2
15	23 24 51.74	+14 38 25.8	23.4±5.2	12.4	54.1
16	23 28 16.77	+14 31 59.6	3.6±0.8	24.3	13.6
17	23 28 03.90	+14 31 08.6	3.4±0.8	19.9	15.6
18	23 25 25.34	+14 29 16.5	41.6±4.6	64.8	48.2
19	23 29 58.90	+14 27 52.8	6.9±1.6	14.5	26.8
20	23 28 14.08	+14 27 45.8	4.0±0.9	22.7	17.9
21	23 28 45.90	+14 19 25.8	5.8±1.3	17.5	25.7
22	23 28 04.44	+14 17 36.0	10.9±1.9	23.5	28.3
23	23 28 37.71	+13 59 32.7	125.0±6.0	522.4	45.5

sources, the 13.3^m K5 star BD +13 5114 can be the counterpart of No.10. The coordinates for BD +13 5114 are $\alpha_{2000} = 23^h27^m34.7^s$ and $\delta_{2000} = +14^\circ44'24''$. There is one source (No.9) located within the D_{25} (= 5.0′) ellipse of the galaxy, but not in the central area (*cf.* Figure 4.12) There is no source detected close to the SIMBAD position for this galaxy and the upper limit count rate is 1.3×10^{-3} s^{-1}. Using the power low model with photon index =2.0 and Galactic column 4.06×10^{20} cm^{-2}, this predicts an unabsorbed (0.1–2.4 keV) flux and luminosity as $f_X = 3.0 \times 10^{-14}$ ergs cm^{-2} s^{-1} and $L_X = 1.2 \times 10^{37}$ ergs s^{-1} at the distance of

1.80 Mpc.

4.13 Carina

Carina was observed with the ROSAT PSPC in April 1992 for about 8,792 seconds. 33 sources are found with $ML \geq 10$ (Table 4.17), among which 2 may have optical counterparts. No.19 is about 4″ away from the star HD 48652 (F2V, 9.7^m), while No.29 is about 1′ away from the star CD-51 2021 (F0, 10^m). The latter one is just within the FWHM of the PSF at the off-axis angle of 32.5′. However, No.29 may be more likely identified with a Seyfert I galaxy which is listed by Tinney et al. (1997)

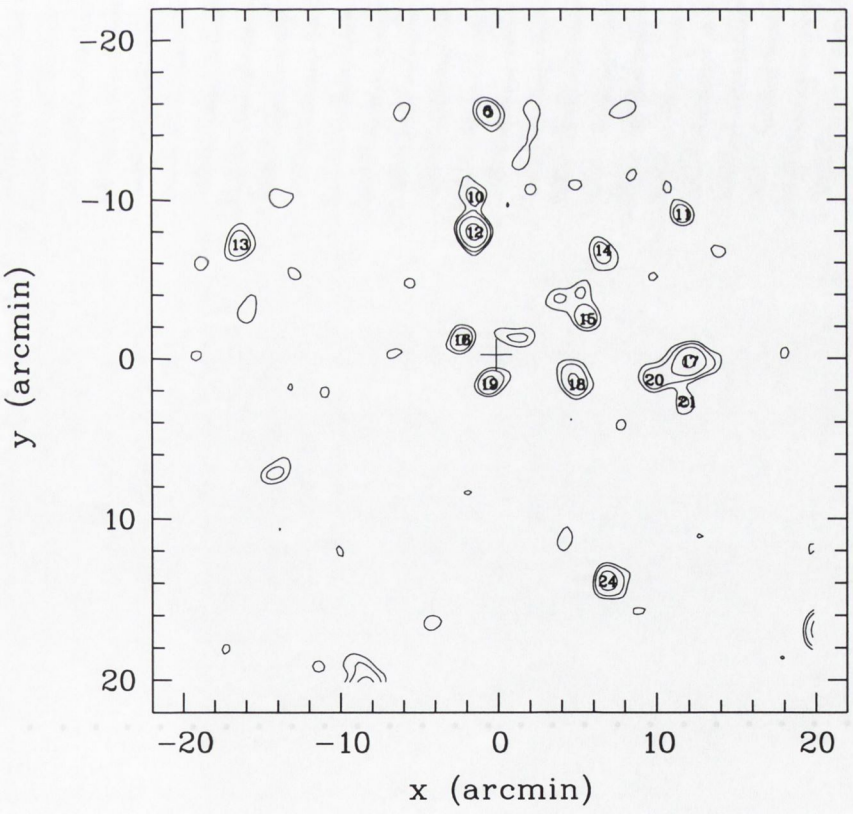

Figure 4.13: ROSAT PSPC contour plot of Carina, central 40′ × 40′ area. The PSPC image has 15″ × 15″ pixels and smoothed with 2-pixel size Gaussians. The background is ~ 0.50 cts pix^{-1}. The contours are 0.76, 0.89, 1.15 and 1.80 cts pix^{-1}. The cross in the centre refers to the SIMBAD/NED position of the galaxy and the X-ray sources are marked with source numbers (see Table 4.17).

Table 4.17: Sources and count rates within ROSAT PSPC field of Carina

Source No.	α_{2000} $h\ m\ s$	δ_{2000} $^\circ\ '\ ''$	Count Rates 10^{-3} s^{-1}	ML	Off-axis $'$	Source Ident.
1	06 42 33.69	-50 21 40.7	9.9±2.3	13.5	37.6	
2	06 43 14.77	-50 23 43.8	12.8±2.5	18.7	37.9	
3	06 39 13.22	-50 25 47.5	21.0±4.2	10.2	39.5	
4	06 40 55.59	-50 31 42.6	45.5±3.0	295.8	27.2	QJ0640-5031
5	06 45 25.85	-50 41 21.0	13.3±2.9	14.0	40.0	
6	06 41 40.42	-50 42 38.2	3.4±0.9	16.7	15.6	
7	06 44 29.84	-50 43 17.3	13.3±2.1	33.9	31.2	
8	06 43 53.30	-50 43 31.0	7.1±1.7	11.3	26.2	
9	06 44 00.88	-50 48 10.8	22.1±2.1	124.6	25.0	
10	06 41 45.12	-50 48 01.8	2.5±0.7	11.5	10.3	
11	06 40 22.54	-50 49 06.3	2.9±0.8	10.7	14.7	
12	06 41 45.46	-50 50 16.4	8.3±1.1	91.0	8.1	GJ0641-5050
13	06 43 19.75	-50 50 58.7	4.4±1.1	15.1	17.9	
14	06 40 53.87	-50 51 23.5	2.6±0.8	11.5	9.5	
15	06 41 00.39	-50 55 43.9	3.2±0.8	18.3	6.1	QJ0640-5055
16	06 41 50.74	-50 57 01.3	3.3±0.7	30.5	2.6	? QJ0641-5057
17	06 40 19.57	-50 58 21.6	7.2±1.1	68.4	12.0	
18	06 41 04.73	-50 59 51.2	3.5±0.8	26.1	5.2	
19	06 41 39.81	-50 59 48.5	3.6±0.8	34.6	1.7	HD 48625
20	06 40 33.52	-50 59 32.1	2.9±0.8	17.7	9.9	
21	06 40 20.74	-51 00 53.6	2.2±0.7	11.2	12.1	
22	06 46 30.68	-51 00 37.6	11.0±2.8	10.2	46.4	
23	06 39 14.73	-51 07 09.7	6.6±1.5	14.4	23.9	
24	06 40 52.02	-51 12 05.5	5.2±1.1	25.4	15.5	QJ0640-5112
25	06 38 32.66	-51 12 47.5	12.7±2.2	27.0	32.3	
26	06 39 21.89	-51 14 51.5	11.9±2.0	27.5	26.8	
27	06 42 30.52	-51 18 42.8	6.3±1.3	22.1	22.2	
28	06 40 38.75	-51 23 15.8	7.6±1.5	21.5	26.6	
29	06 39 40.70	-51 25 16.2	184.2±5.8	1824.0	32.5	GJ0639-5125
30	06 42 38.92	-51 25 40.7	5.2±1.4	10.1	29.2	
31	06 42 25.04	-51 32 27.5	50.9±3.6	217.6	35.1	
32	06 41 32.03	-51 32 44.4	10.7±2.4	13.5	34.5	
33	06 40 42.21	-51 39 44.0	64.3±4.7	161.3	42.4	

as an AGN, GJ0639-5125 ($z = 0.108 \pm 0.001$). 5 other sources can be identified with QSOs Tinney et al. (1997) from as well. We list these identifications in Table 4.17,

with a '?' for No.16 because the offset is well above 10″.)

Apart from No.19, a few other sources are within D_{25} (= 23.4′) ellipse, namely No.12, 15, 16, 18 and 20. No.10, 14, 17 and 21 are just outside the ellipse. At the positions of No.15, 17 and 20, there are visible spots in the POSS image that are catalogued in the GSC. The remaining ones in or near the D_{25} could be associated with the galaxy. No.16 (a QSO?) is the nearest source from the SIMBAD position of the galaxy (Figure 4.13). From the SIMBAD position, the upper limit count rate is 1.5×10^{-3} s^{-1}. This rate actually calculated by EXSAS from the counts collected from the area with two contours just NW to the SIMBAD position. Using the $\Gamma = 2.0$ power law model and Galactic column $N_H = 3.9 \times 10^{20}$ cm^{-2}, the unabsorbed (0.1–2.4 keV) flux $f_X < 3.4 \times 10^{-14}$ ergs cm^{-2} s^{-1} and luminosity $L_X < 3.1 \times 10^{34}$ ergs s^{-1} at the distance of 87 kpc.

4.14 Sculptor

The Sculptor dwarf elliptical galaxy was observed on 1 and 2 July 1992 with the ROSAT PSPC for 9,887 seconds (ROR 600378). 51 sources with $ML \geq 10$ are detected and listed in Table 4.18. No SIMBAD source is found as optical counterpart. Tinney et al. (1997) lists 11 QSO/AGN objects that may all have been detected as X-rays sources.

This galaxy covers a large area of the sky with $D_{25} = 39.8'$ (tidal radius = 76.5′). From the contour plot (Figure 4.14), no source is near the central area around the SIMBAD position. The upper limit count rate for the SIMBAD position is 0.92×10^{-3} s^{-1}. Using the $\Gamma = 2.0$ power law model and Galactic column $N_H = 2.04 \times 10^{20}$ cm−2, the unabsorbed (0.1–2.4 keV) flux $f_X < 1.4 \times 10^{-14}$ ergs cm^{-2} s^{-1} and luminosity $L_X < 1.1 \times 10^{34}$ ergs s^{-1} at the distance of 78 kpc.

Table 4.18: Sources and count rates within ROSAT PSPC field of Sculptor

Source No.	α_{2000} $h\ m\ s$	δ_{2000} $^\circ\ '\ ''$	Count Rates 10^{-3} s^{-1}	ML	Off-axis $'$	Source Ident.
1	01 00 04.78	-33 05 28.7	16.4±3.1	18.3	37.3	
2	01 02 35.30	-33 10 13.7	20.9±3.6	17.1	39.8	
3	01 01 54.94	-33 11 31.3	8.1±1.9	12.3	34.2	
4	01 00 12.11	-33 16 22.6	10.0±2.1	12.0	26.3	
5	01 00 20.46	-33 25 13.5	4.2±1.0	18.9	17.3	
6	00 57 52.28	-33 28 16.5	19.7±2.9	32.5	37.7	
7	00 58 17.08	-33 28 43.1	14.8±2.3	32.2	32.7	
8	01 02 38.01	-33 29 53.7	13.5±2.0	35.0	27.2	
9	01 01 04.83	-33 30 10.7	16.7±1.5	194.8	12.8	GJ
10	01 00 32.17	-33 32 02.8	3.0±0.8	17.0	10.1	
11	01 01 17.61	-33 33 44.8	3.1±0.8	17.1	11.3	
12	01 00 42.21	-33 35 09.4	4.1±0.9	14.8	6.8	
13	00 59 26.65	-33 34 51.5	2.9±0.8	12.0	17.0	
14	01 01 23.24	-33 36 14.5	3.8±0.8	23.3	10.5	
15	01 00 09.52	-33 37 31.2	8.9±1.1	108.1	7.9	
16	00 58 11.91	-33 38 15.5	33.8±2.9	121.0	31.2	? QJ
17	01 00 32.79	-33 38 31.5	7.5±1.0	80.0	3.9	QJ
18	01 00 56.55	-33 40 42.4	8.4±1.1	79.5	3.5	QJ
19	01 00 26.04	-33 41 01.6	2.7±0.7	19.4	3.2	QJ
20	01 03 14.82	-33 40 59.1	7.4±1.8	11.8	32.1	
21	01 01 21.73	-33 42 13.7	6.9±1.0	55.0	8.5	QJ
22	00 59 46.50	-33 43 08.0	2.7±0.7	14.3	11.4	
23	01 01 48.73	-33 43 33.4	26.6±1.9	348.7	14.2	GJ
24	00 58 25.66	-33 45 43.5	12.0±1.7	47.6	28.3	
25	01 01 00.37	-33 46 10.7	2.1±0.6	12.6	5.8	
26	01 02 51.08	-33 47 03.3	9.5±1.8	23.4	27.6	
27	01 01 16.29	-33 47 27.8	4.5±0.9	31.8	9.2	QJ
28	01 00 29.24	-33 47 32.6	7.3±1.0	84.6	6.0	
29	00 57 46.21	-33 50 16.8	30.3±4.0	32.5	37.2	
30	01 00 27.61	-33 51 08.9	54.5±2.5	1272.0	9.6	
31	01 00 00.73	-33 55 24.9	17.8±1.6	195.6	15.8	
32	01 01 15.96	-33 56 11.1	5.9±1.3	12.6	16.0	
33	01 00 45.02	-33 57 07.8	6.3±1.2	27.7	15.2	QJ
34	01 01 34.23	-33 57 59.2	9.8±1.6	27.7	19.5	
35	00 59 50.18	-33 58 05.2	3.1±0.9	10.0	19.2	
36	00 56 57.33	-33 56 23.4	40.2±6.1	18.7	48.6	
37	01 03 46.44	-34 05 01.2	38.8±6.2	11.6	44.9	
38	00 59 23.85	-34 04 56.4	8.7±1.9	12.7	28.0	
39	01 00 30.78	-34 06 23.1	11.8±1.7	39.5	24.5	
40	01 03 13.55	-34 07 20.0	36.1±4.9	25.2	40.6	
41	01 01 13.64	-34 08 35.0	19.3±2.3	55.5	27.4	
42	01 03 19.84	-34 07 54.8	44.3±4.9	48.2	42.0	
43	00 58 47.84	-34 13 20.4	24.7±4.4	10.4	39.1	
44	00 57 49.21	-34 11 56.1	43.1±5.3	35.9	46.5	
45	01 01 56.46	-34 14 08.3	50.0±3.7	152.9	35.8	QJ
46	01 02 24.96	-34 14 41.5	40.8±4.4	68.0	39.2	? QJ
47	01 00 30.07	-34 15 58.6	11.7±2.1	23.6	34.0	
48	00 58 54.85	-34 17 13.6	68.4±5.7	69.5	41.5	
49	00 58 47.26	-34 18 13.7	59.3±5.2	89.2	43.2	
50	00 59 27.66	-34 18 58.6	11.7±3.0	12.9	40.0	
51	01 03 02.59	-34 21 52.1	19.7±4.1	14.6	49.5	

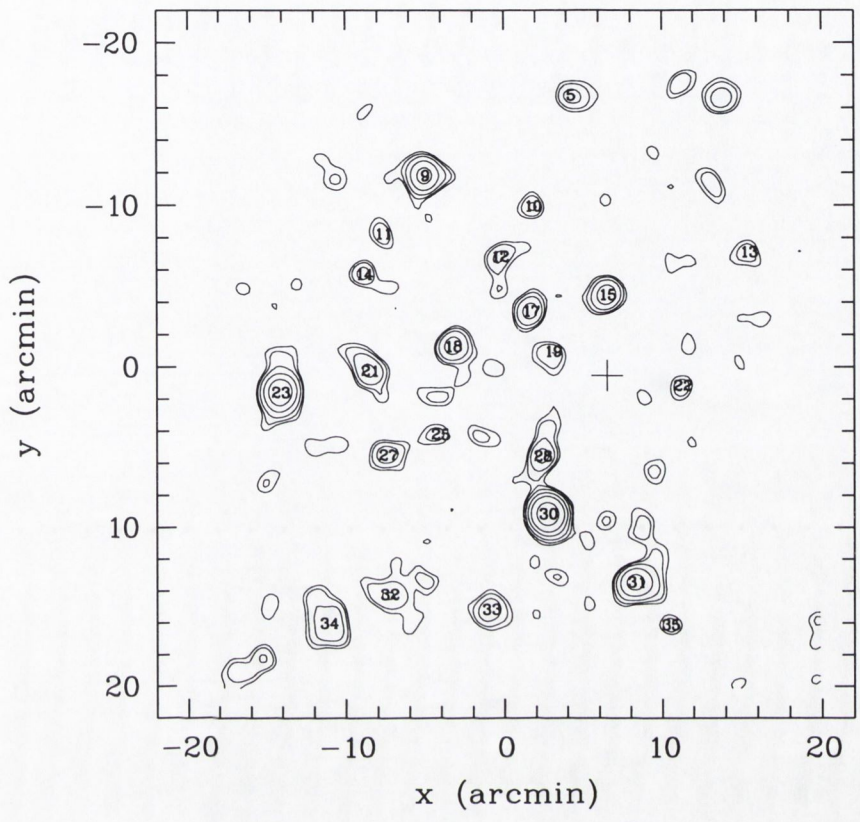

Figure 4.14: ROSAT PSPC contour plot of Sculptor, central $40' \times 40'$ area. The PSPC image has $15'' \times 15''$ pixels and smoothed with 2-pixel size Gaussians. The background level is ~ 0.80 cts pix^{-1}. The contours are 1.10, 1.25, 1.55, 2.30, 3.80 and 8.30 cts pix^{-1}. The cross near the centre is the SIMBAD position of the galaxy and the X-ray sources are marked with source numbers (see Table 4.18.)

4.15 Sextans

The ROSAT PSPC pointed on the Sextans dwarf galaxy on 29 May 1992 for 1,946 seconds (ROR 600148). 13 sources are detected with $ML \geq 10$ (Table 4.19). Among them, No.1 and 2 may belong to one extended source which is associated with galaxy UGC 5515 in a cluster of galaxies. No.3 and 4 can be found near the stars BD-00 2307 (11.6^m, $\alpha_{2000} = 10^h23^m21.9^s$, $\delta_{2000} = -1°11'8''$) and HD 88488 (A3, 8.5^m, $\alpha_{2000} = 10^h12^m14.7^s$, $\delta_{2000} = -1°15'39''$) respectively. No.6 is $4''$ away from a no-stellar object catalogued in GSC 1.2 (GSC 0490_400893, 13.02^m).

This galaxy also covers a large area of the sky, with a tidal radius of $160' \pm 50'$.

Table 4.19: Sources and count rates within ROSAT PSPC field of Sextans

Source No.	α_{2000} h m s	δ_{2000} $^\circ$ $'$ $''$	Count Rates 10^{-3} s^{-1}	ML	Off-axis $'$
1	10 13 22.59	-00 53 35.0	146.2±17.1	31.4	43.3
2	10 13 40.38	-00 55 44.9	268.0±20.4	116.5	41.9
3	10 13 16.65	-01 10 46.3	31.0±5.8	26.5	26.1
4	10 12 13.71	-01 15 13.7	14.8±3.9	15.5	24.6
5	10 12 57.52	-01 20 49.3	10.6±3.2	10.5	15.8
6	10 12 21.34	-01 28 14.0	120.6±8.5	592.4	13.2
7	10 13 39.85	-01 28 42.5	9.6±2.7	18.3	12.2
8	10 12 49.24	-01 29 57.8	5.0±1.9	12.0	7.4
9	10 14 03.55	-01 34 09.6	12.6±3.6	10.7	15.5
10	10 13 28.25	-01 36 38.5	14.8±3.2	25.9	6.5
11	10 10 56.35	-02 01 16.5	74.3±13.0	21.6	40.0
12	10 11 35.24	-02 06 01.1	25.9±6.6	12.5	36.6
13	10 11 29.20	-02 11 57.6	27.8±7.8	10.0	42.3

Near the SIMBAD position, there is no source detected but some emission can be seen from the contour plot, Figure 4.15. From the SIMBAD position, the upper limit count rate is calculated from this emission as 5.3×10^{-3} s^{-1}. Using the $\Gamma = 2.0$ power law model and Galactic column $N_H = 3.86 \times 10^{20}$ cm^{-2}, the unabsorbed (0.1–2.4 keV) flux $f_X < 1.2 \times 10^{-14}$ ergs cm^{-2} s^{-1} and luminosity $L_X < 1.1 \times 10^{35}$ ergs s^{-1} at the distance of 90 kpc.

4.16 Draco

The Draco dwarf galaxy was observed with the ROSAT PSPC, focussing on the centre object Draco C-1 (ROR 200724). The observation was carried out on 1 April 1992 with an exposure time of 5,336 seconds. 33 sources are detected with $ML \geq 10$ (Table 4.20). No.13 is at the centre (Figure 4.16) and listed as a symbiotic binary by Bickert et al. (1996). This source has a supersoft X-ray spectrum (α type, see Mürset et al. 1996). No.31 is an extended source ($> 2'$) which is believed to be associated with a cluster of galaxies. The X-ray position is near the NGC

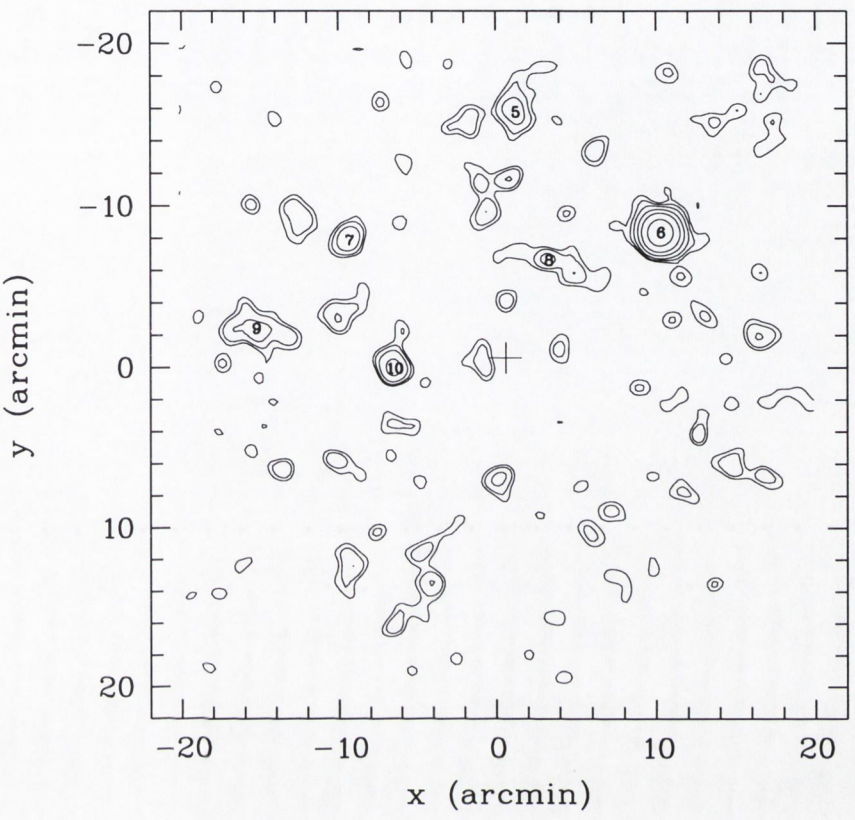

Figure 4.15: ROSAT PSPC contour plot of Sextans, central $40' \times 40'$ area. The PSPC image has $15'' \times 15''$ pixels and smoothed with 2-pixel size Gaussians. The background level is ~ 0.13 cts pix^{-1}. The contours are 0.23, 0.28, 0.38, 0.63, 1.13 and 2.63 cts pix^{-1}. The cross in the centre indicates the SIMBAD position of the galaxy and the X-ray sources are marked with source numbers (see Table 4.19).

6338 in the cluster, that was previously detected in the ROSAT All Sky Survey, namely 1RXS J171519.5+572430 or RX J1715.3+5724 by Brinkmann and Siebert (1994). No.9 can be identified as a binary star HD 238688 (F8, 8.80^m, also SAO 30348 or V* GM Dra) with coordinates $\alpha_{2000} = 19^h20^m21.88^s$, $\delta_{2000} = 57°58'27.0''$. Among the rest, No.6 and 15 probably have stellar objects as counterparts which are GSC 0389600604 ($\alpha_{2000} = 17^h20^m37.69^s$, $\delta_{2000} = +58°2'11.4''$) and GSC 0389600822 ($\alpha_{2000} = 17^h21^m58.30^s$, $\delta_{2000} = +57°49'21.6''$).

The SIMBAD lists coordinates of Draco C-1 ($\alpha_{2000} = 17^h19^m57.5^s$, $\delta_{2000} = 57°50'5''$) as the position of Draco dwarf galaxy as well. But in the NED and RC3 catalogues, the coordinates are several arcminutes away (NED : $\alpha_{2000} = 17^h20^m18.7^s$,

Table 4.20: Sources and count rates within ROSAT PSPC field of Draco

Source No.	α_{2000} $h\ m\ s$	δ_{2000} $^\circ\ '\ ''$	Count Rates 10^{-3} s^{-1}	ML	Off-axis $'$
1	17 17 51.22	+58 15 14.8	104.5±5.7	513.9	30.4
2	17 17 01.48	+58 14 47.5	21.3±4.0	18.6	34.2
3	17 19 43.43	+58 12 33.4	10.1±2.5	10.6	22.8
4	17 18 56.11	+58 08 07.6	5.4±1.5	12.4	20.1
5	17 20 33.99	+58 08 34.0	29.4±2.9	153.3	19.4
6	17 20 37.62	+58 02 09.4	27.5±2.5	256.5	13.5
7	17 14 10.75	+57 58 14.1	101.0±7.5	183.0	46.8
8	17 19 34.81	+57 58 50.3	12.2±1.7	87.7	9.5
9	17 20 21.62	+57 58 26.0	103.8±4.6	1735.4	9.2
10	17 20 51.84	+57 55 10.7	3.9±1.0	18.2	9.0
11	17 21 06.16	+57 53 34.6	3.4±1.1	10.6	9.9
12	17 24 26.32	+57 53 18.1	13.5±3.2	13.1	35.9
13	17 19 57.79	+57 50 07.3	50.1±3.3	402.8	0.3
14	17 19 21.59	+57 49 42.5	4.6±1.1	23.7	4.8
15	17 21 58.31	+57 49 21.3	75.3±4.2	776.9	16.1
16	17 20 37.22	+57 48 54.4	33.9±2.7	353.1	5.4
17	17 17 48.33	+57 47 50.2	4.8±1.3	13.3	17.3
18	17 15 34.90	+57 46 33.5	18.5±4.2	13.2	35.1
19	17 18 15.43	+57 47 01.2	4.3±1.2	13.7	13.9
20	17 18 01.84	+57 42 21.6	4.1±1.3	10.8	17.1
21	17 20 53.38	+57 41 56.5	3.6±1.1	13.3	10.8
22	17 19 28.49	+57 41 29.4	4.4±1.2	16.9	9.2
23	17 15 27.22	+57 40 17.3	25.8±4.4	24.9	37.3
24	17 18 20.18	+57 39 38.2	7.4±1.5	27.6	16.5
25	17 20 33.96	+57 39 07.9	6.1±1.4	26.4	11.7
26	17 24 54.94	+57 37 44.1	29.8±5.0	25.7	41.5
27	17 20 44.65	+57 35 18.4	10.5±2.0	17.4	15.8
28	17 21 00.81	+57 34 47.3	6.1±1.5	17.4	17.2
29	17 18 29.49	+57 34 23.4	125.3±5.5	1213.7	19.4
30	17 23 54.65	+57 30 03.0	13.4±3.5	10.2	37.3
31	17 15 21.96	+57 24 51.9	581.0±16.2	1330.6	44.5
32	17 24 52.01	+57 23 17.2	48.6±9.0	13.1	47.5
33	17 21 50.71	+57 18 29.9	22.8±4.4	16.3	34.8

$\delta_{2000} = 57^\circ 54' 48''$; *cf.* Figure 4.16). For the NED position, the upper limit count rate is 1.6×10^{-3} s^{-1}. Using the $\Gamma = 2.0$ power law model and Galactic column

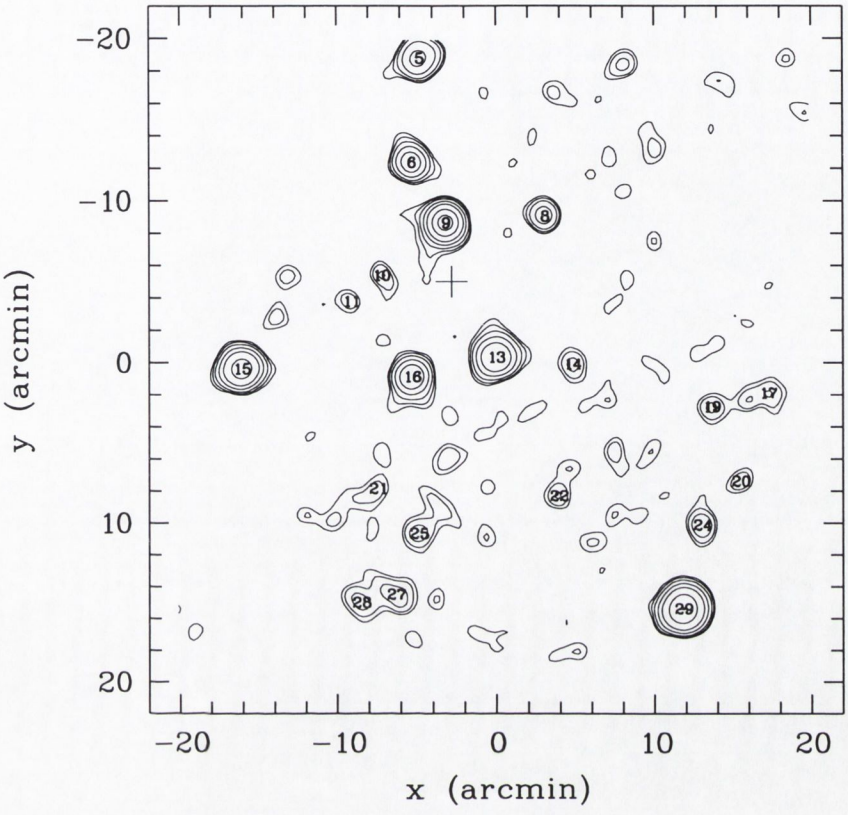

Figure 4.16: ROSAT PSPC contour plot of Draco, central $40' \times 40'$ area. The PSPC image has $15'' \times 15''$ pixels and smoothed with 2-pixel size Gaussians. The background level is ~ 0.42 cts pix^{-1}. The contours are 0.66, 0.78, 1.02, 1.62, 2.82, 6.42 and 12.42 cts pix^{-1}. The X-ray sources are marked with source numbers (see Table 4.19. The NED/RC3 position of the galaxy is marked with a cross. The Draco C-1 is in the centre of the field (No.13).

$N_H = 2.77 \times 10^{20}$ cm^{-2}, the unabsorbed (0.1–2.4 keV) flux $f_X < 3.0 \times 10^{-14}$ ergs cm^{-2} s^{-1} and luminosity $L_X < 2.0 \times 10^{34}$ ergs s^{-1} at the distance of 76 kpc.

4.17 IC 10 and the others

We examined the both frames of the ROSAT HRI observations for IC 10, no source were found at the position of the galaxy. The upper limit count rate from the second observation is listed in Table 6.1. The flux and luminosity are converted with the $\Gamma = 2.0$ power law model and Galactic column $N_H = 4.2 \times 10^{21}$ cm^{-2}.

The same model is used for other three galaxies, Tucana, Ursa Minor and Sagittarius, which are included in the PSPC fields with rather large off-axis angles (35′, 52′ and 44′, respectively). There are no sources detected at the positions of these galaxies. The values of the upper limits are also listed in Table 6.1.

Chapter 5

M32

5.1 Introduction

The Andromeda Galaxy companion M32 (NGC 221) seems to present itself as a promising candidate for a nearby example of low-level nuclear activity. Though small, it is one of the nearest Elliptical galaxies with a correspondingly clear central concentration. Benefitting from recent observational advances, kinematical and dynamical analyses have been pursued that probe regions nearer the nucleus of M32 than were reached before (*e.g.* Kormendy and Richstone 1995, van der Marel et al. 1998). The observed kinematics suggest, together with appropriate dynamical modelling, that the central mass distribution could be consistent with the presence of a 3×10^6 $M_\odot$ black hole.

When a massive black hole is present in the centre of a galaxy, nuclear activity is expected to be a distinct possibility (depending on available fuel). No signs of this were known for M32, but a ROSAT PSPC observation reveals a comparatively strong X-ray source coincident with its nucleus (Eskridge et al. 1996). There is further a suggestion of a weaker source about $0.5'$ NE of the main contributing source. The PSPC resolution (also degraded due to a $17'$ off-axis position of the galaxy in the detector) did not allow to distinguish between a low-level active nucleus or a collection of stellar X-ray sources. No distinction on the basis of the X-ray spectrum could be made between these two possible interpretations either, since as

a result of the limited spectral resolution of the PSPC detector several conceivable spectral shapes appear to fit the data perfectly.

In view of these alternative interpretations, X-ray observations of M32 at higher spatial and spectral resolution are evidently of interest. Results from a dedicated ROSAT HRI observation were recently published (Loewenstein et al. 1998), which provide a spatially much more detailed look at this X-ray source. The fairly strong source associated with M32 appears about 10″ away from a catalogued optical position of the galaxy. After subtraction of this source, some residual emission is suggested to remain at a position close to the centre of M32. After also an analysis of two ASCA observations with greater spectral resolution, the apparent offset of the main X-ray source from the centre of the galaxy and the large flux variations on relatively short timescale led these authors to propose an X-ray binary rather than an AGN as interpretation of this source.

In view of the still ambiguous interpretation of the M32 X-ray source, we have taken a fresh look at the available ROSAT data for this galaxy. Our new analysis of existing ROSAT PSPC and HRI data brings out differences with the results published previously and contributes to a re-assessment of the nature of this X-ray source, with a low-level AGN remaining an appealing possibility.

In the following we include, for completeness, our improved results for the PSPC data. The HRI results follow next, providing stronger constraints on the nature of the M32 X-ray source. Subsequently possible interpretations of this X-ray source are discussed in the light of our improved results.

5.2 X-ray data

The PSPC frame examined by Eskridge et al. (1996) for morphological information is the best targeted frame for M32 out of the first M31 survey in July 1991, which comprised 6 pointed ROSAT PSPC observations with exposure times of tens of ksec (Supper et al. 1997). A second survey of M31 in 1992 was carried out as a raster scan, featuring however short exposures. That best PSPC exposure (Identification

No. 600068p, see Table 5.1) is the only one that combines an exposure time of several tens of ksec with a position of M32 in the inner detector area. Figure 5.1 shows the distribution of all centre positions of PSPC fields with M32 included. Our analysis of this observation benefits from a re-processing of the satellite data. The exposure was taken in July 1991 for 30.0 ksec with M32 at an off-axis angle of 17′. The Photon Event Table was binned at 15″ again to form an image at standard PSPC resolution.

The one relevant HRI observation is centered on M32. This observation (Identification No.600600h) was taken in July 1994 with exposure time 12.7 ksec. Recently a bug in the SASS (Standard Analysis Software System) was discovered (URL:http://hea-www.harvard.edu/rosat/rsdc_www/aspfix.html) that may introduce an additional error term in the HRI PSF (Point Spread Function), depending on the year of observation. Software fixes have been developed in the ROSAT data centres and Dr S. Döbereiner of the Max Planck Institute for Extraterrestrial Physics in Garching kindly corrected our 600600h frame for this effect. We formed an image by binning the Photon Event Table at 5″ again, corresponding to the typical HRI resolution.

There is another HRI observation that included M32 in its field (ROR ID.600931) This observation was carry out during first two months of 1997. This HRI observation has a much longer exposure time, 169.4 ksec, which enables a deep survey of an M31 area in the HRI resolution. Unfortunately M32 is only located at the edge

Table 5.1: ROSAT observation log of M32

ROR ID.	Start Date	Exposure Time sec	Field Centre α_{2000} $h\ m\ s$	Field Centre δ_{2000} $^\circ\ '\ ''$	Off-set
600600h	1994.07.19	12,658	00 42 40.7	+40 52 12.0	0.5′
600931h	1997.01.04	169,416	00 41 24.0	+41 00 00.0	16.9′
600068p	1991.07.27	30,005	00 42 28.7	+41 08 24.0	17′
600064p	1991.07.15	48,760	00 41 02.4	+40 46 12.0	20′
600067p	1991.07.26	27,466	00 43 55.2	+41 30 36.0	41′
600079p	1991.07.14	41,666	00 39 36.0	+40 24 00.0	45′

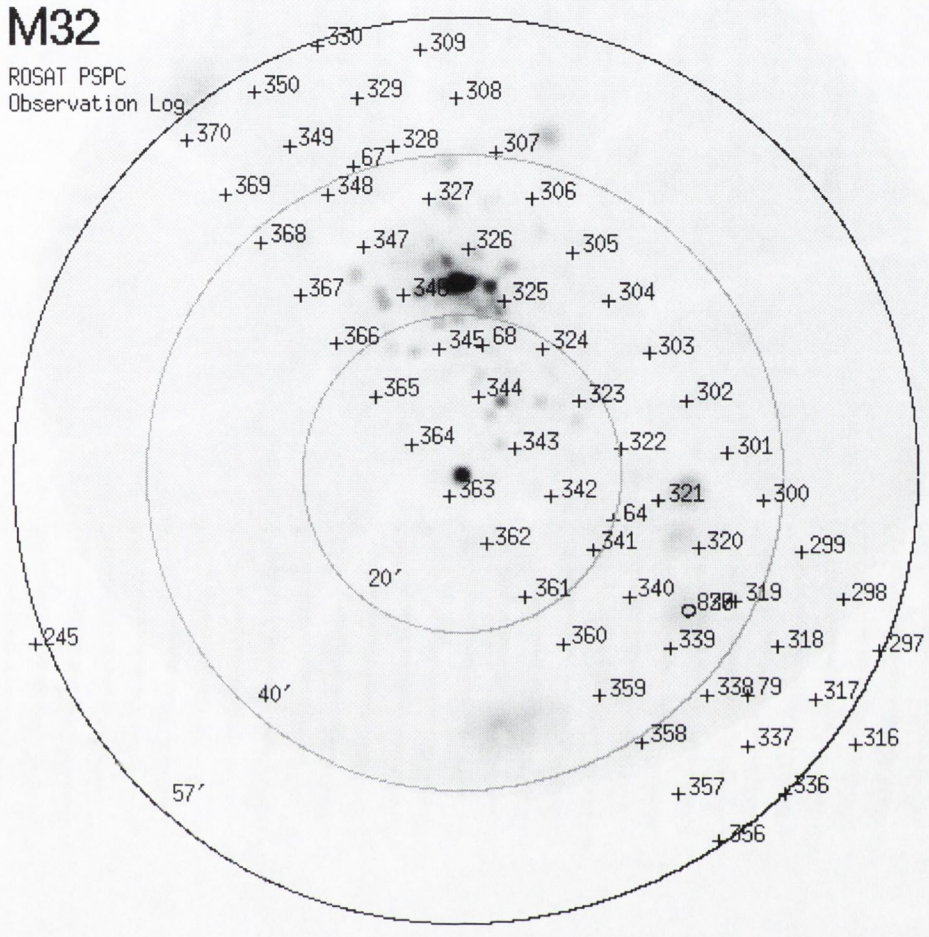

Figure 5.1: ROSAT PSPC observations with M32 in the field. The background is the PSPC image of observation ROR ID.600068 (see text). The centre spot is M32; the radii of the circles are 20′, 40′ and 57′. The numbers marked are the last three digits of observation ID, they begin with 600 for observations with "+", or 141 for "○".

of the field in this exposure (with off-axis angle about 16.9′). We also analyze this data set, in a same way as ROR 600600h, so to compare with the HRI frames with each other. Table 5.1 lists the observation log of long PSPC exposures and the 2 relevant HRI exposures.

5.3 Analysis of reprocessed PSPC observation

5.3.1 Morphology

The region around M32 in the PSPC image is presented in Figure 5.2b and shows no evidence for any additional source located half an arcminute NE of the main source. The previous result of that kind (Figure 5.2a, with several distorted contours, from Eskridge et al. (1996)) may be due to a bad satellite attitude solution. Overall, the PSPC field in this earlier analysis (Figure 5.2a) exhibits hints of diffuse extensions to the NE of a few other sources as well (Figure2a in Eskridge et al.), which would be consistent with the suggested satellite attitude effect. Our result for this X-ray source looks somewhat asymmetric, with wider spaced contours to the South, caused by its 17′ off-axis position to the South off the detector centre in this exposure. A radial profile of the M32 source confirms also for the reprocessed data that it is unresolved, as was concluded previously by Eskridge et al. The radial profile is presented in Figure 5.3a, together with the azimuthal profile in Figure 5.3b. The latter shows some variation, not unlike the HRI azimuthal profile (see Section 5.4.2), but the source asymmetry resulting from its off-axis position renders any interpretation regarding source structure uncertain.

5.3.2 Spectrum

Since for this observation the reprocessed data are now available for analysis, we determined again the X-ray spectrum to check consistency with spectral results published before. Besides improved satellite data, there are in two further respects differences with the previous analysis. Eskridge et al. combined photons from three long observations and used too many spectral bins (more than 100, see their Table 2) for their model fits. We however stay with 21 bins (obtained for S/N $\geq$ 13 per bin) close to an optimum spectral binning for PSPC data (*c.f.* Davelaar 1969) and we restrict our spectral analysis to the 600068p frame, in view of evidence for luminosity–dependent spectral variability of the X-ray source (Loewenstein et al. 1998).

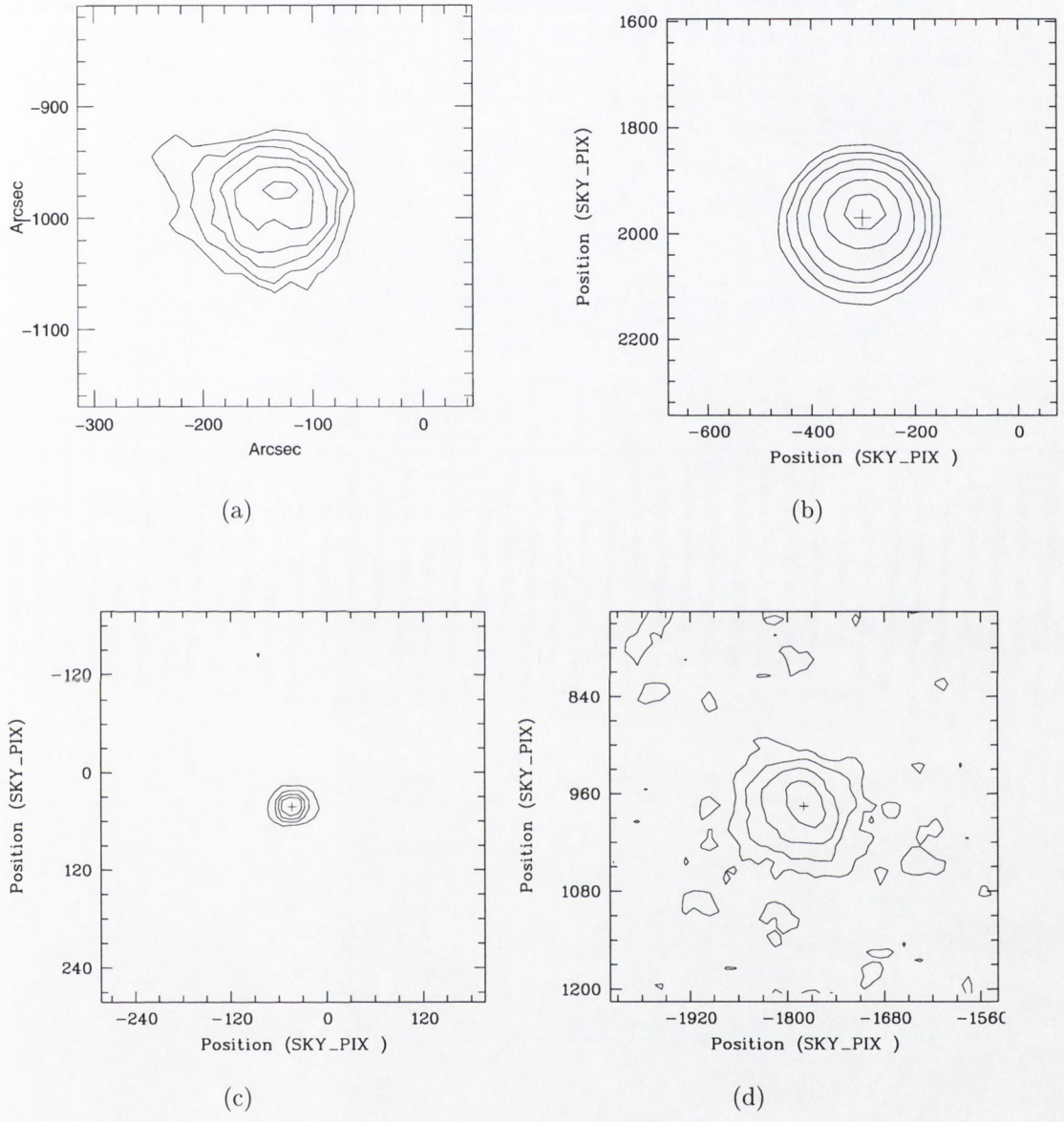

Figure 5.2: Contour plots of the X-ray source associated with M32: (a) ROSAT PSPC analysis of Eskridge et al. (1996), in a $6.25' \times 6.25'$ field, (b) our PSPC result in the same area, (c) and (d) ROSAT HRI contours for 600600 and 600931, respectively, in a $4.0' \times 4.0'$ field. The crosses refer to the position found for the X-ray source; 1 arcsec equals 2 sky-pixels. Contour values are (b) 6.5, 13, 26, 52, 104 and 170 cts pix^{-1}, (c) 1, 4, 7 and 10 cts pix^{-1}, (d) 2, 5, 10 and 20 cts pix^{-1}. The images for the plots have $15'' \times 15''$ pixels for PSPC and $5'' \times 5''$ pixels for HRI, and they have been background subtracted, vignetting and dead time corrected and smoothed by one-pixel size Gaussians.

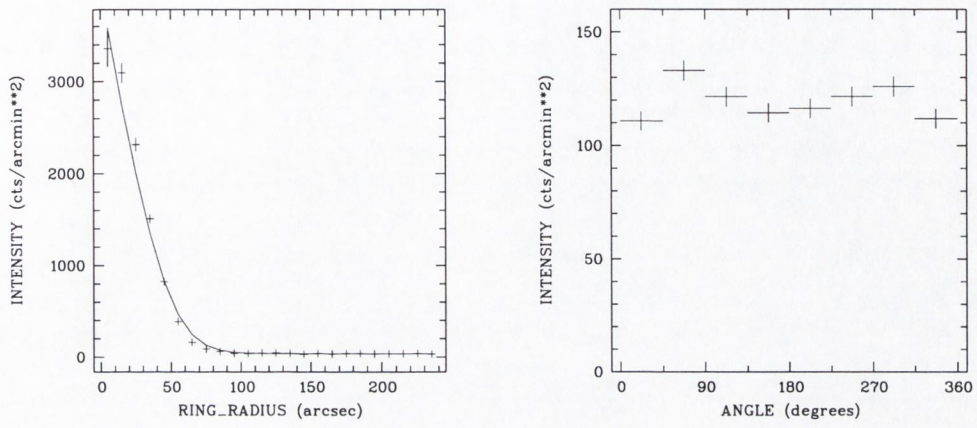

(a) (b)

Figure 5.3: ROSAT PSPC ring profiles of M32: (a) radial profile compared with the model PSF; (b) azimuthal brightness variation, data extracted within 4.0′ around source, the angles start from North clockwise.

The data were extracted within a radius of 2′ around the source centre. The contribution from the background was determined in two source–free regions at either side of the source and subtracted. The same three models were checked as in Eskridge et al., *viz* Power Law, Bremsstrahlung and Raymond-Smith. The results for these spectral model fits are summarized in Table 5.2, for both free N_H and fixed Galactic N_H. As an example, our Thermal Bremsstrahlung model fit for N_H free is shown in Figure 5.4. The fits with N_H fixed are in each case less good than those where N_H is left free, suggesting that during the 600068p observation some extra absorbing material close to the source may have been present. The trend for absorption columns that are higher than the Galactic value is present in all analyses. While considering their fitted N_H values consistent with the observed Galactic column for all models, the derived N_H values of Eskridge et al. lie above the Galactic value for all their three models and the error ranges quoted are inconsistent with the Galactic column for two of the three models. One of the models (Power Law) that Loewenstein et al. try for their ASCA datasets gives also higher N_H values than Galactic when N_H is left free to vary. Supper et al. (1997) include a short discussion of the M32 X-ray spectrum with their results of the first ROSAT M31 survey. Their Ther-

Table 5.2: The spectral fitting parameters of M32 (frame 600068p)

Model	wabs*powerlaw		wabs*bremss		wabs*raymond†	
N_H (10^{20}cm^{-2})	$12.7^{+5.3}_{-2.9}$	6.6‡	$9.7^{+2.5}_{-1.7}$	6.6‡	$9.6^{+2.6}_{-1.8}$	6.6‡
Γ	$2.03^{+0.32}_{-0.21}$	1.53				
kT(keV)			$2.0^{+0.7}_{-0.5}$	$3.5^{+1.2}_{-0.7}$	$2.0^{+0.7}_{-0.5}$	$3.0^{+1.0}_{-0.7}$
Abundance					$0.013^{+0.162}_{-0.013}$	$0.31^{+0.30}_{-0.23}$
χ^2_ν	0.78	2.21§	0.69	1.43	0.73	1.27

* "wabs" stands for photo-electric absorption using Wisconsin cross-sections.

† redshift fixed to 0.

‡ fixed to Galactic value (Stark et al. 1992).

§ error given when $\chi^2_\nu > 2$.

mal Bremsstrahlung and Power Law solutions for N_H are also higher than Galactic, with error ranges quoted that are inconsistent with the Galactic value. Loewenstein et al. refer to a re-analysis of the PSPC exposures examined by Eskridge et al. but give only Power Law indices for two of the three PSPC datasets, derived while fixing N_H to the Galactic column. An absorbing column higher than Galactic thus appears a realistic possibility. It is not straightforward to determine whether this absorbing material is intrinsic to the M32 X-ray source or lies somewhere along the line of sight. The latter could easily occur if M32 is located behind the disk of M31, notwithstanding earlier inferences that this satellite galaxy may be located in front of M31 (Ford et al. 1977). This would indeed generally lead to higher than Galactic columns, although the resulting values for N_H may differ if other fitting parameters change between observations.

We also checked the possible PSPC observations listed in Table 5.1. The 600064p and the 600067p frames have smaller off-axis angles for M32; in both fields, M32 is partially obscured by the supporting structure (ribs) of the PSPC. The count rates for M32 are 0.0459±0.0013 s^{-1} and 0.15069±0.0036 s^{-1}, respectively. Although the latter one has almost the same count rate as 600068p (0.1642±0.0028 s^{-1}), its background could hardly be estimated. The remaining frame is 600079 which has a 41.6 ksec exposure time. This observation had M32 in 45′ off-axis angle and obtained over 4,000 counts, which yields a count rate of 0.1922±0.0037 s^{-1}. This is about 20%

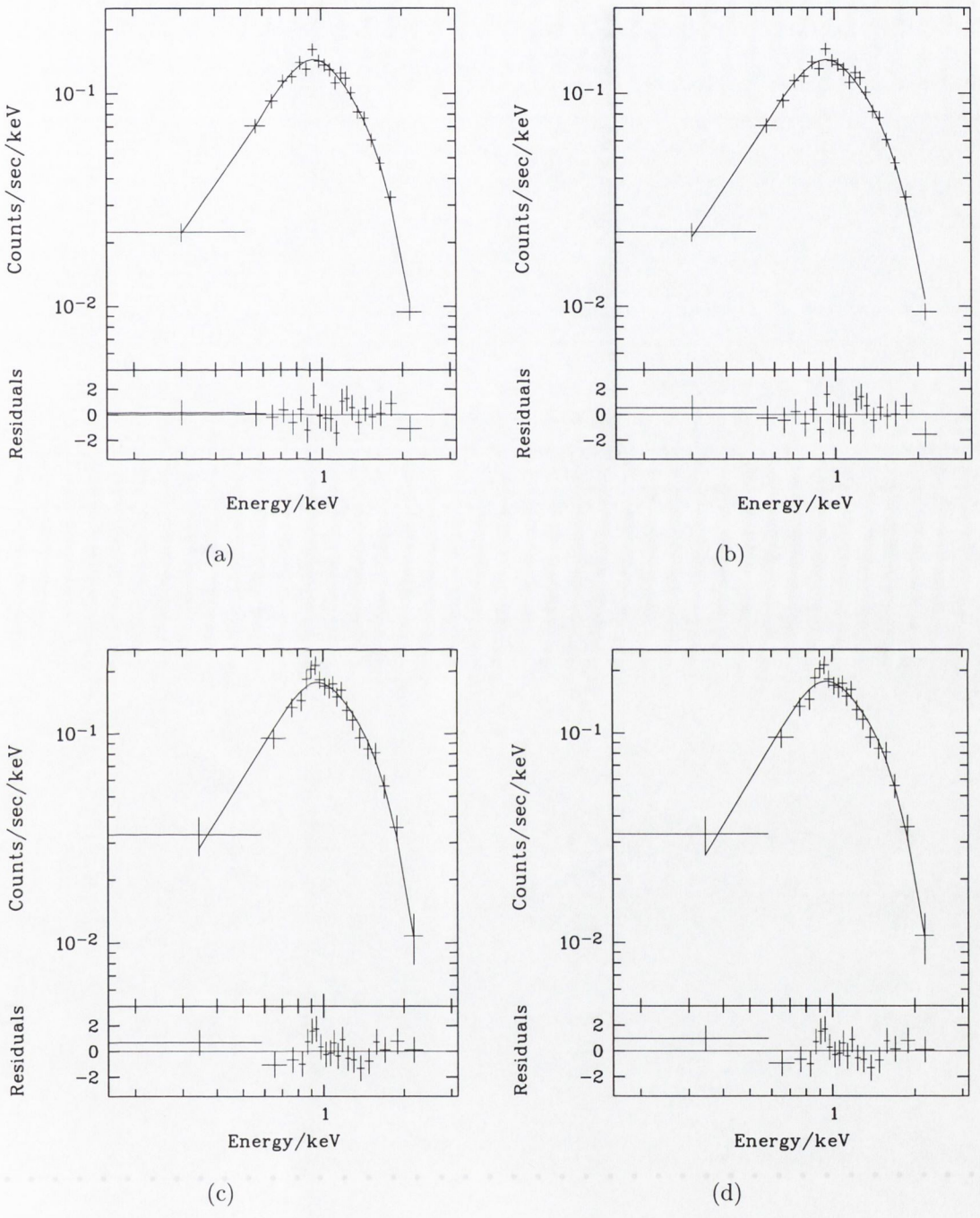

Figure 5.4: ROSAT PSPC spectra of M32 fitted with Thermal Bremsstrahlung model (a,c) and Power Law model (b, d). The data are from frame 600068p (a, b) and 600079p (c, d), respectively. The fitted parameters for frame 600068p are listed in Table 5.2 for details.

more than that of 600068p which was observed two weeks later. (See Section 5.5.2 for the discussion of brightness variations.)

In Figure 5.4, the fits to the Thermal Bremsstrahlung and Power Law models for the data of frame 600079p are also shown. The results are clearly similar to those for data frame 600068p. The spectral data are extracted within a 6.25′ radius area which is roughly 2.5 times the FWHM of the PSF at this off-axis angle. The background is extracted from outer area around the source. The annulus was checked with respect to source detection results in the field and ring profiles from the Photon Event Table to ensure no counts from other possible sources are included. The data are again binned to 21 channels, with $S/N \geq 9$. The best fit Thermal Bremsstrahlung model is with $N_H = 12.6 \pm 3.33 \times 10^{20}$ cm^{-2} and kT=1.95±1.91 keV ($\chi^2_\nu = 0.82$); while the Power Law model gives $N_H = 20.3 \pm 15.2 \times 10^{20}$ cm^{-2} and $\Gamma = 2.28 \pm 0.95$ ($\chi^2_\nu = 0.82$). Although the fitted parameters leave bigger errors than in the case of frame 600068p, the absorption columns come out higher than galactic again.

As for previous spectral analyses of this X-ray source, the various models with N_H free are all acceptable and no preference for one of these can be established from the statistical fitting results. The Raymond-Smith fit (with N_H free) would be consistent with zero abundance, as also Eskridge et al. found, thus tending towards Bremsstrahlung. The most promising descriptions for the M32 X-ray source will be either Power Law or Thermal Bremsstrahlung, the same choice to which Supper et al. (1997) and Loewenstein et al. (1998) restricted their spectral modelling.

Due to some difference in spectral shape of the actual data we get a steeper Power Law respectively lower–kT Thermal Bremsstrahlung or Raymond-Smith than Eskridge et al., but there are no abnormal differences. The results of Supper et al. (for Power Law and Bremsstrahlung) lie in between those obtained by Eskridge et al. and this paper. Since both Eskridge et al. and Supper et al. combined several long PSPC exposures, the results in Table 5.2 cannot be expected to be exactly the same. Loewenstein et al. present spectral analyses of ASCA data, which captured M32 in a low luminosity state. Their results vary sometimes substantially with the PSPC results, but given the possible luminosity-dependent spectral variability that

they notice, a direct comparison with the PSPC data is not straightforward. The effect that Loewenstein et al. refer to is that the M32 X-ray source is harder when the luminosity is higher. Our 600068p PSPC frame has the lowest luminosity of the three PSPC frames analysed by Eskridge et al. (see their Table 3) and our PL index is indeed softer than what they derive for the three frames combined (and softer than for the combination of PSPC exposures in Supper et al.). The PL index that Loewenstein et al. quote for this 600068p PSPC observation is derived for N_H fixed and is nearly the same as ours for N_H fixed (1.47 resp. 1.53). From these results it is clear that an investigation into the exact nature of the M32 spectral variability will be an interesting project for future X-ray observations.

5.4 Analysis of HRI frames

5.4.1 Source detection in ROR 600600h

Loewenstein et al. (1998) found a source position that is shifted peculiarly by ca. 5″ towards the NW from the peak flux. Since after a source subtraction exercise some residual emission is left closer to the centre of M32, where also their source detection algorithm finds a weak second source, they hint at the possibility that a weak X-ray source in the nucleus of M32 pulls the detection position towards it. Since this shift seems a bit large in view of the relative strengths of the main source and the possible residue, we decided to re-analyse the HRI data (ROR ID. 600600h).

In the field of 600600, 14 sources are detected with $ML \geq 10$, listed in Table 5.3. No.6 is the brightest and is located at the edge of the field. M32 (No.9) is the second brightest with a count rate of $11.69 \pm 0.99 \times 10^{-3}$ s^{-1}. 6 of them may have optical counterparts, most of which are globular clusters. Figure 5.5 shows the contour plot of the whole field overlaid on the optical image. In next two sections, the morphology and the position will be described in detail.

Table 5.3: Point sources within ROSAT HRI field of M32

Source No.	α_{2000} $h\ m\ s$	δ_{2000} $^\circ\ '\ ''$	Count Rate 10^{-3} s^{-1}	ML	Off-axis $'$	Optical* Counterpart
1	00 42 29.45	+41 08 18.4	4.38±0.91	19.4	16.3	Bol 101
2	00 43 13.61	+41 07 21.1	4.14±1.00	12.5	16.4	Bol 158
3	00 42 29.19	+41 04 37.4	4.86±0.77	49.2	12.6	
4	00 42 15.88	+41 01 16.3	7.56±0.85	148.0	10.2	Bol 82
5	00 41 49.85	+41 01 02.3	2.14±0.60	11.6	13.1	
6	00 43 58.34	+40 59 53.2	16.65±1.49	145.3	16.5	
7	00 42 22.22	+40 59 25.3	2.61±0.50	46.3	8.0	
8	00 42 16.55	+40 55 51.9	2.17±0.45	39.3	5.9	
9	00 42 42.71	+40 51 51.3	11.69±0.99	383.0	0.5	M32
10	00 42 35.08	+40 48 34.8	2.43±0.49	31.2	3.8	Bol D63
11	00 42 03.14	+40 46 08.0	2.03±0.47	25.9	9.4	
12	00 43 55.40	+40 45 27.4	2.88±0.79	10.5	15.6	
13	00 42 40.15	+40 43 15.9	1.37±0.41	13.7	8.9	
14	00 42 14.11	+40 39 14.4	2.52±0.66	12.7	13.9	

* Bol numbers are globular cluster candidates listed by Battistini et al. (1987)

5.4.2 Morphology

At an off-axis angle of 0.5′, the X-ray emission associated with M32 appears as a single source for which the source detection algorithm returns a position that agrees closely with the brightness peak (Figure 5.2b). In Section 5.5.1 we show that a shift by about 5″ for the position determined by the detection algorithm, due to a putative source associated with the M32 nucleus at ca. 10″ distance as suggested in Loewenstein et al. (1998), is an unlikely interpretation, which supports the correctness of our plotted detection result.

The source detection routine attributes a small extension to the source associated with M32. To investigate this further we determined the radial brightness profile and the azimuthal brightness variation for this source and also for a few other sources in this HRI field. The radial brightness profiles indicate that the M32 source is broadened by about 2.7″ (Figure 5.6a), while such a broadening is not observed for a couple of other sources in the inner portion of the HRI detector (Figure 5.7). The

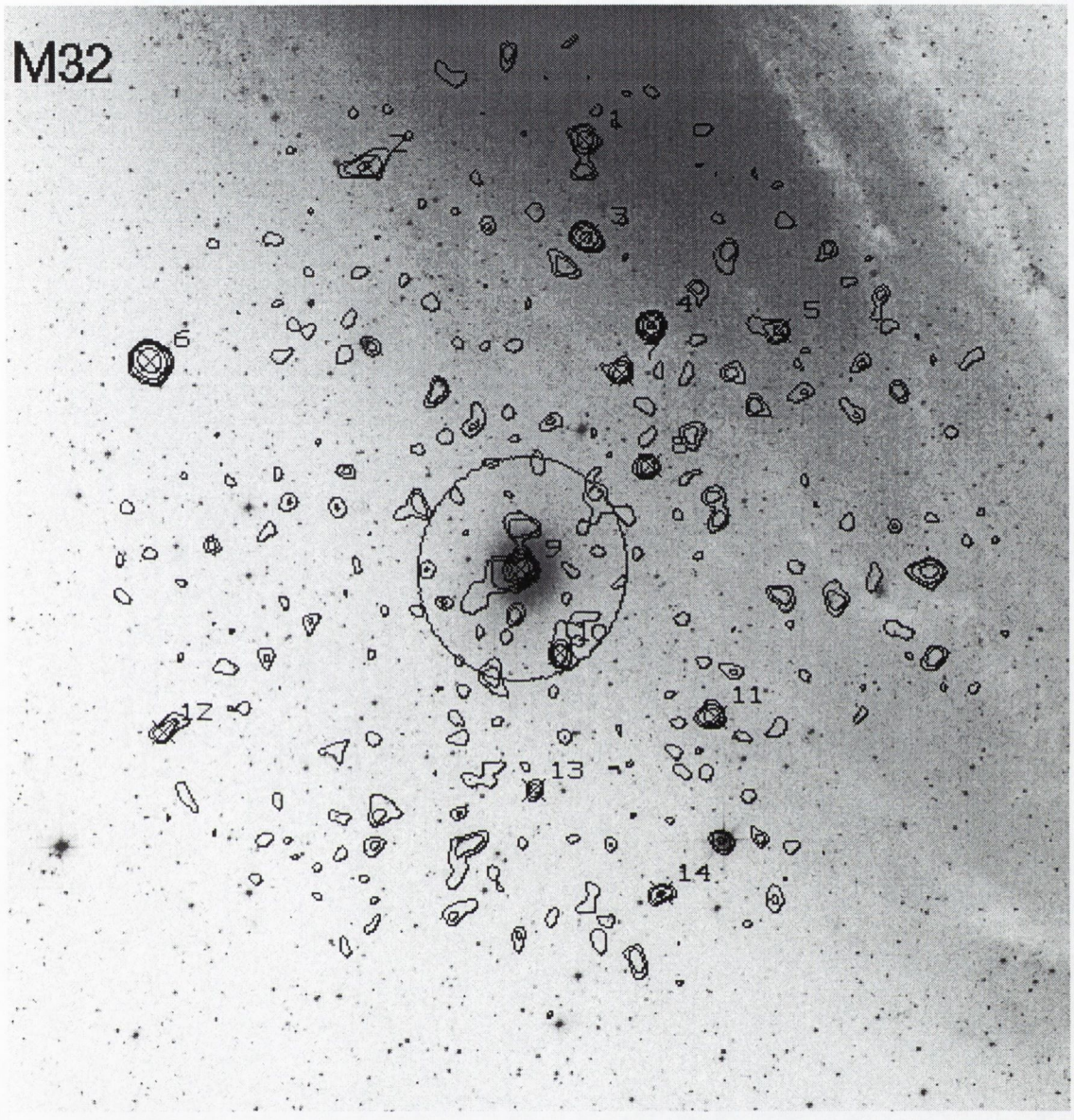

Figure 5.5: ROSAT HRI contour plot of M32 overlaid on optical image covering the whole HRI area. The D_{25} ellipse (from the RC3 catalogue) is indicated. The background level in the HRI image is ~ 0.35 cts pix^{-1}. The contour levels are 0.47, 0.53, 0.65 0.95 and 1.55 cts pix^{-1}. The HRI image has $5'' \times 5''$ pixels and is smoothed with 3-pixel size Gaussians. The optical image is taken from the DSS.

broadening that is apparent for M32 itself is on the other hand a small extension and the neighbouring sources that can be used for comparison have less counts than M32. In Figure 5.2c M32 appears as a slightly elliptically shaped source, elongated roughly E-W, which may just be recognizable in the azimuthal profile

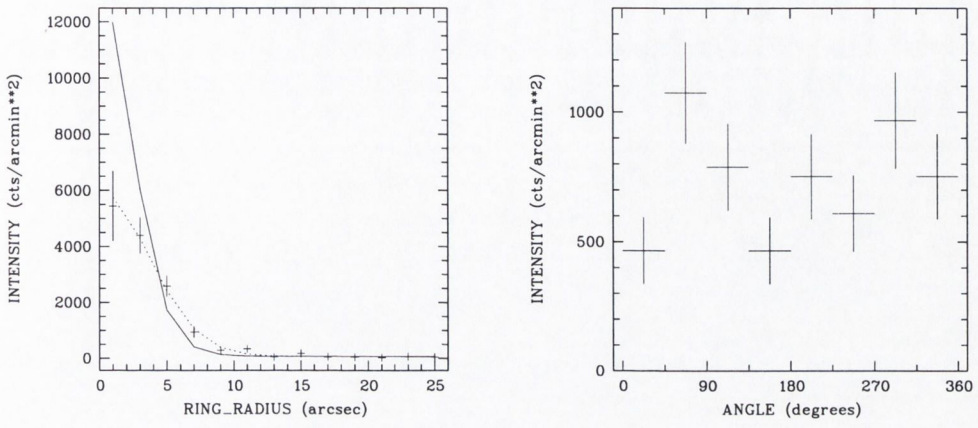

(a) (b)

Figure 5.6: ROSAT HRI ring profiles of M32: (a) radial profile compared with model PSF (solid line) and PSF broadened by 2.7″ (dotted line); (b) azimuthal brightness variation, data extracted within 16″ around source.

(Figure 5.6b) as somewhat higher bins around angles 90° and 270°. Comparing N–S and E-W annular sectors between 8″ and 16″ as shown in Figure 5.8 (*cf.* Elvis et al. 1983), we find N–S 6 ± 2.5 counts and E–W 26 ± 5.1 counts, which reflects this elongation. Other sources in the field exhibit different azimuthal variation. The HRI

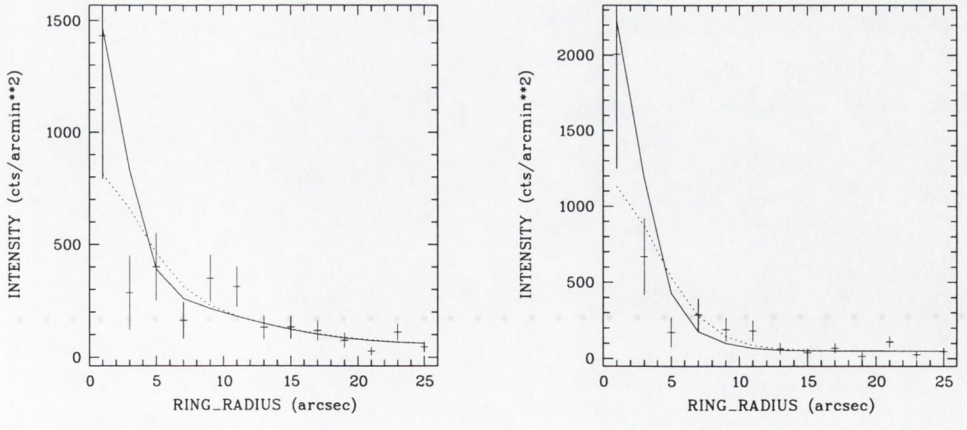

(a) (b)

Figure 5.7: ROSAT HRI radial profiles of two sources in the same field of view as M32, compared with their model PSFs (solid line) and PSFs broadened by 2.7″ (dotted line).

data do not present great photon statistics and we conclude only that the M32 source could well be elongated in the E–W direction, which needs confirmation from future Chandra/AXAF observations. In Section 5.5.3 we discuss what the implications are of a source extension.

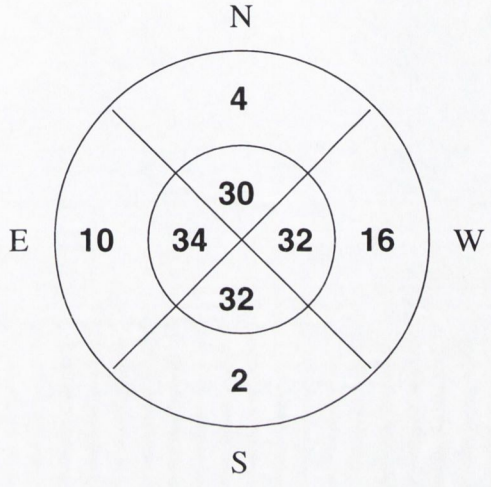

Figure 5.8: ROSAT HRI integrated counts of M32 within 16″ radius. The inner circle is 8″ and four 90° sectors around the cardinal directions are indicated.

5.4.3 X-ray position versus optical positions

A couple of the (non-M32) HRI sources not too far from the field centre have optical counterparts (objects Bol 82 and Bol D63 from Battistini et al. (1987), see Table 5.3) that suggest positional corrections of $-2''$ in RA and $+3''$ in DEC for M32 itself. When these adjustments are applied, the X-ray position will be $\alpha_{2000} = 0^h42^m42.5^s$ and $\delta_{2000} = +40°51'55''$. The offset of the X-ray source from the optical nucleus of M32 is still ca. 8″, (see Figure 5.9) roughly in Easterly direction. This refers to the most accurate optical position ($\pm 0.7''$) returned by the NED, but the original reference for these particular measurements (Palumbo et al. 1988) indicates that for very extended objects like M32 greater errors might occur. In that case the results by Gallouët et al. (1973) and Dressel and Condon (1976) are also of interest (errors $\pm 4''$), yielding offsets of ca. 4″ – 7″. When all optical positions with errors of at most a few arcsec are considered, it is clear that no agreement exists between the various results (differences between them of the order of the X-ray/optical offsets)

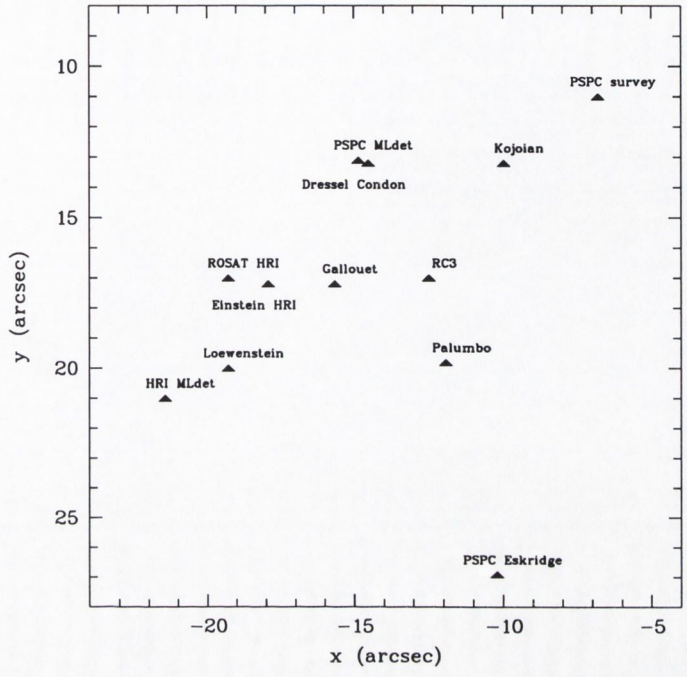

Figure 5.9: M32 positions in various observations and catalogues. Top is North, left is East. X-ray positions: PSPC and HRI MLdets are directly from ML detection results; 'ROSAT HRI' is corrected position; 'Loewenstein' from Loewenstein et al. (1998); 'PSPC Eskridge' from Eskridge et al. (1996); 'PSPC survey' from Supper et al. (1997). Optical positions are from NED and marked with author's surname(s), except 'RC3'.

and that an association of the M32 X-ray source with the nucleus of the galaxy is perhaps difficult to exclude on the basis of presently available data. M32 will require a dedicated optical position measurement before any X-ray/optical offset can be reliably established.

5.4.4 The other HRI observation (ROR 600931h)

M32 was included in the other HRI observation (ROR 600931h) in 1997. In this observation, M32 collected over 2,000 counts during the observation time (169 ksec). The corresponding count rate is $13.28 \pm 0.37 \times 10^{-3}$ s^{-1}, which is a little higher than that in frame 600600h. The variability measurement is 1.5.

The contour map is shown in Figure 5.2d. The large off-axis angle gives of course

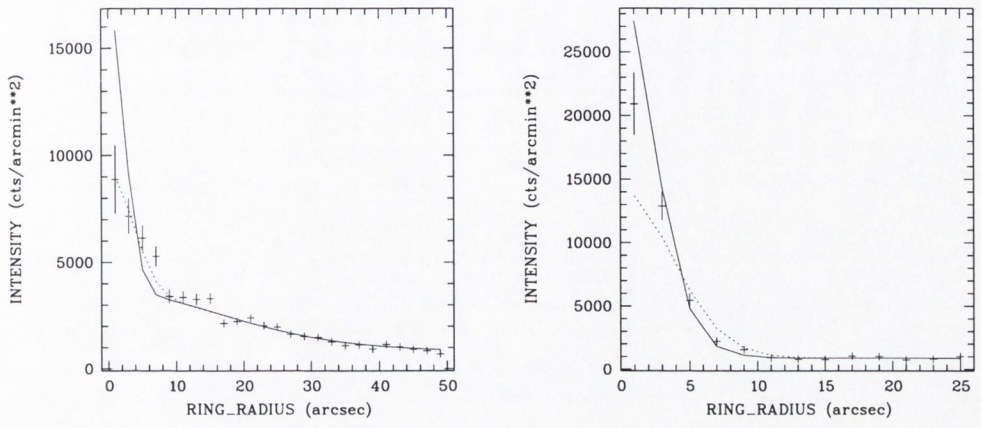

(a) (b)

Figure 5.10: ROSAT HRI radial profiles of two sources in the field of 600931h: (a) M32 and (b) another source, compared with their model PSFs (solid line) and PSFs broadened by 2.7″ (dotted line).

much wider distribution of source photons. The asymmetry of the contours is clearly seen along the radial direction from the field centre which is NW from the source position. Nevertheless, the countours are again with no sign of an additional source to the NE. This agree with the results from our PSPC and HRI analyses above.

To study the possible extension of the source, the ring profile is again plotted to compare with the model PSF (Figure 5.10). From the profile, a PSF model broadened with 2.7″ would fit the data well. The profiles for a few other sources in the field, which are not extended according to the detection routine, have been compared with their PSF models. We find that any extra broadening is less than 1″ (which is of minor influence on the possible M32 broadening), which may be due to the bug in SASS which affects half of the data of 600931h (observed before 16 January 1997, when a yearly reset of time is carried out), or to other effects. Figure 5.10b shows one example of these source.

As of the source position, the globular clusters Bol 82 and Bol 117 may be used for astrometric correction. The X-ray position then can be adjusted to $\alpha_{2000} = 0^h42^m42.31^s$, $\delta_{2000} = +40°51'51''$; this is a few areseconds from the corrected position obtained for 600600h, which can be easily occur in view of the great off-axis angle

in this HRI exposure ($\sim 17'$).

5.5 Discussion

5.5.1 Residual emission close to the centre of M32?

The idea that a source at a few arcsec distance could cause a shift in detection position (see Section 5.4.2) as reported by Loewenstein et al. (1998) can be tested with a simple simulation. Two HRI sources are generated (with the EXSAS software) and added together at $10''$ separation with count ratios varying between 12:12 and 12:1 (the latter roughly the ratio quoted in Loewenstein et al. and $10''$ being close to the separation between main source and possible residue). Figure 5.11 shows the effect of the second source on the position returned by the detection algorithm, as average of 16 simulations for each of the plotted points.

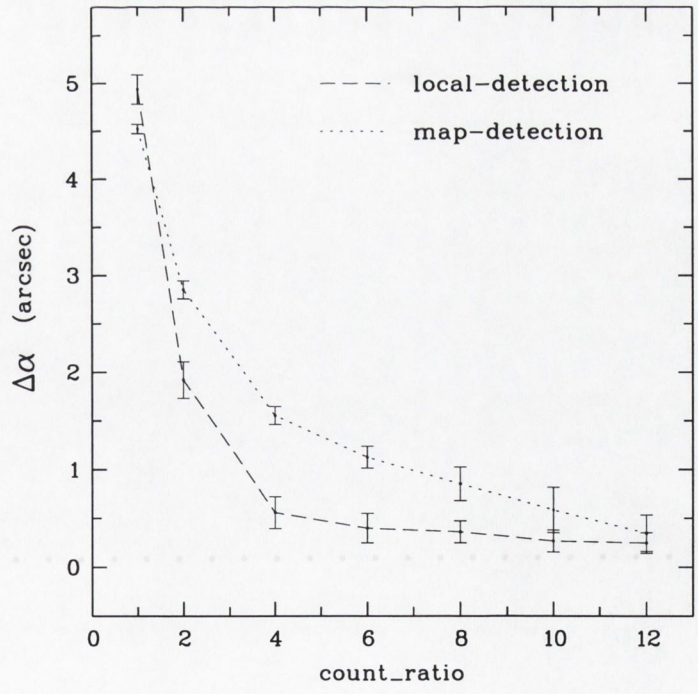

Figure 5.11: Source position affected by an additional source for various count ratios from 12:12 to 12:1. Two sources are simulated for the ROSAT HRI detector with $10''$ separation. Averages for 16 simulations are connected by dashed and dotted lines; the error bars represent the rms errors for these simulations.

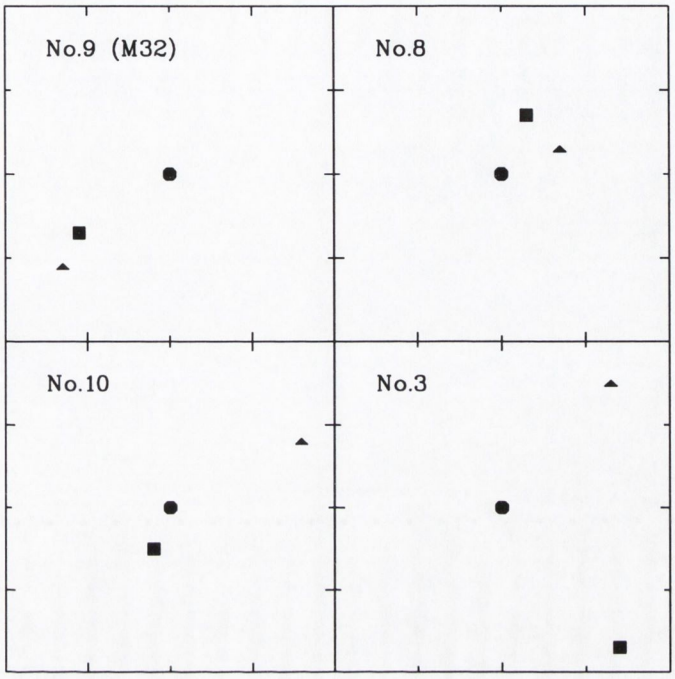

Figure 5.12: Examples for differences among positions given by local, map and ML detection method. The sources are in frame 600600h and are M32 itself plus three sources not too far from the centre. The box size for each source is $2'' \times 2''$. The triangle, squre and dot are local, map and ML position respectively.

As expected a halfway position is found for two equal sources, but for the ratio relevant for the case of M32 any shift is less than $1''$. Figure 5.11 displays the effect for the local- and map detection steps, since the simulations do not produce a photon event file as is required for the normally reported ML (Maximum Likelihood) detections. We have checked however that for sources near the centre of the image and with strengths like the M32 source the ML detections are generally some $0.5''$ differing from the positions found with local- and map detections (see Figure 5.12 for examples). Since also our own detection result coincides with the peak of the brightness distribution, we conclude that the much larger offset from the brightness peak in Loewenstein et al. is probably not correct. The uncertainties in positioning also cast doubt on the subsequent source subtraction attempt. Furthermore, their banana-shaped residue is not typical of a proper source being uncovered. It is noted that the residue is only midway between the main source and the M32 optical

position that is referred to, which somewhat diminishes its meaning. It is more likely that the small residue was caused by the broadening effects of the software bug mentioned in Section 5.2, which were corrected for the present analysis.

5.5.2 PSPC and HRI fluxes

Loewenstein et al. (1998) have summarized the X-ray brightness history of the M32 source (Figure 5.13). The PSPC data points are often above the HRI flux, but some are comparable. This implies real increases in brightness rather than the PSPC resolution allowing a completer flux measurement of an extended source. Over the entire timespan available, from Einstein till ASCA, there seems to be a base level for the M32 flux and only the ROSAT PSPC appears to have witnessed a flaring interval. Perhaps the base level indicates the X-ray flux from an extended component, in which the source of the X-ray variation is situated.

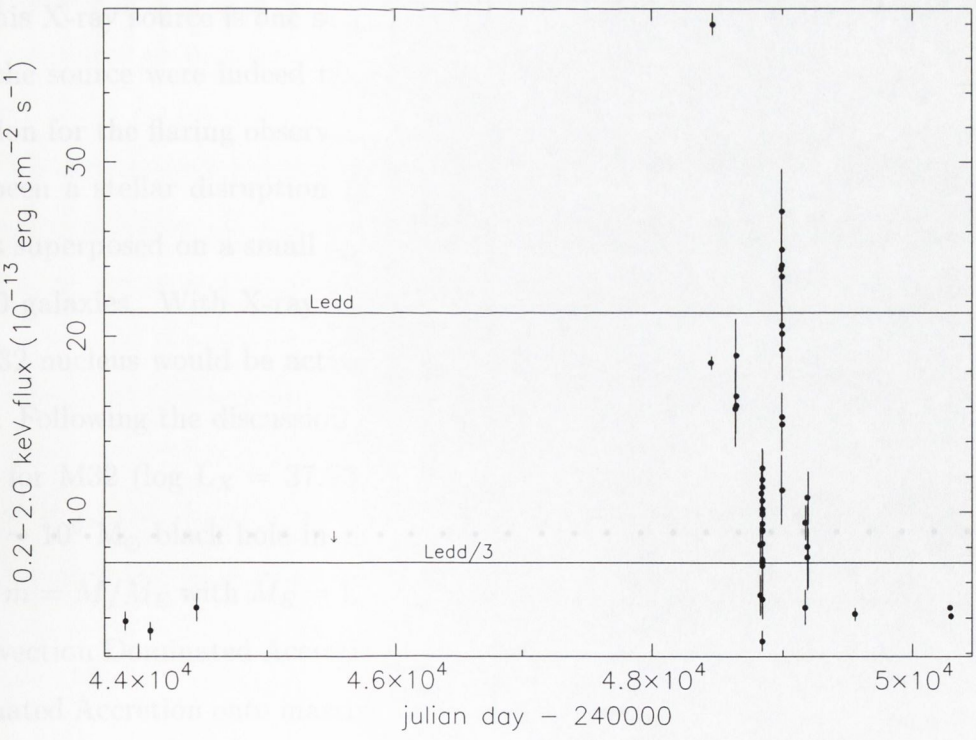

Figure 5.13: X-ray brightness history of the M32 source, from Loewenstein et al. (1998).

5.5.3 Nature of the M32 source

The present study shows the X-ray source associated with M32 as one source, both at PSPC and at HRI resolution, but possibly with intrinsic structure and at an uncertain offset from the optical nucleus. If a source extension can be confirmed with future observation then this will provide an important clue as to the nature of this source. It is interesting to discuss what the implications of an extended source in or near the nucleus of M32 would be. Depending on the possible positional consistency with the centre of M32, the source could be a low-level active nucleus, a SNR or perhaps a star-formation complex. The last possibility is not likely since no on-going starformation is known for M32, unless the source is a chance superposition and belongs to M31; in both cases such a complex would be only some twenty parsecs in size. Another possibility is a chance superposition of a Galactic source. Given the notable coincidence of one of the brightest sources in the general M31 field with this satellite galaxy of the Andromeda Galaxy, we will proceed on the assumption that this X-ray source is one source complex that does belong to M32.

If the source were indeed the nuclear source in M32, then an interesting interpretation for the flaring observed with the PSPC (see Section 5.5.2) is that it could have been a stellar disruption flare as described by Rees (1988). Perhaps such a flare is superposed on a small specimen of hot gas halo as often observed around E and S0 galaxies. With X-ray luminosities between roughly 10^{37} and 10^{38} erg s^{-1}, the M32 nucleus would be active at a remarkable low luminosity (see Loewenstein et al.). Following the discussion of Mahadevan (1997) and using the Einstein luminosity for M32 ($\log L_X = 37.73$, Fabbiano et al. (1992)), the mass accretion rate of the $\sim 10^6$ $M_\odot$ black hole in the core of M32 is around $\dot{m} = 10^{-9}$ (in Eddington units: $\dot{m} = \dot{M}/\dot{M}_E$ with $\dot{M}_E = L_E/c^2$), which because of its low rate is suggestive of an Advection Dominated Accretion Flow. For comparison, discussions of Advection Dominated Accretion onto massive black holes indicate that LINERs may have $\dot{m} \sim 10^{-2}$–10^{-3} (Lasota et al. 1996), regular Ellipticals $\dot{m} \sim 10^{-3}$–10^{-5} (Mahadevan 1997) and Sgr A* in the centre of our Galaxy $\dot{m} \sim 10^{-6}$ (Narayan et al. 1995). The M32 black hole thus takes the most extreme position into the Advection Dominated Ac-

cretion regime. Various authors (*e.g.* Narayan 1996; Lasota et al. 1996; Reynolds et al. 1996) have drawn the attention to the possibility that relatively small increases in $\dot{m}$ can cause appreciable increases in the X-ray luminosity, as a result of a transition from Advection Dominated to thin disc accretion. This is a potentially relevant interpretation for the observed X-ray lightcurve of M32, with a basic low state and a temporary transition into a high state during the ROSAT PSPC observations.

The current status of positional information in the optical leaves a SNR interpretation as an alternative option for an extended source. A broadening by 2.7″ would correspond to nearly 20 pc at the distance of M32, which is quite normal for SNRs in our Galaxy and in the LMC. The observed brightness increases during the PSPC exposures could originate from an associated pulsar. Notice that Eskridge et al. (1996) found a weak indication for a period of 1.27 days. This is slow for a pulsar but it could be part of a binary that survived the supernova explosion. Its age is easily consistent with the intermediate population that several authors have inferred from optical spectroscopy. Given the expected lifetimes involved, the supernova itself should have been of type Ia, which is indeed typical of spheroidal systems. The observed X-ray luminosity during the ROSAT PSPC measurements (up to $\sim 10^{38}$ erg s^{-1}) is consistent with such a LMXB, but X-ray binaries are normally not found together with SNRs. (NB A LMXB unrelated to SNR or AGN would require perhaps too special an alignment of two sources with this galaxy.) The low-state X-ray emission does on the other hand not produce detectable line emission in the ASCA SIS spectrum of Loewenstein et al., as would be characteristic for shell-type SNRs (but Crab-like SNRs may not show line emission, *e.g.* Wang and Gotthelf 1998). A SNR could further be expected to produce detectable radio radiation. The study of Berkhuijsen (1986) allows to estimate the expected level of radio flux density at 1000 MHz for a SNR with known X-ray emission. For the Einstein luminosity of $L_X=10^{37.73}$ erg s^{-1} (Fabbiano et al. 1992) a f_{1000} of around 10 mJy is expected, which is contrasted by an upper limit at 1400 MHz of 4 mJy (Roberts et al. 1991). The scatter in the X-ray and radio properties of SNRs let us cautiously interpret this – together with the absence of X-ray lines – as lending more weight to an AGN

interpretation for an extended source. If the weak indication for periodicity were substantiated, a possible explanation could be an emission feature in the accretion flow around the central object.

It is interesting that the present study leaves a low-level active nucleus as a conceivable possibility. This would be particularly relevant for issues like the prevalence of active nuclei in the Universe and generally the measurable high-energy signatures of the very cores of galaxies. In this regard it is intriguing that several of the nearest normal galaxies do have a source in their centre that shows up as an outstanding source in at least one wavelength interval: the Milky Way (at radio), M32 and M33 (at X-rays). Future X-ray observations of the spatial structure and of the spectral and temporal behaviour of the M32 X-ray source will no doubt allow to establish the nature of this source in a definite way.

Chapter 6

The population of nuclear cores in Local Group galaxies

6.1 Introduction

In a search for "Dwarf" Seyfert Nuclei, Ho et al. (1997) use the sample of emission-line nuclei derived from a recently completed optical spectroscopic survey of nearby galaxies (Ho et al. 1995), in an attempt to quantify the incidence of local ($z \sim 0$) nuclear activity. They conclude that the population of AGNs is very large: approximately 43% of the galaxies in their survey (over 400) can be regarded as active. They distinguish three classes of AGN: Seyfert nuclei, low-ionization nuclear emission-line regions (LINERs), and transition objects assumed to be composite LINER/H II–nucleus systems.

On the other hand, dynamical analyses suggest that at least 20% of nearby kinematically hot galaxies (*i.e.* ellipticals and spiral bulges) have massive dark objects (MDOs) in their centre (Kormendy and Richstone 1995). Because the black hole quasar remnants are expected to be common in galaxy centres, the MDOs are probably supermassive black holes. Recently, based on the HST photometry and ground-based kinematics, Magorrian et al. (1998) examined a sample of 36 nearby galaxies, of which 32 fit well to their models. They further concluded that 97% of early-type galaxies would have MDOs. Their sample include two Local Group

galaxies M31 and M32.

In the X-ray band, many nuclei of galaxies exhibit some level of recognizable activity. Very low level AGNs were recognized in this way in some of the nearest galaxies: the Milky Way (10^{35} erg s^{-1}, Genzel and Townes 1987), M31 (2.1×10^{37} erg s^{-1}, Trinchieri and Fabbiano 1991), M81 (1.7×10^{40} erg s^{-1}, Elvis and Van Speybroeck 1982).

As seen in previous chapters, the ROSAT Data Archive allows us to check several of the very nearest galaxies (namely members of the Local Group) for high energy emission. In this chapter, the X-ray examinations of the nuclear region for the galaxies in the Local Group are summarized, and the overall X-ray characteristics are discussed.

6.2 Results on cores from ROSAT observations

6.2.1 Overview

For most of the Local Group galaxies (Table 2.1), ROSAT X-ray data are available. Table 6.1 summarizes those 22 galaxies with the X-ray results from their nuclear region. Many of the galaxies listed here are analyzed for the first time or have been re-analyzed in order to ensure homogeneous data, except for M33 and the Milky Way which are taken from the literature (respectively Schulman and Bregman (1995) and Predehl and Trümper (1994)). The PSPC results (most are upper limits) are listed only if no HRI data are available. The optical positions are from SIMBAD or NED, except that for Sagittarius the position of the central cluster M54 is used. The X-ray positions are the result of ML detections. In only a few instances sources were detected in the central areas of the galaxies, or even in the bodies of these galaxies at all. For undetected centres, upper limits were determined for the known optical positions of these systems. In the EXSAS upper limit detection routine, the position at which the X-ray upper limit is evaluated may move a bit away from the optical one, especially in the PSPC field. In the case of the Tucana dwarf galaxy the position for X-ray upper limit evaluation is fixed to avoid contamination by a

detected source.

The present results are listed in Table 6.1, together with results published previously(*i.e.* M33 and Milky Way), as confirmed cores (+), possible cases ($\diamond$), suspicious associations (:) and non-detections (−). Low-level activity is well-established only for the Milky Way and M31. M32 remains a promising candidate. M33 features a strong source (M33 X-8) very close to its nucleus. A period was suggested that could imply a stellar binary (Dubus et al. 1997), but widely and fairly regularly spaced observations could produce spurious periods (*cf.* Deeming 1975, Matsuoka et al. 1990) and we keep this source as a possible core. The LMC and SMC have many sources but it is perhaps not sufficiently clear where their centres are located for deciding anything; in Table 6.1 we mark these two satellites of our Galaxy with a "?" and do not attempt to derive upper limits. Observational work on the Magellanic Clouds is also often like Milky Way research in character rather than like extragalactic work and may need a different approach from the other Local Group galaxies.

6.2.2 Comments on detections

By far the strongest case in the present work is M32 for which we re-analyzed PSPC and HRI observations that had already been reported in the literature. Eskridge et al. (1996) suggested either a low-level AGN or a collection of stellar sources on the basis of ROSAT PSPC data. Loewenstein et al. (1998) interpret the higher resolution data (ROSAT HRI), in conjunction with ASCA observations, as a low-mass X-ray binary on the basis of strong variability on short timescales and an apparent offset from the optical nucleus. Re-analysing these data we find that the M32 source may be slightly extended and that an offset from the centre is not well established. At the present stage a nuclear source remains thus an interesting possibility. The detailed discussion is in Chapter 5.

Table 6.1: X-rays from the cores of the Local Group galaxies

Name	Optical α_{2000} h m s	Optical δ_{2000} ° ′ ″	X-ray α_{2000} h m s	X-ray δ_{2000} ° ′ ″	Count rate and error 10^{-3} s^{-1}		Unabsorbed flux f_X (0.1–2.4 keV) 10^{-14} ergs cm^{-2} s^{-1}	Luminosity L_X and $\log L_X$ 10^{36} ergs s^{-1}		Central X-ray source?
Pegasus	23 28 34.40	+14 44 50.0	23 28 37.79	+14 44 40.1	<1.3		<3.0	<12.0	37.08	–
Sextans A	10 11 05.70	−04 42 28.0	10 11 01.65	−04 42 47.5	<0.21		<1.4	<2.8	36.45	–
NGC 3109	10 03 06.80	−26 09 32.0	10 03 07.70	−26 09 25.8	<0.82		<1.9	<3.6	36.56	–
IC 10	00 20 24.70	+59 17 30.0	00 20 24.64	+59 17 32.4	<0.24		<4.5	<8.4	36.92	–
WLM	00 01 58.00	−15 27 50.0	00 01 58.24	−15 27 56.7	0.48	±0.11	3.23±0.74	3.4±0.78	36.53	:
Tucana	22 41 49.70	−64 25 10.0	22 41 49.70	−64 25 10.0	<11.8		<21.5	<20.9	37.32	–
M33†	01 33 54.00	+30 40 07.0	01 33 51.18	+30 39 39.0	226.09	±2.73	1750±21	1320±16	39.12	◇
IC 1613	01 05 05.50	+02 09 39.9	01 05 02.56	+02 09 24.8	<0.41		<2.4	<1.7	36.23	–
M31	00 42 45.90	+41 16 18.0	00 42 44.20	+41 16 08.0	7.72	±0.32	45.4±1.9	26.5±1.1	37.42	+
M32	00 42 41.93	+40 51 51.8	00 42 42.50	+40 51 55.0	11.69	±0.99	79.1±6.7	49.9±4.2	37.70	◇
NGC 205	00 40 22.07	+41 41 25.7	00 40 22.70	+41 41 28.0	<0.42		<3.3	<2.1	36.32	–
NGC 185	00 39 01.50	+48 20 27.0	00 38 58.75	+48 20 16.7	<0.41		<3.9	<1.5	36.18	–
NGC 147	00 33 12.09	+48 30 29.3	00 33 11.79	+48 30 27.2	<0.22		<2.1	<0.8	35.90	–
NGC 6822	19 44 56.20	−14 48 04.0	19 44 55.44	−14 48 12.2	0.43	±0.12	3.69±1.03	1.29±0.36	36.11	:
Fornax	02 39 59.30	−34 26 57.0	02 39 57.07	−34 26 22.2	<1.4		<2.6	<0.053	34.72	–
Sextans	10 13 02.90	−01 36 53.0	10 13 04.94	−01 36 33.0	<5.3		<1.2	<0.11	35.04	–
Carina	06 42 36.70	−50 57 58.0	06 41 37.58	−50 56 42.7	<1.5		<3.4	<0.031	34.49	–
Sculptor	01 00 05.90	−33 42 32.0	01 00 08.77	−33 42 01.2	<0.92		<1.4	<0.011	34.04	–
Draco	17 20 18.70	+57 54 48.0	17 20 24.82	+57 54 35.3	<1.6		<3.0	<0.020	34.31	–
Ursa Minor	15 09 11.40	+67 12 52.0	15 09 59.02	+67 10 45.7	<14.6		<24.3	<0.14	35.15	–
Sagittarius	18 55 03.28	−30 28 42.6	18 55 06.44	−30 31 53.6	<24.2		<86.1	<0.06	34.78	–
SMC	00 52 44.80	−72 49 43.0								?
LMC	05 23 34.50	−69 45 22.0								?
Galaxy‡	17 45 40.06	−29 00 28.2	17 45 40.40	−29 00 23.0	0.8			0.74	35.87	+

† Data from Schulman and Bregman (1995); ‡ data from Predehl and Trümper (1994).

Among the small (dwarf) systems in the Local Group, we found only in three other cases a ROSAT source close to the optical centres: NGC 6822, WLM, Draco. These are all Irregular or dwarf-Spheroidal systems and it is doubtful whether optical positions are close to their actual centres or would refer to proper nuclei at all (*cf.* Mateo 1998, Ho et al. 1995, and references therein). The source close to the centre of NGC 6822 is resolved in the HRI image from a nearby, much stronger (10 times brighter) source. The hardness ratio from the HRI data hints at a hard spectrum, in the PSPC observation the contours of the hand band image do also show a little extension in the direction of this source from the nearby stronger source. The luminosity is low, but is comparable to that of the centre source in the Milky Way Galaxy, although they are different type of galaxy. The WLM galaxy has no PSPC observation, its hardness ratio from the HRI is hardly meaningful. The luminosity of this source remained at the same level between two observations that were carried out within half a year. Referring to the observational results we have had so far, one cannot find clear indications for these two sources being low-level nuclei. The central source of the third case, Draco, has a supersoft X-ray spectrum and has been identified with a Carbon star.

6.2.3 Comments on non-detections

NGC 205, which being an Elliptical galaxy contains a recognizable optical center, has no X-ray source detected. However, some indication for diffuse emission may be present in the HRI image. In the current data, the level of this emission is only 2σ over the background. Given that the exposure time of this galaxy is only about half of that for WLM and NGC 6822, one could expect that more X-ray photons will be collected if the observation time increased.

The same considerations apply to another Elliptical, NGC 185 which has the same exposure time (and a distance comparable to NGC 205). The diffuse emission is not obvious but still visible from the HRI image. The upper limit luminosity is a little less than that for NGC 205, but is double that of NGC 147, which is consistent with the contour plots.

Among the others, The PSPC observations of Pegasus and Sextans show some X-ray emission that reaches 3σ over the background around the central area. Such emission may be from a point source with low count rate which may be associated with the centre, or could be due to some diffuse central emission. In the case of Sextans A, the source observed with the PSPC appears actually to be out of the central area when viewed with the HRI image. In NGC 6822 on the other hand, the higher resolution HRI data reveal a secondary source next to the main central X-ray source, that is actually coincident with the putative optical centre of this galaxy. For most of the irregular galaxies (including NGC 6822 and WLM) the centres are however difficult to define. It is not obvious to find the right position to get the upper limits and to discuss if they have active 'cores'. This is particularly a problem for the Local Group members which are 'too' close to us. Apart from two Magellanic Clouds mentioned above, Sagittarius is the nearest member to us (24 kpc), which covers $\sim 2^\circ$ of sky. The globular cluster M54 is close to the centre of symmetry of the galaxy and is thought to be its nucleus (*cf.* Mateo 1998). No X-ray source is detected with this globular cluster and the upper limit luminosity is low.

6.2.4 X-ray Luminosities and galaxy morphology

A histogram of inferred luminosities (assuming standard Power Laws for most galaxies, see sections in Chapter 4) for the detected core sources and also for the upper limits is shown in Figure 6.1. Some of the upper limits achieved are at quite low luminosities thanks to the closeness of the galaxies.

The M33 has a outstanding nucleus which is more than 100 times brighter than any other one. The nuclei of M31 and M32 emit nearly at the same level; depending on the observation epoch, one can be a little brighter than the other. The Milky Way stays at the low end of the luminosity axis; this is actually the lowest level of the nuclear X-ray emission found so far. The "suspicious" sources have luminosities around 10^{36} ergs s^{-1}, which may be close to the sensitivity limit for individual sources in these observations. Among the upper limits, particularly the two galaxies Pegasus and Tucana could still have the same 'active' level as M32. It will be interesting to

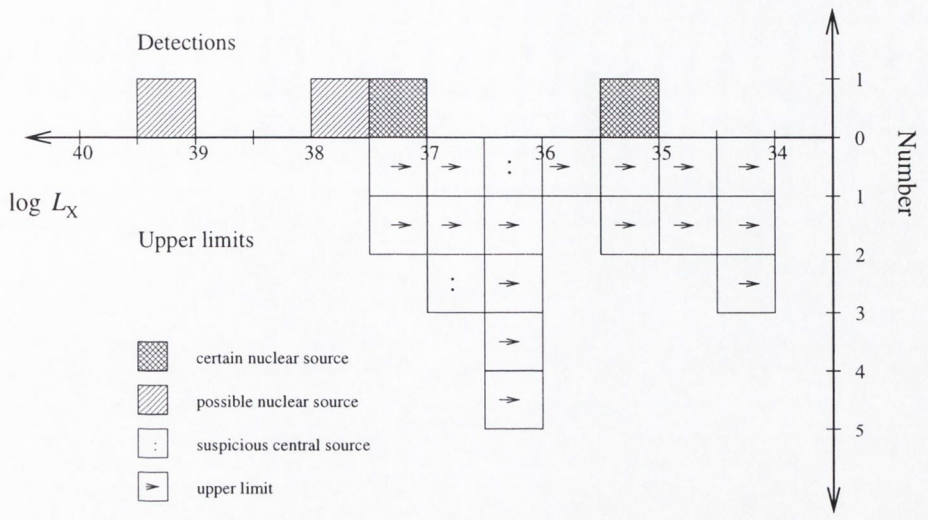

Figure 6.1: Histogram of luminosities of Local Group galaxy cores

see their results from more sensitive observations in the future.

A set of histograms illustrating the detected or possibly detected cases as function of optical galaxy luminosity, divided according to morphological types, is presented in Figure 6.2. All the Spirals have certain or possible nuclear sources; these are the three most luminous stellar systems in the Local Group. The most luminous Elliptical (M32) also has a possible nuclear source. Beyond M_V = -14.0 all Spheroidal systems are classified as dwarfs. M32 is the only Elliptical or dwarf Elliptical with a likely core and none of the Irregulars provide good candidate nuclear cores.

6.3 Discussion

6.3.1 μAGNs

As seen from the example of low-luminosity AGN (μAGN) M32, the ROSAT soft X-ray luminosities of the central X-ray sources are several orders of magnitude less than typical Seyfert galaxies. If the sources are AGNs, one would expect this difference to be due to either a lower black hole mass ($\sim 10^4 M_\odot$) or a lower accretion rate (for M32, 10^{-9}). For such a low mass accretion rate, the standard thin disk model for accretion (Shakura and Sunyaev 1973) is probably not applicable and the model for advection-dominated accretion flows (ADAFs), provides possible solutions (Narayan

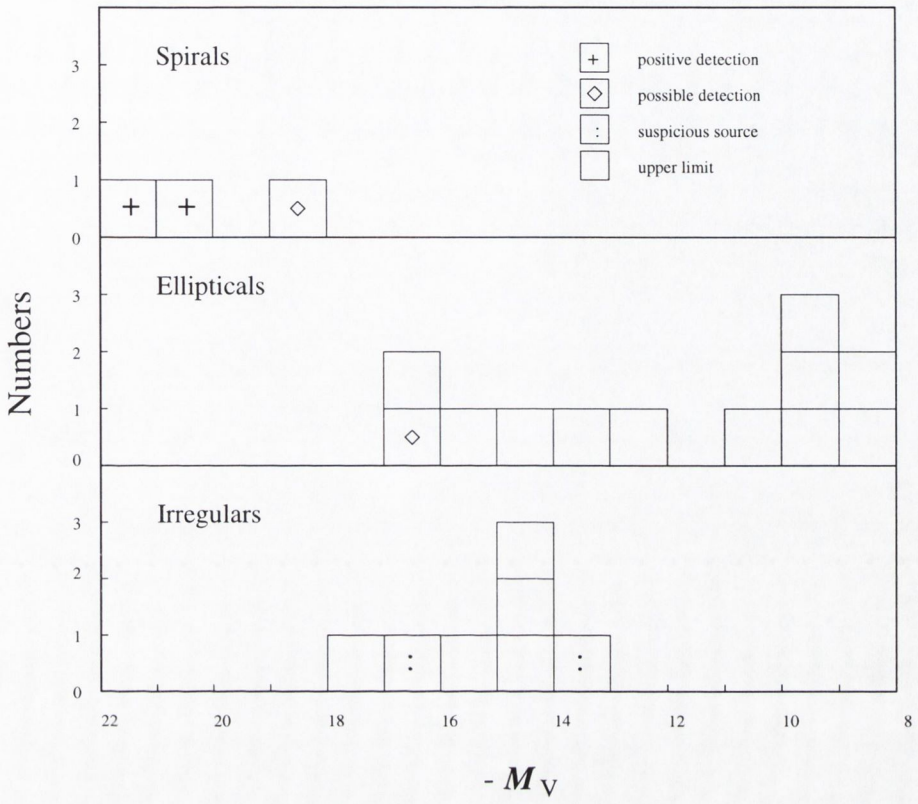

Figure 6.2: Status of detections of nuclear sources in Local Group members

and Yi 1994). In the advection-dominated accretion very little energy is radiated away during the accretion process.

Lasota et al. (1996) have used an ADAF model to explain the spectrum of the low-luminosity AGN NGC 4258. In their model, the outer disk is a standard optically thick, geometrically thin accretion disk, but at smaller radii their model is taken over by an advection-dominated flow. It is consistently observed that mass accretion rates are low in low-luminosity AGNs. For example, L/L_E is estimated to be 10^{-4} for the LINER galaxy NGC 4258 (Lasota et al. 1996). while the values for classical AGNs are taken to be 10^{-3} to 10^{-2} (*cf.* Wandel 1991).

Masses for the central condensed objects have been determined for the Milky Way (2.6×10^6 $M_\odot$, Genzel et al. 1997) and for M32 (3.4×10^6 $M_\odot$, Van der Marel et al. 1998). In both cases the accretion rate is extremely low (in Eddington units: $\dot{m} \sim 10^{-6}$ for Sgr A* in the Milky Way centre, $\dot{m} = 10^{-9}$ for the nucleus of M32) and well into the expected Advection Dominated Accretion Flow regime. If the

X-ray source in M32 were offset from the nucleus, then the true nucleus would be simmering at an even lower fuelling rate.

6.3.2 MDOs and BHs

At some stages, an AGN with a low mass $\ll 10^6\ M_\odot$ black hole (BH) is not that much different from a massive BH binary with a BH mass ($> 10\ M_\odot$). ADAF models are also possible to explain the X-ray emission from X-ray binaries (Narayan 1997). The X-ray binaries are thought to be common in galaxies, which make a significant contribution to the total X-ray luminosity of the host galaxy (*cf.* Fabbiano et al. 1989). For the detected nuclear X-ray sources, however, Colbert and Mushotzky (1999) found that the X-ray luminosities for the sources found in 21 nearby face-on Spirals and Ellipticals, are much higher than those predicted for X-ray binaries by Canizares et al. (1987) from an $L_X - L_B$ relationship.

In the Local Group, since many galaxies do not have well-defined nuclear position, one may generally compare the total blue luminosities with the nuclear X-ray emission. The Figure 6.3 shows the diagram of the relation between log L_X (0.1–2.4 keV) and total blue luminosities in solar units (log $L_B/L_{\odot,B}$). From the diagram, it is clear that the higher blue luminosities are associated with higher X-ray emission, although the detected cases are too few to calculate a reasonable regression. For both galaxies with suspicious central sources, the blue luminosities are at mid-level of the group. For most dwarf Ellipticals with $L_B \lesssim 10^7\ L_\odot$, the X-ray emission is at a very low level and there is not likely any activity in their nuclei. But galaxies with total blue magnitude $L_B \simeq 10^8\ L_{\odot,B}$ or more may have some central X-ray emission at the level of the central object in the Milky Way.

6.3.3 Limitations and further work

We have noticed that all the X-ray data used for this search are from observations not specially intended for survey purposes. Each observation has a unique object which requires different exposure times, dates and even observation modes. The data

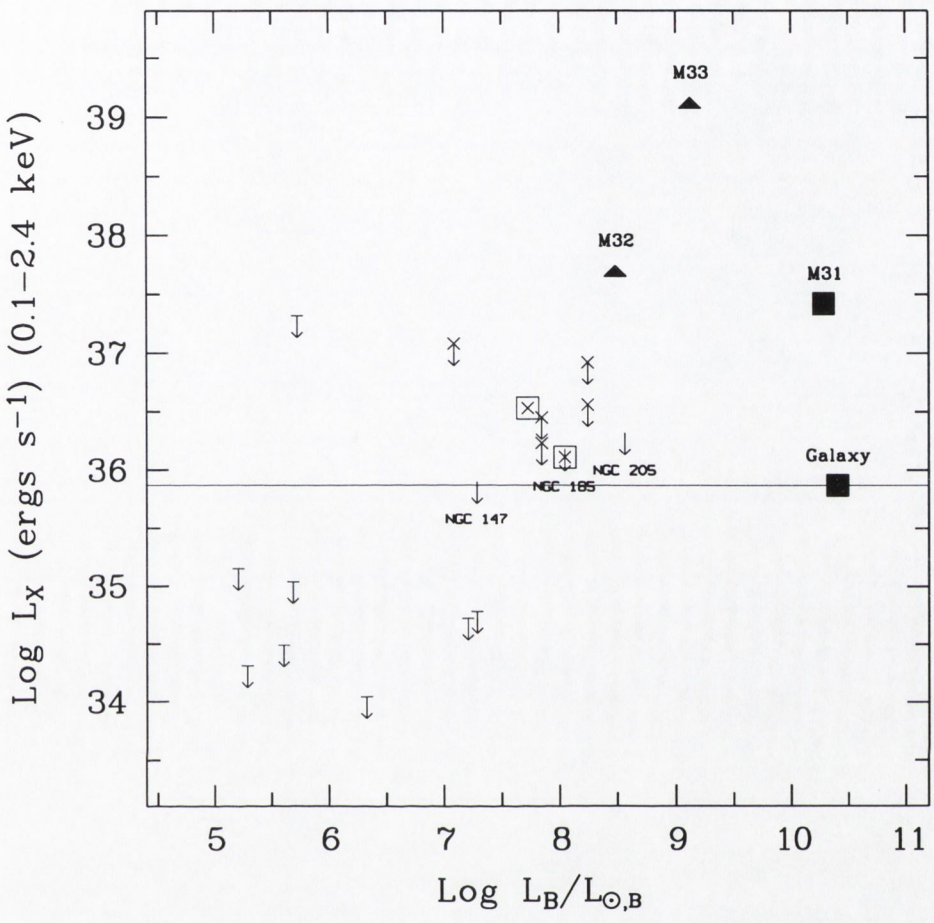

Figure 6.3: Local Group galaxies in $L_X - L_B$ diagram. Filled squares for the galaxies with certain nuclear source; filled triangles for possible nuclear sources, square for suspicious central sources and arrows for upper limits. Dwarf Ellipticals and Irregulars are marked with '–' and '×', respectively. The solid line is the L_X level of the nuclear source in the Milky Way.

with unequal sensitivity limits maybe not straightforward to interpret, especially if statistical analyses were attempted in the presence of many upper limits.

Although a huge amount of research work has been done for the Local Group, it is not clear, for most small systems, where the nuclei are actually located. There is also little information in other waveband that can be found for our two detected suspicious sources. One possibility which can be investigated is that there may be unknown QSOs/AGNs as X-ray sources behind the target galaxy. The example is that many X-ray sources detected in Carina, Sculptor and Fornax have been

identified as QSOs.

While the X-ray detectors/telescope are getting more sensitive, one can expect that more X-ray sources will be detected or resolved. From the current results of X-ray emission and optical study (*cf.* Figure 6.3), NGC 205 might be the most promising one to detect some nuclear X-ray emission. It would be too great a surprise if some kind of nuclear activity were found in those galaxies which appear at the mid-area of $L_X - L_B$ diagram (Figure 6.3).

As of our two "suspicious" cases, for NGC 6822, Chandra (AXAF) X-ray telescope may be the better one which would resolve the possible nuclear source completely from the nearby stronger source with the higher resolution detectors, and provide a spectrum as well. XMM may be used to detect more photons from the source in the centre of WLM to determine its spectral properties. We have proposed to observe M32 with XMM for which better spectral information will help us to understand the nature of the X-ray source in M32. Of course, these new satellites will also facilitate further study of the temporal properties of these sources.

6.3.4 Summary

Central X-ray sources are found among the most luminous members of the Local Group. These are candidate massive Black Holes, for which confirmation can be found from data at other wavelengths in the cases of the Milky Way and M31. If also M32 and M33 have massive Black Holes in their nuclei, there could be at least four massive Black Holes immediately around us. For the moment one could conclude that the 20 or so smaller and/or Irregular and dwarf-Spheroidal systems do not seem to possess massive Black Holes, but the sample of M32 shows that the activity level can be so low that a non-detection may not necessarily imply no Black Hole.

Chapter 7

Sculptor Group of galaxies: NGC55, NGC247 and NGC300

7.1 Introduction

The Sculptor Group is the nearest group of bright galaxies beyond the Local Group (distance ~ 2.5 Mpc) and forms a loose association of about 15 members within an area 20° in diameter not far from the South Galactic Pole. The five bright members of the group are of morphological type Sc or later (Table 7.1). In the X-ray band the starburst galaxy NGC 253 has been well studied (*e.g.* Vogler and Pietsh 1999). Recently, the ROSAT PSPC observations have been analyzed as well (*cf.* Read and Pietsch 1999), whereas there are not much published data on ROSAT HRI data. Before the ROSAT, there was only an Einstein IPC observation of NGC 247 which revealed a total X-ray luminosity $L_X \sim 10^{39}$ erg s^{-1} (0.5–3.0 keV) in three discrete sources apparently associated with the galaxy (Long and Van Speybroeck 1983).

The ROSAT observation log of each data set used is shown in Table 7.2. The PSPC data for NGC 55, NGC 247 and NGC 300 were obtained from the UK ROSAT Data Archive Centre at Leicester. The Starlink Asterix software package was used to sort the data and perform the image processing. In the case of NGC55 512×512 pixel images of a central 1° square region of the PSPC field were constructed in three bands (soft, 0.2–0.4 keV; hard, 0.4–2.0 keV and total, 0.2–2.0 keV), whereas

Table 7.1: Sculptor group galaxies

Name	α_{2000} $h\ m\ s$	δ_{2000} $^\circ\ '\ ''$	Type	D Mpc
NGC 55	00 15 08.45	−39 13 13.3	SBS9	1.3
NGC 247	00 47 08.28	−20 45 37.6	SXS7	2.1
NGC 253	00 47 34.37	−25 17 17.8	SXS5	3.0
NGC 300	00 54 53.72	−37 40 56.9	SXS7	1.2
NGC 7793	23 57 49.21	−32 35 23.8	SAS7	3.4

for NGC 247 and NGC 300 256 × 256 pixel images were employed. The Asterix PSS algorithm was used to detect discrete X-ray sources in these fields and the XSPEC package was used to perform X-ray spectral fitting on a subset of the sources (*i.e.* several of the brightest X-ray sources in each field). The PSPC data for NGC 7793 are obtained from the MPE archive and MIDAS/EXSAS is used for data reduction.

In order to distinguish the X-ray emission from different areas within each galaxy, the HRI data are particular useful as could also be seen in the analyses of Local Group galaxies. The HRI data are obtained from ROSAT Data Archive at MPE, Garching, and the MIDAS/EXSAS software is used for the image processing. Again, the HRI images are formed by binning the Photon Event Table at 5″.

In this Chapter, the results from PSPC observations are present briefly and the more detailed searches on HRI data follow. A discussion about possible X-ray

Table 7.2: ROSAT observation log of Sculptor Group galaxies

Name	ROR ID.	Start Date	Exposure Time ksec	Field Centre α_{2000} $h\ m\ s$	Field Centre δ_{2000} $^\circ\ '\ ''$
NGC 55	600107p	1991.11.22	18.7	00 15 09	−39 13 12
	600766h	1994.12.12	27.5	00 15 09	−39 13 12
NGC 247	600159p	1991.12.21	18.8	00 47 09	−20 45 36
	600622h+1	1995.06.29	17.8	00 47 07	−20 45 36
NGC 300	600025p	1991.11.28	46.0	00 54 52	−37 41 24
	600621h+1	1995.05.27	19.1	00 54 52	−37 41 24
NGC 7793	600386p	1992.12.07	13.3	23 57 50	−32 35 24

emission from the centres of these galaxies is given at the end.

7.2 NGC 55

NGC 55 is a nearby edge-on galaxy. It has an off-centre bar which is not at the centre of the disc but offset to the North-West by 2.7′ from the centroid of total optical light.

7.2.1 PSPC observation

Figure 7.1 shows the background subtracted hard band X-ray image (the X-ray data have been smoothed with a circular Gaussian function of width 4 pixels). The PSS routine detected a total of 36 X-ray sources in the hard band image at a significance $> 5\sigma$ within a 18′ radius of the field centre (the full field-of-view within the circular window support rib of the PSPC). As is evident from Figure 7.1, a number of relatively bright discrete sources is coincident with the disk of NGC 55, the brightest appearing 3.8′ East of the nominal centre of the galaxy. There is also an extended X-ray source coincident with a prominent bar structure (to the West of centre). The source to the South of this bar structure may be identified with a foreground star, CD-39 43, (12.42^m).

Table 7.6 summarizes the X-ray spectral properties and derived luminosities for the bright source and the extended bar emission. The total X-ray luminosity of NGC 55 in the 0.4–2 keV band amounts to $L_X \sim 9 \times 10^{38}$ ergs s^{-1}.

7.2.2 HRI observation

The HRI observation (ROR 600766) was carried out in December 1994 with 27.5 ksecs exposure time. In the whole field within 16′ from the centre, 23 sources are detected with $ML \geq 7$ (12 of them with $ML \geq 10$). Table 7.3 lists all source positions and count rates. These sources are also marked on Figure 7.2 which shows the HRI contours overlaid on the optical image.

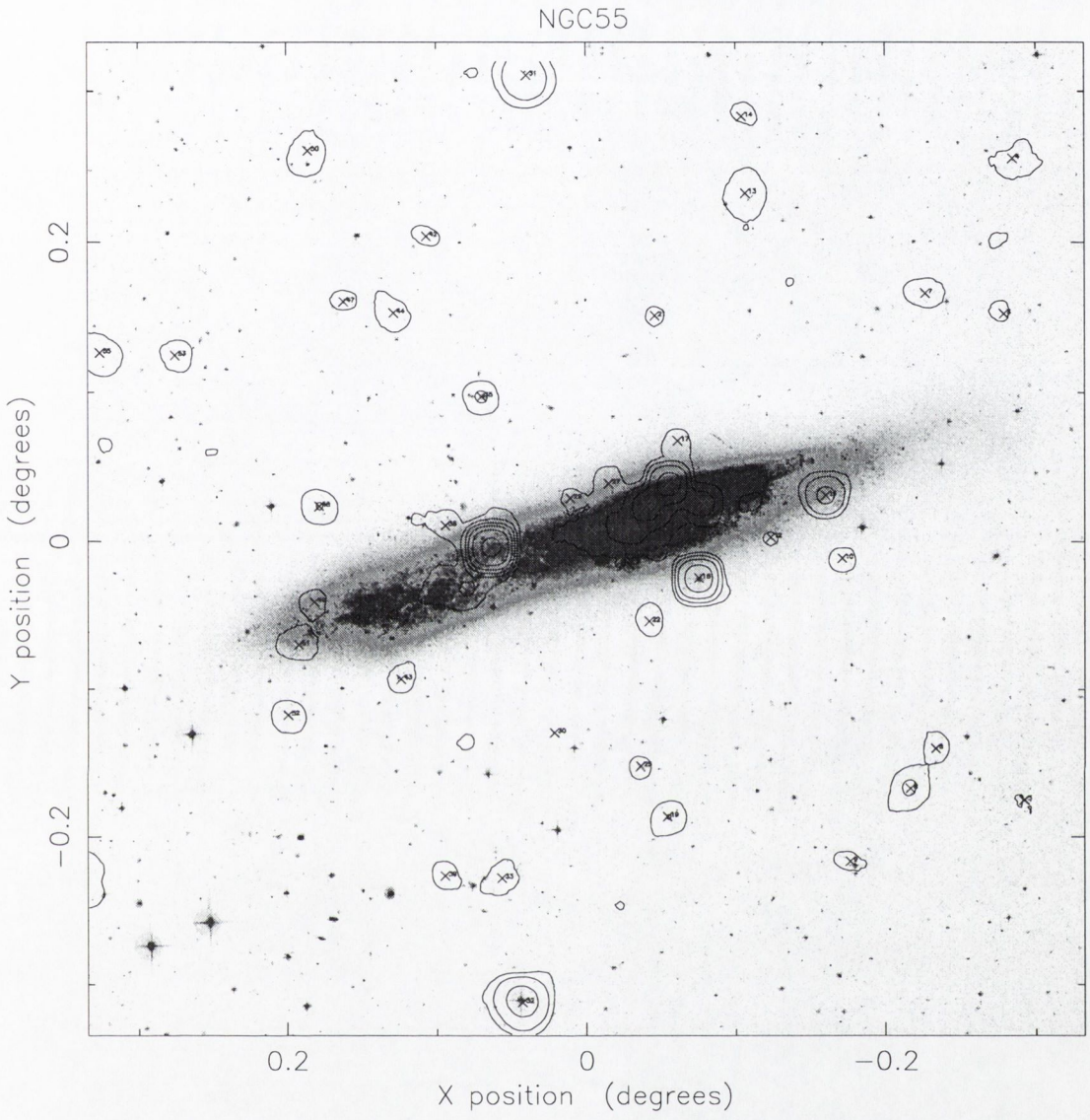

Figure 7.1: NGC 55 ROSAT PSPC (hard band 0.4-2.0 keV) image overlaid on the digital optical image. The displayed field of view is $40' \times 40'$. The contour levels of the PSPC image are 0.11, 0.33, 1.0, 3.0, 9.0 and 27.0 cts pix^{-1}. The detected sources are marked with '×'.

The HRI contour plot appears similar to the PSPC's (Figure 7.1), the bright sources detected in PSPC appear also in HRI. But the source to the South of this bar structure (No.16) appears to be over 20″ away from the foreground star, CD-39 43, and is not likely its counterpart.

For the central area of the galaxy, there is no source detected and no sign of

Table 7.3: ROSAT HRI point sources in the field of NGC 55

Source No.	α_{2000} $h\ m\ s$	δ_{2000} $^\circ\ '\ ''$	Count Rate 10^{-3} s^{-1}	ML	Off-axis $'$
1	00 15 58.16	-39 03 20.5	1.34±0.40	7.8	13.6
2	00 15 15.99	-39 05 57.7	0.58±0.19	9.8	7.3
3	00 15 14.88	-39 07 30.6	0.44±0.16	8.6	5.8
4	00 14 46.44	-39 08 30.6	0.79±0.24	7.7	6.5
5	00 14 50.17	-39 08 57.4	1.48±0.26	53.8	5.7
6	00 14 35.05	-39 09 02.1	0.65±0.21	9.7	7.9
7	00 14 51.66	-39 10 42.5	4.53±0.42	316.3	4.3
8	00 14 18.76	-39 11 12.8	2.67±0.37	73.4	10.0
9	00 14 44.20	-39 11 32.1	0.64±0.18	19.6	5.2
10	00 14 56.61	-39 11 37.0	3.05±0.35	177.3	3.0
11	00 15 44.21	-39 12 06.5	0.51±0.18	7.1	6.8
12	00 15 01.80	-39 12 28.3	0.31±0.13	7.2	1.7
13	00 15 37.83	-39 12 32.4	0.59±0.18	13.6	5.5
14	00 15 28.69	-39 13 17.5	24.93±0.97	2656.0	3.7
15	00 15 28.71	-39 14 21.8	0.39±0.15	7.1	3.9
16	00 14 45.33	-39 14 35.2	12.58±0.70	1151.6	4.9
17	00 15 33.62	-39 15 11.8	0.59±0.17	15.0	5.1
18	00 14 54.82	-39 15 20.9	0.59±0.19	8.4	3.6
19	00 15 48.25	-39 18 40.0	0.68±0.22	8.3	9.3
20	00 14 56.75	-39 20 45.7	0.66±0.21	10.6	8.0
21	00 16 19.29	-39 20 44.6	1.75±0.49	9.0	15.5
22	00 15 16.28	-39 20 59.1	0.72±0.22	11.0	7.9
23	00 14 51.22	-39 24 12.5	1.22±0.31	13.2	11.6

diffuse emission either. The upper limits are derived for several positions around the optical centroid, the upper limit value is near that of the weak source located on the bar (No.12). The typical upper limit value obtained is valid for the position from NED, the count rate $< 0.18 \times 10^{-3}$ s^{-1}. Using the $\Gamma = 2.0$ power law model with the Galactic $N_H = 1.72 \times 10^{20}$ cm^{-2}, as in Chapter 4, the (0.1–2.4 keV) unabsorbed flux $f_X < 0.53 \times 10^{-14}$ ergs cm^{-2} s^{-1} and luminosity $L_X < 1.86 \times 10^{36}$ ergs s^{-1}. Because of the high inclination, the absorption column can be much larger than the Galactic one for the X-ray emission from the centre. Using the fitted Thermal

Figure 7.2: ROSAT HRI contour plot of NGC 55 overlaid on optical image. The centre of the galaxy (from the NED) is marked with a cross and the D_{25} ellipse is taken from the RC3 catalogue. The background level in the HRI image is ~ 0.82 cts pix^{-1}. The contour levels are 0.96, 1.03, 1.17, 1.52, 2.22 and 4.32 cts pix^{-1}. The HRI image has $5'' \times 5''$ pixels and is smoothed with a 3-pixel size Gaussian. The optical image is taken from the DSS. Detected X-ray sources are indicated.

Bremsstrahlung model in the Table 7.6 for the bar region, the flux and the luminosity will be doubled.

7.3 NGC 247

7.3.1 PSPC observation

From the PSPC image of NGC 247, a total of 26 sources was detected in the hard X-ray band within 18′ of the field centre. A number of these X-ray sources is coincident with the disk of the galaxy, although several sources of comparable intensity are distributed across the full PSPC field. For example, the relatively bright source $\sim 4'$ West of the galactic disk can be identified with a known QSO. Thus in NGC 247 there appears to be a source confusion problem. The brightest source, which is probably associated with NGC 247, lies $\sim 2'$ South of the nominal centre of the galaxy; Table 7.6 provides relevant details for its spectral properties. Integrating all the X-ray emission coincident with the galactic disk gives a total X-ray luminosity (0.4–2 keV) for NGC 247 of $\sim 3 \times 10^{38}$ erg s^{-1}.

Table 7.4: ROSAT HRI point sources in the field of NGC 247

Source No.	α_{2000} $h\ m\ s$	δ_{2000} $^\circ\ '\ ''$	Count Rate 10^{-3} s^{-1}	ML	Off-axis $'$
1	00 46 35.30	-20 36 45.1	1.21±0.37	9.6	11.6
2	00 47 03.30	-20 36 56.7	3.35±0.49	84.5	8.7
3	00 46 47.80	-20 38 35.7	1.42±0.33	24.5	8.3
4	00 47 03.72	-20 40 14.4	1.05±0.29	15.1	5.4
5	00 46 51.85	-20 43 26.6	5.65±0.58	267.2	4.2
6	00 47 10.09	-20 47 10.1	1.21±0.28	33.3	1.7
7	00 47 27.52	-20 47 24.3	3.69±0.48	144.3	5.1
8	00 47 03.94	-20 47 44.7	11.82±0.84	579.6	2.3
9	00 47 05.53	-20 49 25.9	0.64±0.23	9.4	3.9
10	00 47 43.63	-20 49 40.7	1.41±0.38	12.4	9.4
11	00 47 16.27	-20 49 53.2	0.49±0.19	9.4	4.8
12	00 47 42.04	-20 52 37.2	1.54±0.43	10.3	10.8
13	00 47 39.84	-20 53 20.8	1.10±0.35	8.8	10.9
14	00 47 25.39	-20 54 45.8	1.10±0.33	11.4	10.1

7.3.2 HRI observation

The HRI observation (ROR 600622) was carried out in 1994 and 1995. The longer exposure (17.8 ksec, see Table 7.2) has been analyzed. Within 16′ from the center

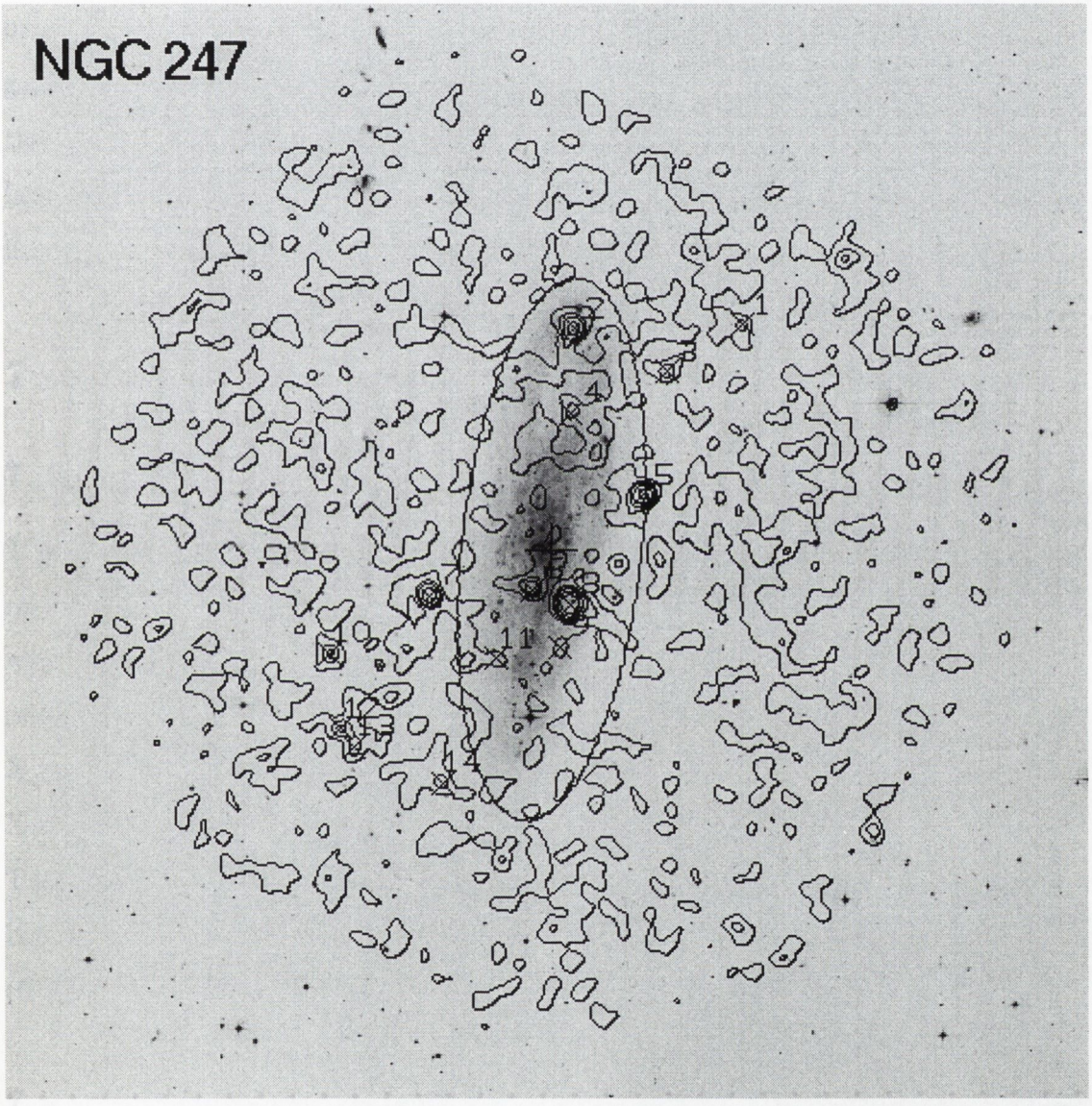

Figure 7.3: ROSAT HRI contour plot of NGC 247 overlaid on optical image. The centre of the galaxy (from the NED) is marked with a cross and the D_{25} ellipse is taken from the RC3 catalogue. The background level in the HRI image is ~ 0.42 cts pix^{-1}. The contour levels are 0.49, 0.63, 0.77, 1.10 and 1.82 cts pix^{-1}. The HRI image has $5'' \times 5''$ pixels and is smoothed with a 3-pixel size Gaussian. The optical image is taken from the DSS. Detected X-ray sources are indicated.

of the field, 14 sources are detected with $ML \geq 7$. Table 7.4 lists all these sources for reference.

The source No.5, which also detected by the PSPC, can be identified as the QSO which is studied in detail by Elvis et al. (1997). Figure 7.3 shows the HRI contours overlaid on the optical image. There may be a few sources associated with the galaxy, but none of them is located at the centre. The upper limit is calculated for the position from the NED, the count rate $< 0.21 \times 10^{-3}$ s^{-1}. Using the $\Gamma = 2.0$ power law model with the Galactic $N_H = 3.36 \times 10^{20}$ cm^{-2} the (0.1-2.4 keV) unabsorbed flux $f_X < 1.30 \times 10^{-14}$ ergs cm^{-2} s^{-1} and luminosity $L_X < 6.88 \times 10^{36}$ ergs s^{-1}.

7.4 NGC 300

7.4.1 PSPC observation

This X-ray field is complicated by the presence of a bright extended complex of X-ray emission to the North-East of NGC 300, corresponding to a galaxy group/cluster which is unassociated with the Sculptor Group. Restricting to a 9′ radius from the centre of the field, 19 hard X-ray sources were detected. There is a relatively bright X-ray source 3.4′ East of the centre of the galaxy and some evidence for an extended X-ray emission complex coincident with the inner 5′ (2.5 kpc) region of the galaxy. Table 7.6 details the X-ray spectral results for the brightest sources. Integrating all the X-ray emission coincident with the galactic disk gives a total X-ray luminosity (0.4–2 keV) for NGC 300 of $\sim 1.3 \times 10^{38}$ erg s^{-1}.

7.4.2 HRI observation

The HRI observation (ROR 600621) was carried out in 1994 and 1995. The latter data set has a longer exposure time (19.1 ksec). Within 16′ from the field centre, 18 sources are detected with $ML \geq 7$. Table 7.5 lists all these sours with their count rate.

Source No.3 may be identified with a foreground star, HD 5043 (G5V, 5.37^m).

Table 7.5: ROSAT HRI point sources in the field of NGC 300

Source No.	α_{2000} $h\ m\ s$	δ_{2000} $^\circ\ '\ ''$	Count Rate 10^{-3} s^{-1}	ML	Off-axis $'$
1	00 55 22.11	-37 29 15.6	1.47±0.46	8.0	13.5
2	00 54 14.56	-37 29 39.1	3.76±0.61	38.7	14.0
3	00 55 27.08	-37 31 22.7	8.49±0.77	196.7	12.1
4	00 53 52.75	-37 33 53.8	2.27±0.54	14.8	14.1
5	00 55 41.97	-37 35 31.3	2.03±0.42	27.3	11.4
6	00 54 23.67	-37 35 39.0	0.67±0.25	7.0	8.1
7	00 54 50.68	-37 38 47.2	0.60±0.21	10.6	2.6
8	00 55 11.34	-37 40 05.4	0.46±0.18	8.3	3.9
9	00 54 40.78	-37 40 44.4	1.04±0.28	16.3	2.5
10	00 54 44.41	-37 41 18.1	0.38±0.17	7.3	1.7
11	00 54 24.63	-37 42 08.6	0.53±0.20	8.2	5.6
12	00 55 10.30	-37 42 12.9	7.92±0.67	335.6	3.6
13	00 55 54.52	-37 43 38.7	1.47±0.46	7.2	12.4
14	00 54 33.88	-37 44 45.1	0.50±0.20	7.8	5.0
15	00 55 02.91	-37 45 37.3	0.51±0.20	7.8	4.7
16	00 55 04.15	-37 48 00.4	0.58±0.22	7.7	7.0
17	00 55 11.15	-37 48 37.5	3.07±0.44	85.3	8.1
18	00 54 44.95	-37 51 02.6	1.50±0.36	18.5	9.8

There are several sources located within the D_{25} ellipse (Figure 7.4), but no source is located in the centre of the galaxy. The upper limit is calculated for the position from the NED, the count rate $< 0.29 \times 10^{-3}$ s^{-1}. Using the $\Gamma = 2.0$ power law model with the Galactic $N_H = 3.24 \times 10^{20}$ cm^{-2} the (0.1-2.4 keV) unabsorbed flux $f_X < 1.78 \times 10^{-14}$ ergs cm^{-2} s^{-1} and luminosity $L_X < 3.07 \times 10^{36}$ ergs s^{-1}.

7.5 NGC 7793

NGC 7793 was observed only with the ROSAT PSPC, which was carried out in December 1992 and May 1993 with a total exposure time of 23.8 ksec. Read and Pietsch (1999) gave the detailed results of this observation, by merging the two data sets to one. From the contours of the images that are created for different

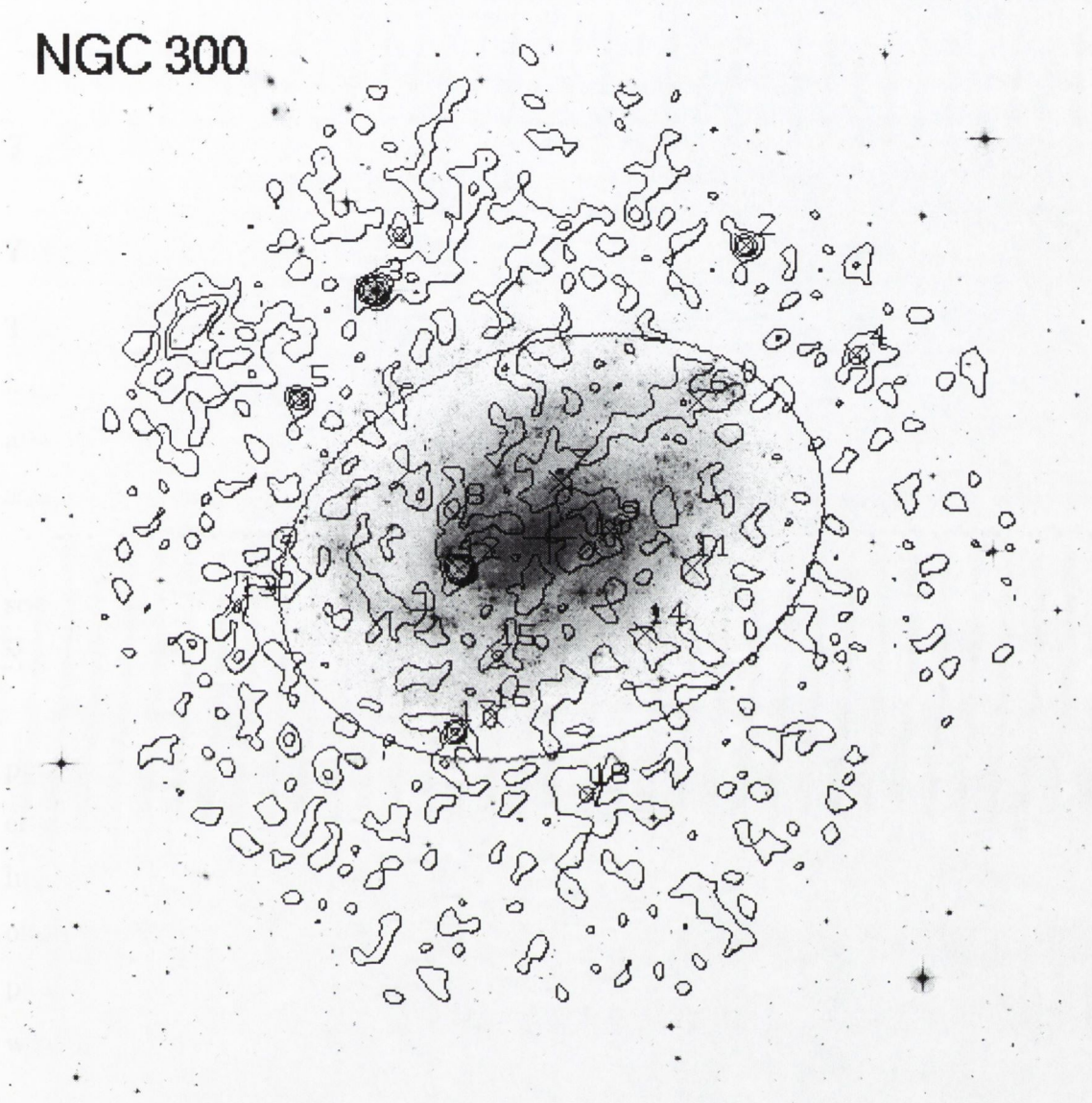

Figure 7.4: ROSAT HRI contour plot of NGC 300 overlaid on optical image. The centre of the galaxy (from the NED) is marked with a cross and the D_{25} ellipse is taken from the RC3 catalogue. The background level in the HRI image is ~ 0.52 cts pix^{-1}. The contour levels are 0.60, 0.76, 0.92 and 1.32 cts pix^{-1}. The HRI image has $5'' \times 5''$ pixels and is smoothed with a 3-pixel size Gaussian. The optical image is taken from the DSS. Detected X-ray sources are indicated.

energy bands, they found that the unresolved residual emission is quite uniformly distributed over the galaxy.

Their result is tested here with a single data set observed in December 1992 with 13.3 kpc exposure time. Neither ring profile from the Photon Event Table or radial

profile from the binned image shows any clear increase at the center of the galaxy.

7.6 Discussion

7.6.1 X-ray bright sources and luminosities

The brightest sources in NGC 55, 247 and 300 are listed in Table 7.6 with their best fitted spectral parameters. All of the fitted absorption columns of these source are much larger than the corresponding Galactic value, which suggests that these sources might be associated with the host galaxies.

The derived X-ray luminosities of NGC 55, NGC 247 and NGC 300 are in reasonable agreement with the previously established correlation for spiral galaxies of X-ray luminosity with the integrated B magnitude (Fabbiano 1989).

Based on the present study it is clear that source confusion can be a significant problem in the X-ray band when studying extended objects of relatively low average X-ray surface brightness such as nearby late-type spirals. For example, the luminosity of NGC 247 we derive here is just 30% of that measured in the Einstein observation (Long & Van Speybroeck 1983); this is partly due to the exclusion in the present analysis of the X-ray flux from a bright nearby background object identified with a QSO.

The total X-ray luminosities derived for these three galaxies, and also the luminosities of individual sources probably associated with each of the galaxies, are at

Table 7.6: The best spectral fitting parameters of bright sources of NGC 55, NGC 247 and NGC 300

Galaxy	NGC 55		NGC 247	NGC 300	
Source	brightest	extended bar	brightest	brightest	2nd brightest
Model	wabs*brem	wabs*brem	wabs*raymond	wabs*brem	wabs*brem
$N_H(10^{20}$ cm$^{-2})$	22.1 ± 2.9	16.6 ± 5.9	7.02 ± 0.30	4.56 ± 0.44	8.38 ± 1.60
kT (keV)	0.87 ± 0.23	1.72 ± 0.84	0.30 ± 0.03	0.60 ± 0.18	0.35 ± 0.47
Abundance			0.24 ± 0.27		
χ^2_ν	1.37	0.92	0.65	0.90	1.695
$L_X^\dagger$ (10^{37} ergs s^{-1})	61.2	17.6	14.1	8.97	3.05

† 0.4–2.0 keV

Table 7.7: Upper limits of X-ray emission from the cores of Sculptor Group galaxies

Name	X-ray α_{2000} $h\ m\ s$	X-ray δ_{2000} $^\circ\ '\ ''$	Count Rate 10^{-3} s^{-1}	Unabsorbed flux f_X (0.1–2.4 keV) 10^{-14} ergs cm^{-2} s^{-1}	Luminosity L_X and $\log L_X$ 10^{36} ergs s^{-1}	
NGC 55	00 15 08.35	−39 13 17.3	<0.18	<0.91	<1.86	36.26
NGC 247	00 47 08.56	−20 45 38.2	<0.21	<1.30	<6.88	36.87
NGC 300	00 54 53.13	−37 40 53.0	<0.29	<1.78	<3.07	36.48

levels compatible with sources of a stellar origin.

7.6.2 X-ray emission from the centres

There is no point-like source detected in the centres of these four Sculptor Group galaxies, NGC 55, 247, 300 and 7793 from either PSPC or HRI observations. Diffuse emission is detected all over NGC 7793, but there are no signs of extended source in the central area of other three galaxies. The upper limits of the X-ray emission from these three galaxies are summarized in Table 7.7.

Compare with the galaxies in the Local Group, these values are well below that of the centre object in M31. If there is any nuclear activity in these galaxies, the levels are certainly below or almost comparable that of the nuclear object in the Milky Way.

Chapter 8

Conclusions

In this thesis, a dedicated search for X-ray emission from the cores in the Local Group galaxies is performed to establish whether low levels of nuclear activity occurs in these nearest galaxies. The data are from ROSAT HRI or PSPC pointing observations which are available for 21 Local Group galaxies in the centre of the observing fields, and for another 3 in the outer detector area, covering 70% of all Local Group members. The HRI data are particular useful, since the nuclear source may be more resolvable from their HRI images. 14 galaxies have HRI data, while 9 of them have PSPC observations as well.

M31 is the brightest galaxy of the group, and is considered to contain a massive dark object in its nucleus. The X-ray emission from the nuclear source (known for some time) is also detected in the HRI data observed in 1996. The X-ray luminosity in the ROSAT broad band (0.1–2.4 keV), $L_X = 2.7 \pm 0.1 \times 10^{37}$ ergs s^{-1}, is at nearly same level of that detected 6 years before (the variability measurement is 1.5). M32 is a small Elliptical with a clear central concentration, and would contain a 3×10^6 $M_\odot$ black hole. The HRI observation in 1994 shows a little extension ($\sim 2.7''$) of the X-ray source in M32. Although the X-ray position of this source is a few arcseconds off the optical centre, this offset is not yet reliably established. The HRI observation in 1997 confirms this extension. The long exposure PSPC observations in 1991 obtained enough counts to attempt the spectral fitting. The results are reasonable from both data sets used; for the power law model the photon

index $\Gamma \sim 2$ and thermal Bremsstrahlung model $kT \sim 2$ keV. All fitted models give higher absorption columns than the Galactic one. The HRI observation of 1994 yields an X-ray luminosity $L_X = 5.0 \pm 0.4 \times 10^{37}$ ergs s^{-1}, which increased little in 1997 (the variability measurement is 1.5). But some PSPC observations detected as much as 3 times this luminosity from the same source. In the view of the small source extension and still uncertain central or non-central position of the source, conceivable interpretations are either a Supernova Remnant or a mini-AGN. An ASCA spectrum and a radio upper limit suggest that a low-level AGN is a more attractive explanation.

The HRI image of the observation in 1995 for NGC 6822 resolved a weak source from the nearby 10 times stronger source. The position of this weak source is consistent with the optical centre of the galaxy as listed in the NED/SIMBAD database. The PSPC data indicate that this source may exhibit a hard spectrum. The X-ray luminosity is low, ($L_X = 1.3 \pm 0.4 \times 10^{36}$ ergs s^{-1}), but is comparable to that of the central source in the Milky Way (Sgr A*, $L_X = 0.74 \times 10^{36}$ ergs s^{-1}). The WLM galaxy has also an HRI source in the central position, detected in 1996. The count rate for this source is at the same level of that of NGC 6822, but the the luminosity ($L_X = 3.4 \pm 0.8 \times 10^{36}$ ergs s^{-1}) is higher because of the greater distance to us. This luminosity did not change much between two data sets observed within half a year (the variability measurement is 0.5). In both cases the galaxy is in a Irregular system and the optical position will refer to the centroid of the overall light distribution rather than a well-defined centre. These two central sources can therefore only be considered suspicious cases until there nature is firmly established with help of data from other wavebands and from new high-energy measurements. Among the rest of the Local Group galaxies, no sources are detected in their central area. The upper limits of the X-ray luminosities derived for the central regions show that most dwarf Ellipticals have little X-ray emission ($L_X \lesssim 10^{35}$ erg s^{-1}), and that the galaxies with total blue magnitude of at least $L_B \simeq 10^8\ L_{\odot,B}$ may contain a central source at the level of the core in the Milky Way or stronger.

In addition, among 5 large members of the Sculptor Group, NGC 253 is a well-

known starburst galaxy; NGC 7793 has some diffuse emission detected all over the galaxy but without significant enhancement in the centre position. For NGC 55, 247 and 300 no sources are detected in the central regions, yielding rather low upper limits ($L_X \lesssim 10^{36}$ ergs s^{-1}).

As seen from the example of M32, the X-ray luminosities of the nuclear X-ray sources are several orders of magnitude less than typical Seyfert galaxies. If the sources are AGNs, one would expect this difference to be due to either a lower black hole mass ($\sim 10^4\ M_\odot$) or a lower accretion rate (for M32, 10^{-9}, in Eddington units). For such a low mass accretion rate, the standard thin disk model for accretion is probably not applicable and the model for Advection-Dominated Accretion Flows provides possible solutions. In the advection-dominated accretion very little energy is radiated away during the accretion process.

Masses for the central condensed objects have been determined for the Milky Way (2.6×10^6 M$_\odot$) and for M32 (3.4×10^6 M$_\odot$). In both cases the accretion rate is extremely low (in Eddington units: $\dot{m} \sim 10^{-6}$ for Sgr A* in the Milky Way centre, $\dot{m} = 10^{-9}$ for the nucleus of M32) and well into the expected Advection Dominated Accretion Flow regime.

In brief, the central X-ray sources are found among the most luminous members of the Local Group. These are candidate massive Black Holes, for which confirmation can be found from data at other wavelengths in the cases of the Milky Way and M31. If also M32 and M33 have massive Black Holes in their nuclei, there could be at least four massive Black Holes immediately around us. For the moment one could conclude that the 20 or so smaller and/or Irregular and dwarf-Spheroidal systems do not seem to possess massive Black Holes, but the sample of M32 shows that the activity level can be so low that a non-detection may not necessarily imply no Black Hole. For future work, inclusion of data from several other wavelengths will allow to tighten this overall assessment of the nuclear status of the Local Group galaxies, which likely has to be carried through with reference to the Advection Dominated Accretion Flow emission predictions.

Bibliography

Battistini, P., Bònoli, F., Braccesi, A., and et al. 1987, *A. Ap. Suppl.*, **67**, 447.

Bender, R., Kormendy, J., and Dehnen, W. 1996, *Ap. J. Lett.*, **464**, L123.

Berkhuijsen, E. M. 1986, *A.Ap.*, **166**, 257.

Bickert, K. F., Greiner, J., and Stencel, R. E. 1996, in *Supersoft X-Ray Sources*, Lecture Notes in Physics, Vol. 472, J. Greiner (ed.), Springer, p.225.

Brinkmann, W., and Siebert, J. 1994, *A. Ap.*, **285**, 812.

Bowyer, S., Margon, B., Lampton, M., and Cruddace, R. 1974, *Ap. J.*, **190**, 285.

Bradt, H. V. D., Ohashi, T., and Pounds, K. A. 1992, *Annu. Rev. A. Ap.*, **30**, 391.

Brandt, W. N., Ward, M. J., Fabian, A. C., and Hodge, P. W. 1997, *MNRAS*, **291**, 709.

Canizares, C. R., Fabbiano, G., and Trinchieri, G. 1987, *Ap. J.*, **312**, 503.

Charles, P. A., and Seward, F. D. 1995, *Exploring the X-ray Universe*, Cambridge University Press, Cambridge.

Clark, G. W. 1965, *Phys. Rev. Lett.*, **14**, 91.

Colbert, E. J. M., and Mushotzky, R. F. 1999, *Ap. J.*, **519**, 89.

Crampton, D., Cowley, A. P., Hutchings, J. B., Schade, D. J., Van Speybroeck, L. P. 1984, *Ap. J.*, **284**, 663.

Cruddace, R., Hasinger, G., and Schmitt, J. 1988, in *Astronomy from Large Databases. Scientific objectives and methodological approaches, Proceedings of the Conference, 12-14 October 1987, Garching, Federal Republic of Germany*, ESO Conference and Workshop Proceedings, (eds.) F. Murtagh and A. Heck, p177.

Davelaar, J. 1969, *PhD Thesis*, University of Leiden.

de Vaucouleurs, G., de Vaucouleurs, A., Corwin, H. G., Buta, R. J., Paturel, G., and Fouque, P. 1991, *Third Reference Catalog of Bright Galaxies*, Springer, New York. (RC3)

Deeming, T. J. 1975, *Ap. Space Sci.*, **36**, 137.

Dressel, L. L., and Condon, J. J. 1976, *Ap. J. Suppl.*, **31**, 187.

Dubus, G., Charles, P. A., Long, K. S., and Hakala, P. J. 1997, *Ap. J. Lett.*, **490**, L47.

Elvis, M., Briel, U. G., and Henry, J. P. 1983, *Ap. J.*, **268**, 105.

Elvis, M., Fiore, F., Giommi, P., and Padovani, P. 1997, *MNRAS*, **291**, L49.

Elvis, M., and Van Speybroeck, L. 1982, *Ap. J.*, **257**, L51.

Eskridge, P. 1988, *A. J.*, **96**, 1614.

Eskridge, P. 1995, *Publ. A. Soc. Pac.*, **107**, 561.

Eskridge, P. B., White, R. E., and Davis, D. S. 1996, *Ap. J. Lett.*, **463**, L59.

Fabbiano, G. 1989, *Annu. Rev. A. Ap.*, **27**, 87.

Fabbiano, G., Kim, D.-W., Trinchieri, G. 1992, *Ap. J. Suppl.*, **80**, 531.

Filippenko, A. V., and Sargent, W. L. W. 1985, *Ap. J. Suppl.*, **57**, 503.

Ford, H. C., Jacoby, G., and Jenner, D. 1977, *Ap. J.*, **213**, 18.

Forman, W., Jones, C., Cominsky, L., Julien, P., Murrey, S., and et al. 1978, *Ap. J. Suppl.*, **38**, 357.

Gallagher, J. S., Hunter, D. A., and Mould, J. 1984, *Ap. J. Lett.*, **281**, L63.

Gallouët, L., Heidmann, N., and Dampierre, F. 1973, *A. Ap. Suppl.*, **12**, 89.

Gallouet, L., Heidmann, N., and Dampierre, F. 1975, *A. Ap. Suppl.*, **19**, 1.

Genzel, R., and Townes, C. H. 1987, *Annu. Rev. A. Ap.*, **25**, 377.

Genzel, R., Eckart, A., Ott, T., and Eisenhauer, F. 1997, *MNRAS*, **291**, 219.

Giacconi, R., Gursky, H., Paolini, F., and Rossi, B. 1962, *Phys. Rev. Lett.*, **9**, 439.

Giacconi, R., Kellogg, E., Gorenstein, P., Gursky, H., and Tananbaum, H., 1971, *Ap. J. Lett.*, **165**, L27.

Giacconi, R., Branduardi, G., Briel, U., Epstein, A., and et al. 1979, *Ap. J.*, **230**, 540.

Gizis, J. E., Mould, J. R., and Djorgovski, S. 1993, *Publ. A. Soc. Pac.*, **105**, 871.

Gottwald, M., Pietsch, W., and Hasinger, G. 1987, *A. Ap.*, **175**, 45.

Griffiths, R. E., and Padovani, P. 1990, *Ap. J.*, **360**, 483.

Gursky, H., Giacconi, R., Paolini, F., and Rossi, B. 1963, *Phys. Rev. Lett.*, **11**, 530.

Heckman, T. M. 1980, *A. Ap.*, **87**, 152.

Helfand, D. J. 1984, *Publ. A. Soc. Pac.*, **96**, 913.

Ho, L. C., Filippenko, A. V., and Sargent, W. L. 1995, *Ap. J. Suppl.*, **98**, 477.

Ho, L. C., Filippenko, A. V., and Sargent, W. L. 1997, *Ap. J.*, **487**, 568.

Hubble, E. 1932, *Ap. J.*, **76**, 44.

Kormendy, J., and Richstone, D. 1995, *Annu. Rev. A. Ap.*, **33**, 581.

Lasota, J.-P., Abramowicz, M. A., Chen, X., and et al. 1996, *Ap. J.*, **462**, 142.

Loewenstein, M., Hayashida, K., Toneri, T., and Davis, D. S. 1998, *Ap. J.*, **497**, 681.

Long, K. S., Charles, P. A., Blair, W. P., and Gordon, S. M. 1996, *Ap. J.*, **466**, 750.

Long, K. S., and Van Speybroeck, L. P. 1983, in *Accretion-driven stellar X-ray sources*, Cambridge University Press, Cambridge, p. 117.

Lozinskaya, T. A., Silchenko, O. K., Helfand, D. J., and Goss, W. M. 1998, *A. J.*, **116**, 2328.

Magorrian, J., Tremaine, S., Richstone, D., and et al. 1998, *A. J.*, **115**, 2285.

Mahadevan, R. 1997, *Ap. J.*, **477**, 585.

van der Marel, R. P., Cretton, N., de Zeeuw, P. T., and Rix, H.-W. 1998, *Ap. J.*, **493**, 613.

van der Marel, R. P., de Zeeuw, P. T., and Rix H.-W. 1997, *Ap. J.*, **488**, 119.

Markert, T. H., and Donahue, M. E. 1985, *Ap. J.*, **297**, 564.

Markert, T. H., and Rallis, A. D. 1983, *Ap. J.*, **275**, 571.

McKechnie, S. P., Jansen, F. A., de Korte, P. A. J., Hulscher, F. W. H., van der Klis, M., and et al. 1984, in *X-ray Astronomy '84*, ed. M. Oda and R. Giacconi, Tokyo, Inst. Space Aeronaut. Sci., p.376.

Mateo, M. 1998, *Annu. Rev. A. Ap.*, **36**, 435

Mateo, M., Olszewski, E., Welch, D., et al. 1991, *A. J.*, **102**, 914.

Matsuoka, M., Piro, L., Yamauchi, M., and Toshio, M. 1990, *Ap. J.*, **361**, 400.

Matt, G., Piro, L., Antonelli, L. A., Fink, H. H., Meurs, E. J. A., and Perola, G. C. 1994, *A. Ap. Lett.*, **292**, L13.

Mürset, U., Jordan, S., and Wolff, B. 1996, in *Supersoft X-Ray Sources*, Lecture Notes in Physics, Vol. 472, J. Greiner (ed.), Springer, p.251.

Narayan, R., and Yi, I. 1994, *Ap. J.*, **428**, L13.

Narayan, R., Yi, I., Mahadevan, R. 1995, *Nature*, **374**, 623.

Narayan, R., 1996, *Ap.J.*, **462**, 136.

Narayan, R., 1997, in *Accretion Phenomena and Related Outflows*, ASP Conf. Ser. 121, eds. D. Wickramasinghe, L. Ferrario and G. Bicknell, San Francisco:ASP, p.75.

Palumbo, G. G. C. 1988, *Accurate positions of Zwicky galaxies.* October 1988 special version, includes 1987 *A. Ap. Suppl.*, Vol. 70, p.189 and p.191 and additional measurements.

Parma, P., Cameron, R. A., and de Ruiter, H. R. 1991, *A. J.*, **102**, 6.

Peres, G., Reale, F., Collura, A., and Fabbiano, G. 1989, *Ap. J.*, **336**, 140.

Peterson, L. E., Jacobson, A. S., and Pelling, R. M. 1966, *Phys. Rev. Lett.*, **16**, 142.

Predehl, P., and Trümper, J. 1994, *A. Ap. Lett.*, **290**, L29.

Primini, F. A., Forman, W., and Jones, C. 1993, *Ap. J.*, **410**, 615.

Read, A. M., and Pietsch, W. 1999, *A. Ap.*, **341**, 8.

Rees, M. J. 1988, *Nature*, **333**, 523.

Reynolds, C. S., Di Matteo, T., Fabian, A. C., and et al. 1996, *MNRAS*, **283**, L111.

Roberts, M. S., Hogg, D. E., Bregman, J. N., and et al. 1991, *Ap. J. Suppl.*, **75**, 751.

Sargent, W. L. W., Young, P. J., Boksenberg, A., Shortridge, K., Lynds, C. R., Hartwick, F. D. A. 1978, *Ap. J.*, **221**, 731.

Schulman, E., and Bregman, J. N. 1995, *Ap. J.*, **441**, 568.

Seyfert, C. K. 1943 *Ap. J.*, **97**, 28.

Stark, A., Gammie, C., Wilson, R., and et al. 1992, *Ap. J. Suppl.*, **79**, 77.

Supper, R., Hasinger, G., Pietsch, W., Trümper, J., Jain, A., and et al. 1997, *A. Ap.*, **317**, 328.

Takano, M., Mitsuda, K., Fukazawa, Y., and Nagase, F. 1994, *Ap. J. Lett.*, **436**, L47.

Tinney, C. G., Da Costa, G. S., and Zinnecker, H. 1997, *MNRAS*, **285**, 111.

Trinchieri, G., and Fabbiano, G. 1991, *Ap. J.*, **382**, 82.

Trinchieri, G., Fabbiano, G., and Peres, G. 1988, *Ap. J.*, **325**, 531.

Vettolani, G., Palumbo, G., Santagata, N. 1986, *A. Ap. Suppl.*, **64**, 247.

Vogler, A., and Pietsh, W. 1999, *A. Ap.*, **342**, 101

Wandel, A. 1991, *A. Ap.*, **241**, 5.

Wang, Q. D., and Gotthelf, E. V. 1998, *Ap. J.*, **494**, 623.

Whiting, A. B., Hau, G. K. T., and Irwin, M. J. 1997a, *Spectrum*, No. 14, p.4.

Whiting, A. B., Irwin, M. J., and Hau, G. K. T. 1997b, *A. J.*, **114**, 996.

Wilson, A. S., Elvis, M., Lawrence, A., and Bland-Hawthorn, J. 1992, *A. J. Lett.*, **391**, L75.

Zimmermann, U., Boese, G., Becker, W., Belloni, T., and et al. 1998, *EXSAS User's Guide*, ROSAT Scientific Data Center.